THE MULTIPLE FUNCTIONS OF EFHC1 IN *TETRAHYMENA* AND *XENOPUS*

By

Ying Zhao

B.S., University of Science and Technology of China

A thesis submitted to the

Faculty of the Graduate School of the

University of Colorado in partial fulfillment

of the requirement for the degree of

Doctor of Philosophy

Department of Molecular, Cellular, and Developmental Biology

2015

This thesis entitled:

The Multiple Functions of EFHC1 in *Tetrahymena* and *Xenopus*

written by Ying Zhao
has been approved for the Department of Molecular, Cellular, and Developmental Biology

Mark Winey, Ph.D., Advisor

Gia Voeltz, Ph.D., Chair of Committee

Date

The final copy of this thesis has been examined by the signatories, and we
Find that both the content and the form meet acceptable presentation standards
Of scholarly work in the above mentioned discipline.

Zhao, Ying (Ph. D., Molecular, Cellular, and Developmental Biology)

The Multiple Functions of EFHC1 in *Tetrahymena* and *Xenopus*

Dissertation directed by Professor Mark Winey

The basal body is the microtubule-organizing center that nucleates the axoneme of the cilium. Both basal bodies and cilia are complex intracellular organelles composed of hundreds of polypeptides found throughout the eukaryotes. Different types of cilia have various and often over-lapping functions, from driving fluid flow and cellular motility, to the establishment of distinct cellular domains and morphologies, to mediating and modulating intracellular signaling involved in tissue patterning. Dysfunction of basal body or ciliary components has been implicated in a variety of human diseases. EFHC1 is conserved from single cell alga to human beings. Members of this protein family contain three tandem DM10 domains and a putative EF-hand Ca2+ binding motif at the C terminal end. In some organisms, the EF-hand motif appears to be missing. Mutations of EFHC1 have been linked to juvenile myoclonic epilepsy (JME). The EFHC1 paralog, EFHC2, is also present in many species and mutant forms are reported to be pathological. Despite their wide spread conservation, the cellular functions of EFHC family proteins and the underlying mechanisms associated with the pathology of mutant forms remains obscure. In this study, both the ciliate *Tetrahymena thermophila* and the frog *Xenopus laveis* were used as distinct systems to investigate the functions of EFHC1. Here I have shown that there are two EFHC1-like genes in *Tetrahymena*. Both of them encode proteins that localize to the basal bodies and the cilia, and their localization is independent on each other. Cells lacking either individual gene do not exhibit obvious growth or basal body defects. However, both of them have structural defects, missing the MIP1a complex inside the axonemal doublet microtubules. Unlike *Tetrahymena*, only the EFHC1b in *X.laveis* was confirmed to be expressed. I have demonstrated XlEFHC1 was associated with both motile and immotile cilia. It is involved in ciliated cell formation and cilia genesis. Knockdown of XlEFHC1 by morpholino resulted in disrupted central nervous system patterning and deficient neural crest formation and migration. Reduction of XlEFHC1 leads to increased level of Wnt8a RNA, suggesting XlEFHC1 acts as an antagonist of canonical Wnt signaling. Together, this thesis work uncovered unexpected roles of EFHC1 in maintaining axoneme structure, in ciliogenosis and in regulating Wnt signaling pathway, which might well be relevant to the etiology of JME.

Acknowledgments

First, I would like to thank my advisor Mark for his intellectual and moral support over the past six years. Mark had made himself available to answer my numerous questions. He always had suggestions on the experiments that I could be doing and at the same time gave me a lot of freedom to pursue my own ideas. I have also learned from him that never give up easily. None of this work would have happened without Mark's support to follow the stories where they took me.

Thanks for all the current and previous members of Winey lab for providing such a fun place to learn how to do good science and making my graduate school experience very enjoyable. And I also thank my collaborators, without whom the work would not have been as successful. I would like to express my thanks to my committee members, Gia, Min, Mike and Dan, for providing me all the guidance and suggestions for my research.

I would like to thank my family for their love, encouragement and support over the years, especially my mom and dad, who always believe in me; without them, I definitely would not make this far today. Finally, I would like to thank my fiancé, Qian, for his support over the years we have been together. I'm looking forward to share new adventures with you in the future.

Table of Contents

Chapter 1. Introduction 1

I. Cilia structure and function 1

II. Cilia signaling 3

III. Basal body structure and function 5

IV. Microtubule inner protein 7

V. Ciliopathies 9

VI. Juvenile myoclonic epilepsy 11

VII. EFHC1 protein family 12

VIII. EFHC1 function 16

Chapter 2. Localization of four conserved basal body component proteins 20

I. Introduction 20

II. Material and method 24

III. Results 27

IV. Discussion 41

Chapter 3. Genetic analysis of *BBC73* in *Tetrahymena thermophila* 46

I. Introduction 46

II. Material and Method 47

III. Results 52

IV. Discussion: 72

Chapter 4. Functional analysis of EFHC1 in *Xenopus* embryos 79

I. Introduction 79

II. Material and Methods 81

III. Results: 83

IV. Discussion 105

Chapter 5. Conclusion 108

References: 115

List of Tables

Table 2-1. The four BBC protein candidates are conserved 28

List of Figures

Figure1-1. Diversity of ciliary axonemes 2
Figure1-2. The Structures and function of centrioles/basal body 6
Figure1-3. 3D structures of DMT and MIP1–4 organization in *Chlamydomonas* axonemes 8
Figure1-4. Genes involved in ciliopathies 10
Figure1-5. Phylogenetic analysis and sequence alignment of *EFHC* family 13
Figure2-1. *Tetrahymena* basal body organization 22
Figure2-2. Bbc31 is associated with the accessory structures of basal bodies 29
Figure2-3. Bbc31 is required for maintaining the cortical row alignment 31
Figure2-4. Bbc57 localizes to both basal bodies and cilia 33
Figure2-5. Bbc52 is associated with both basal bodies and cilia 34
Figure2-6. Capsl does not localizes to the centrosome 36
Figure2-7. Bbc73 is associated with both basal bodies and cilia 39
Figure2-8. Bbc60, the homolog of Bbc73, exhibits the similar localization pattern to Bbc73 in *Tetrahymena* 42
Figure3-1. Ultrastructural localization of Bbc73-GFP 53
Figure3-2. *BBC73* is not an essential gene in *Tetrahymena* 55
Figure3-3. Bbc73 is not required for overall cortical organization and basal body assembly or maintenance 56
Figure3-4. Loss of *BBC73* leads to subtle behavior defects 58
Figure3-5. *bbc73Δ* cells has MIP defect 61
Figure3-6. Localization of GFP-luciferase-Bbc73 fusions 63
Figure3-7. Localization of GFP-mCherry-Bbc73 fusions 64
Figure3-8. The N-terminus of Bbc73 is sufficient but not required for its basal body and ciliary localization 66
Figure3-9. *bbc60Δ* cells has MIP defect 69
Figure3-10. Localization of GFP-luciferase-Bbc60 rescue fusion in wild type cells and *bbc60Δ* cells 70
Figure3-11. Localization of Bbc73 and Bbc60 are independent on each other 71
Figure4-1. Expression of *EFHC1* RNA in *Xenopus* embryos 84
Figure4-2. Localization of EFHC1 in various cilia 87
Figure4-3. The N-terminus of EFHC1 is required for its ciliary localization 89
Figure4-4. Specificy of EFHC1 morpholino 90
Figure4-5. Loss of EFHC1 leads to motile cilia defects on ectoderm explants 92
Figure4-6. EFHC1 truncation mutants cannot rescue the ciliary defects in EFHC1b morphants 94
Figure4-7. Depletion of EFHC1 affects neural crest induction and migration 96

Figure4-8. Knocked down of EFHC1 results in Neural crest migration both in vivo and in vitro 98
Figure4-9. Effects of EFHC1 overexpression on neural crest markers..... 99
Figure4-10. Depletion of EFHC1 disrupts central nervous system patterning 101
Figure4-11. The CNS and NC defects in EFHC1 morphants cannot be rescued by Cby RNA, and vice versa 102
Figure4-12. Gene expression and Wnt signaling are altered in EFHC1b morphants 104
Figure4-13. Notch1 RNA level is changed in EFHC1 morphant explants..... 105

Chapter 1. Introduction

I. Cilia structure and function

Cilia are highly conserved hair-like microtubule-based structures that emanate from the cell surface. There are two types of cilia: motile cilia and non-motile primary cilia. Both types of cilia are widely found in eukaryotic cells and in human the primary cilia are present on almost every cell (Yuan and Sun, 2013). Their structures have been well characterized back to 1980s, with the featured incredibly stable axoneme, the outside membrane and the matrix in between(Gibbons, 1981). While the two kinds of cilia share some common features, they differ both structurally and functionally(Ferkol and Leigh, 2012; Marshall and Nonaka, 2006). Cilia contain axonemes, composed of the nine outer doublet microtubules. Motile cilia typically have a "9+2" axoneme, which has two central pair singlet microtubules in addition to the nine doublet microtubles. Each of the nine doublet microtubules is composited of a complete A-tubule of 13 protofilaments and an incomplete B-tubule of 10 protofilaments. Besides the basic building block for microtubules, α and β-tubulin, there are more than 200 polypeptides predicted present in a ciliary axoneme (Luck, 1984). These components further participate in formation of inner dynein arm, outer dynein arm, radial spokes and etc., contributing to the complex 3-dimensional architecture of the axoneme. Specifically, these subunits are arranged periodically with folds of 8nm tubulin dimer along the axial axoneme. For decades, researchers have been studying how this complexity is achieved. Motile cilia play a critical role in cell locomotion and fluid movement around the cell surface, as is the case of motile cilia on trachea in human sweeping the mucus out of the lung. In contrast, non-motile, primary cilia have a 9+0 axoneme, lacking the central pair microtubules and the dynein arms required for mobility(Satir and Christensen, 2007). They function as sensory cellular antennae, regarding their role in external stimuli sensation, signaling transduction and coupling the signal to cell division and differentiation. We rely on the specialized primary cilia in our eyes and nose to see the light and smell the rose.

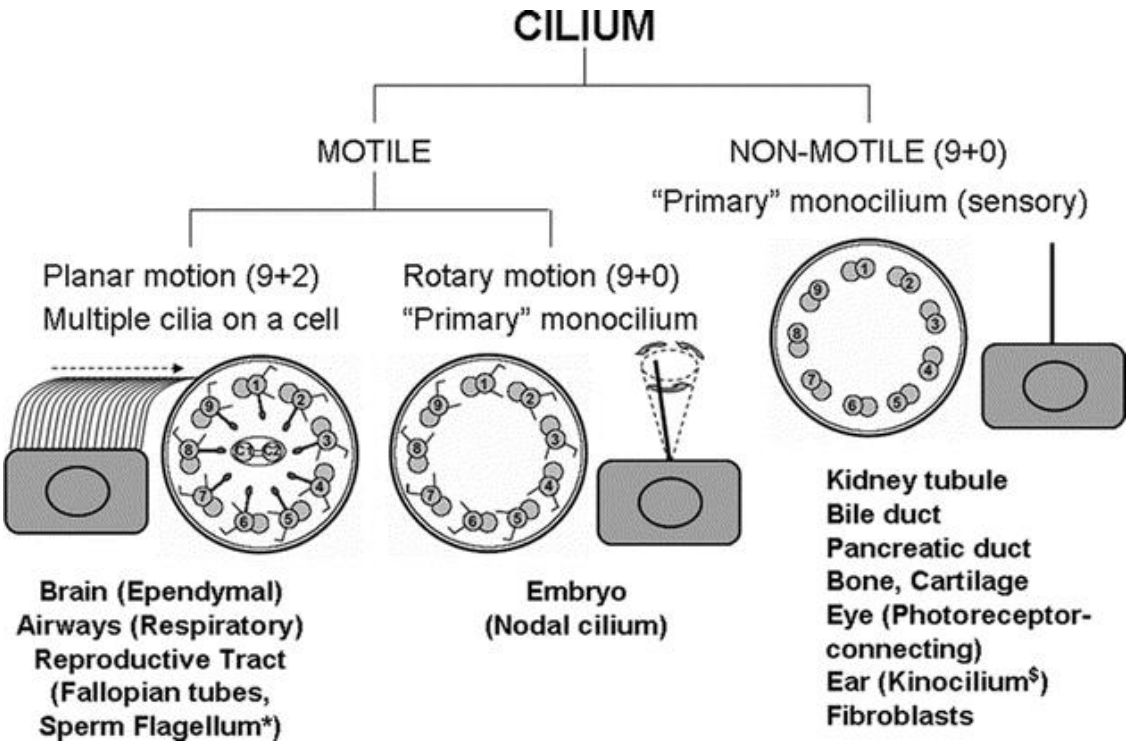

Figure1-1. Diversity of ciliary axonemes. Model showing Cross-sectional view of the motile and non-motile cilia axoneme arrangement and the motion of two types of motile cilia. *Solitary axoneme in the sperm mirrors the structure of the cilium. $Subcellular structure of the kinocilum is debatable. Some reports indicate 9 + 0, whereas others indicate 9 + 2 configuration. Adapted from" Clinical and genetic aspects of primary ciliary dyskinesia/Kartagener syndrome" Margaret W Leigh et al 2009

II. Cilia signaling

Recently, cilia, especially primary cilia have become a spotlight for intensive research studies because more and more evidence shows that they are required for transducing multiple signals critical for vertebrate development(Basten and Giles, 2013; Goetz and Anderson, 2010). Moreover, ciliogenesis is regulated and by some signaling pathways. Therefore, the cilium seems to be a center for signal transduction. The best-understood cilia-dependent signaling pathway is the hedgehog signaling. This pathway is important for various developmental processes, such as cell proliferation, cell differentiation and tissue patterning(Varjosalo and Taipale, 2008). The first evidence came from mutations causing some defect in mouse embryonic patterning, where the mutant morphological phenotype was very similar to impaired hedgehog signaling(Huangfu and Anderson, 2005; Huangfu et al., 2003; May et al., 2005). The ventral tube cell types were lost in the mutants, which is specified by the sonic hedgehog gradient in wild type embryos. It turned out that the genes disrupted in the mutants encoded components of intraflagellar transport machinery, IFT88, IFT172 and DYNC2H1. The IFT machinery is responsible for transporting cargo particles along the ciliary axoneme, which is required for cilia formation. Loss of ift88 in zebrafish leads to analogous Hh-dependent defects in neural tube and somite(Huang and Schier, 2009). Kif3a$^{-/-}$ mice also exhibited a similar deficiency in neural patterning regulated by SHh signaling, where Kif3a is a kininsin-2 motor required for anterograde trafficking in cilia(Zhou, 2009). Experiments have found the enrichment of hedgehog pathway key components in the cilia, including the Hh receptor PTCH1 and its downstream effector SMO, Gli transcription factors and the negative regulator SUFU(Corbit et al., 2005; Haycraft et al., 2005; Rohatgi et al., 2007).

Although most of the cells can form primary cilia, only a small number of them response to Hh signaling at some specific stage(Goetz and Anderson, 2010). This raised the question whether there are other signaling pathways depending on cilia. Most studies have been focused on the canonical and non-canonical Wnt signaling pathways. Wnt signaling is known to be involved in regulating diverse

developmental and homeostatic processes(Gao and Chen, 2010). The key components of the two pathways have been identified. Briefly, the activation of the signaling pathways starts with the extracellular Wnt ligand proteins binding to the Frizzled family receptors. Upon the activation of the receptors, the biological signal is transmitted to Dishevelled proteins inside the cells(van Amerongen and Nusse, 2009; MacDonald et al., 2009; Widelitz, 2005). Then the canonical Wnt signaling leads to regulation of gene transcription through activation of transcriptional coactivator β-catinen. Experiments in cultured cells and zebrafish showed that canonical Wnt signaling was elevated when cilia associated proteins were knocked down(Bergmann et al., 2008; Gerdes et al., 2007; Ross et al., 2005). Chibby mutant mice resulted in inappropriate canonical Wnt activation(Voronina et al., 2009). The non-canonical Wnt signaling can be further divided into two sub signaling pathways: planar cell polarity pathway and calcium pathway. Neither require β-catenin to conduct their functions. The PCP pathway regulates the cytoskeleton of the cell and participates in establishing the polarity of the cilia(Seifert and Mlodzik, 2007). Disruption of activation of the Dishevelled proteins in Xenopus embryos by morpholinos resulted in impaired ciliary polarity of the motile cilia on the epidermis(Park et al., 2008). On the other hand, defects in non-canonical Wnt signaling dependent process, like convention extension, were observed in the zebrafish embryos lacking ciliary protein(Gerdes et al., 2007). The non-canonical Wnt/calcium pathway plays a role in regulating the release of calcium from the endoplasmic reticulum inside the cell and calcium is a critical general second messenger for multiple downstream processes. Physical sensation can influence the cellular calcium concentration. Upon shear stress, the flow induced cilia bending leads to the opening of polycystin complex iron channel and the extracellular calcium influx(Habas and Dawid, 2005; Nauli et al., 2003). The elevated calcium level is believed to affect the canonical Wnt signaling by switching it off and turning on the non-canonical Wnt signaling. Therefore it is proposed that the primary cilium may work as the switch between the canonical and non-canonical Wnt signaling pathways(Corbit et al., 2008; Simons et al., 2005). Despite the evidence that Wnt signaling

is connected with cilia, the details and basis of the process are still unclear and there is conflicting data. It is known abnormal activation of canonical Wnt signaling affects gastrulation, axis duplication and early embryonic patterning. Mouse IFT mutant did not show any of these Wnt-dependent phenotypes. Moreover, alternation of Wnt activity was not detected in ift88 and ift172 mutant mice(Ocbina et al., 2009). Similarly, zebrafish embryos lacking ift88 showed defects in Hh signaling, but not any defect in convention extension regulated by non-canonical Wnt-signaling(Huang and Schier, 2009). Taken together, it seems like the relationship between Wnt signaling and cilia is cell type and stage specific and the role of cilia in these pathways is more complicated and subtle than hedgehog signaling. Thus more work on this issue would surely contribute to understanding the details. I attempt to figure out the connection of a ciliary component and the canonical Wnt signaling pathway by using *Xenopus laveis* embryos in Chapter4.

III. Basal body structure and function

Cilia are nucleated from the basal bodies, which are also well conserved cellular organelles in eukaryotes, featuring a nine-fold symmetry of triplet microtubules(Marshall, 2008). This cylindrical structure can be further divided into several discrete structural domains besides the major structure of the microtubule scaffold wall(Carvalho-Santos et al., 2011; Pearson and Winey, 2009). The cartwheel is a structure at the base, or proximal end of the basal body, important for new basal body assembly. The transition zone is at the distal end of the basal body where there is a transition from the triplet microtubules of the basal body to the doublet microtubules of the ciliary axoneme. Between the transition zone and the cartwheel is the lumen of the basal body containing a density of unknown function and composition distinct from cytoplasm. Basal bodies reside beneath the cell surface where they act as a template for nucleating the axoneme of the cilia. Basal bodies are closely related to the centrioles within centrosomes, and are interconverted in many cell types(Kobayashi and Dynlacht, 2011). Centrioles also have the nine-fold symmetry, but the arrangement of microtubules varies from singlets,

as in the C. elegans(Li et al., 2004), to triplets, as in vertebrates and many other organisms. In animal cells, a pair of linked centrioles along with the pericentriolar material functions as a microtubule organizing center to establish the cellular polarity and assure mitotic fidelity. However, during the cell cycle, when cells enter a quiescence state, the mother centriole of the centriole pair will migrate to the cell surface to act as a basal body to form the primary cilium. This cilium can be disassembled and resorbed once the cell needs to re-enter the cell cycle and the centrioles will migrate back and recapture the role of organizing microtubules near the nucleus. Although the morphology of basal bodies and centrioles has been well described, there is still not much known about their molecular composition and regulators and how they work together to secure the normal function of the structures. Here I present my thesis work of studying the localization and function of basal body proteins in *Tetrahymena thermophile* in Chapter2 and Chapter3.

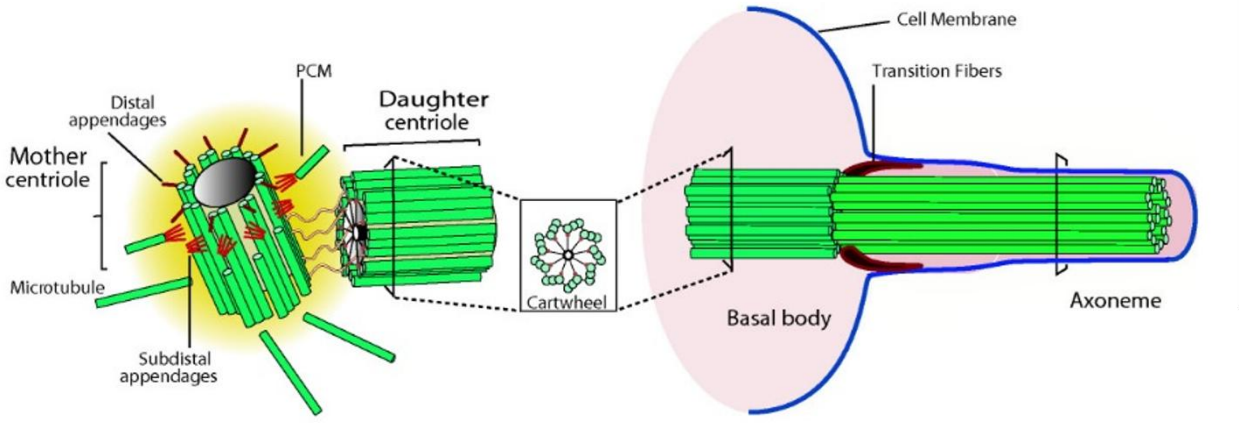

Figure1-2. The Structures and function of centrioles/basal body. The canonical centriole/basal body has nine microtubule triplets. A mother-daughter pair of centrioles composes the centrosome with surrounding matrix pericentriolar material (PCM). There are accessory structures (distal and subdistal appendages) attached to the mother centriole. In many cells, centrioles migrate to the cell surface to act as the basal bodies to form the cilia or flagella. Adapted from Bettencourt-Dias *BMC Biology* 2013

IV. Microtubule inner protein

Electron microscopy and cryo-electron microscopy of axonemes have revealed many interesting features (Ishikawa, 2015). These include microtubule inner proteins (MIPs), which are protein complexes identified recently on the inside of the microtubule wall. They were described as discrete electron-dense material in the lumen of microtubules. So far, MIPs have been reported associated with doublet microtubules in insect, *S. purpuratus* and *Chlamydomonas* flagella, subpellicular microtubules in sporozoites of apicomplexan parasites and cytoplasmic microtubules in rat embryonic hippocampal neurons axons and pluripotent P19 embryonal carcinoma cell line (Cyrklaff et al., 2007; Garvalov et al., 2006; Nicastro et al., 2006, 2011; Popodi et al., 2008; Romano Dallai, 2005; Sui and Downing, 2006). In contrast, no similar structures have been identified in epithelia cell lines like Ptk2 and HeLa cells, and in vitro nucleated-microtubules from purified pig brain tubulin (Garvalov et al., 2006). Both of the axonemal doublet microtubules and the subpellicular microtubules are highly stable and the MIPs seemed to be attached to the microtubule walls, while MIPs found in less stable cytoplasmic microtubules in neural and stem cells were loosely connected to the microtubules. However, these MIPs share a common feature: they all display periodicity along the microtubule walls although the periodicities differ among species (Nicastro et al., 2011). The most well-studied MIPs are from axonemal doublet microtubules of *Chalmydomanos* and Sea urchin flagella. Cryo-electron tomography and isosurface renderings clearly demonstrated that at least four sets of distinct MIPs were localized at the interior of the doublet microtubule wall in *Chlamydomanos* flagella axoneme. The structures MIP1, MIP2 and MIP4 are found in the A tubule of doublet microtubules, while MIP3 is associated with the B tubule of doublet microtubules. More specifically, MIP1 contains two globular subunits, the longer MIP1a and shorter MIP1b, arching from protofilament A5 to A7 (MIP1a) and only in protofilament A5 (MIP1b, Fig1-3). Both MIP1a and MIP1b repeat every 16nm with alternative manner as “a-b”, producing

a 16nm periodicity with an 8nm subperiodicity. The 8nm subperiodicity matches the length of the tubulin dimer repeat. Similarly, MIP2,

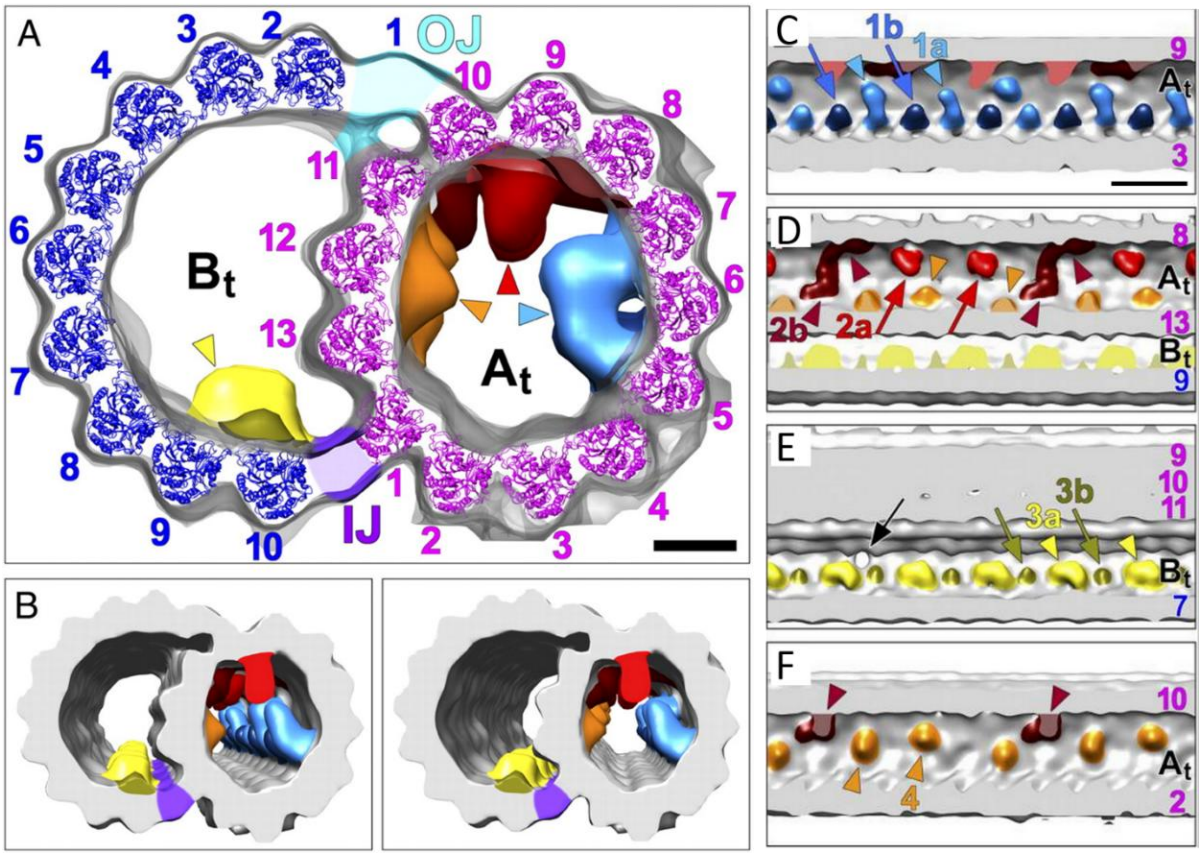

Figure1-3. 3D structures of DMT and MIP1–4 organization in *Chlamydomonas* axonemes. Isosurface renderings of the averaged axonemal repeat from *Chlamydomonas* pseudo-WT show the DMT in cross-sectional views (A, B) and longitudinal view (C, D, E, F). Tubulin dimers and PF numbers are both colored pink in the A-tubule (A_t) and dark blue in the B-tubule (B_t). In the isosurface renderings, the electron densities for MIP1–4 are color-coded (including the arrows and arrowheads pointing toward the MIPs): MIP1a and MIP1b (light and dark blue, respectively), MIP2a and MIP2b (light and dark red, respectively), MIP3a and MIP3b (yellow and olive, respectively), and MIP4 (orange). The black arrows in *E* point to the hole in the IJ-density. Scale bar: 5nm (A) and 20nm(C, D, E, F A). The figures were adapted from Nicastrao D et al. 2011 Proc Natl Acad Sci U S A. 2011 Oct 18; 108(42).

arching from protofilament A8 to A12, also consist of two subunits MIP2a and MIP2b. They generate the "a-a-b" 48nm periodicity with 16nm subperiodicity. The last A-tubule MIP, MIP4 distributes along the inner side of protofilament A12 and A13 with 48nm periodicity of three electron densities. Two subunits were discovered within the B-tubule associated MIP3. The larger globular MIP3a and the smaller spike-shaped MIP3b form the "a-b" pattern 16nm periodicity along the axial of protofilament B8 to B10 (Fig1-3). Despite their wide-spread occurrence and the relevant comprehensive morphological description, the composition and functional roles of MIPs are unknown. There are predictions of MIPs function based on their position and special arrangement(Nicastro et al., 2011). MIPs may help to stabilize the axoneme integrity during flagella or cilia motility. They might also facilitate the anchoring of other axonemal complexes, such as the dynein arms, to the doublet microtubules. Another idea is that MIPs may be involved in post-translational modification of microtubules, like the luminal acetylation. Tubulin acetyltransferase has been localized to lumen of microtubules and was found connected with the microtubule walls (Topalidou et al., 2012). Moreover, additional work is required to understand the connection between MIP complexes and cilia associated proteins implicated in human disease, like ARL13b, which is related to Sonic Hedgehog signaling dependent diseases. My thesis explores the relationship in *Tetrahymena* between MIPs and a protein involved in human epilepsy.

V. Ciliopathies

With the comprehensive functions and wide distribution of basal bodies and cilia, it's not surprising to find that the two organelles have been implicated in a growing class of pleiotropic disorders called ciliopathies. The underlying mechanism of these diseases arises from defects in cilia formation or function(Hildebrandt et al., 2011). During embryonic development, the motile cilia in the node generate a directed fluid as a cue guiding the embryo to establish the left-right asymmetry(Ferkol

and Leigh, 2012). Immobility of the nodal cilia underlies defects in body patterning, like situs inversus and dwarfism. In the female reproductive system, the ovum moves from the ovary to the uterus through

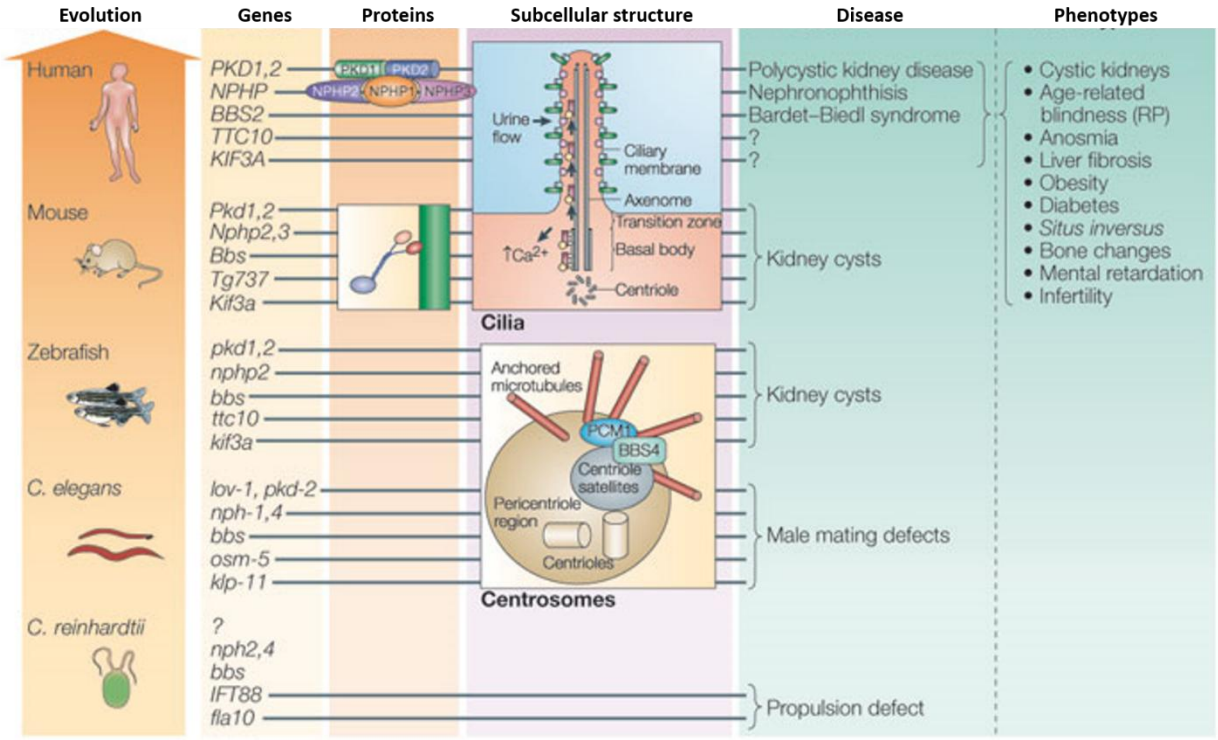

Figure1-4. Genes involved in ciliopathies. Description of a number of ciliopathies, the corresponding genes, protein products, the affected subcellular structure and the phenotypes. A high percentage of these genes are conserved for more than 1.5 billion years of evolution. Adapted from "Cilia and centrosomes: a unifying pathogenic concept for cystic kidney disease?" Friedhelm Hildebrandt & Edgar Otto 2005

the beating of the motile cilia in the fallopian tubes. Malfunctioning cilia can lead to ectopic pregnancy since the ovum may not reach the ovary. Impaired primary cilia no long sense extracellular stimuli and coordinate multiple signaling pathways properly, often resulting in defects in organ development. The syndromes include but are not limited to obesity, heart defects, retinal degeneration, diabetes, polydactyl, hydrocephalus and polycystic kidney(Bachmann-Gagescu, 2014; Hildebrandt et al., 2011; Lee and Gleeson, 2011). The list of ciliopathies is expanding with more basal body and cilia components

implicated in these disorders. The genetic basis of these diseases is extraordinarily complex with more than 89 loci implicated. The connection between the cilia and the signaling pathways involved in development may shed light on the basis of ciliopathies. Beyond that, different genes can contribute a similar syndrome, while similar genes or mutations within the same gene cause a range of different diseases.

VI. Juvenile myoclonic epilepsy

Juvenile myoclonic epilepsy, the most common form of genetic generalized epilepsies, accounts for ~10% of all reported epilepsy cases(Grünewald and Panayiotopoulos, 1993). The patients may exhibit a range of seizure types, including tonic-clonic seizures, myoclonic jerks and sometimes absence seizures. The syndromes usually appear between late childhood and early adulthood with myoclonus occurring in the early morning. In general, the JME patient brain anatomy appears normal revealed by advanced imaging techniques, such as Magnetic resonance Imaging (MRI) and computer tomography (CT scan)(Meador, 2010). Although several studies indicated subtle structural and functional changes associated in the frontal lobe, a following study suggested the deficit should be interpreted with more care. The genetics underlying JME is complex and not yet fully understood. So far genetic mapping of suspicious loci from JME families has linked five Mendelian genes to this disease(Delgado-Escueta et al., 2013). Specifically, four of them are: CACNB4, GABRA1, CLCN2 and GABRD(Cossette et al., 2002; Escayg et al., 2000; Haug et al., 2003; Kapoor et al., 2003), the gene product encoded is an ion channel, which is quite reasonable. Historically, genes encoding ion channel proteins have been thought to be the genetic origin for idiopathic epilepsy(Armijo et al., 2005), since seizures, the primary syndrome of epilepsy, are the outcome of abnormal electronic discharges in neurons, which is regulated by ion channels. However, the fifth gene associated with JME is an exception to this long standard paradigm. The gene, EFHC1, encodes a non-ion channel protein, mutations of which have been discovered in several unrelated JME families(Subaran et al., 2015; Suzuki et al., 2004, 2006). So far the nature of genetic inheritance of EFHC1

mutations in JME patients is still unknown. Most of the mutations reported are heterozygous missense mutations, indicating JME as an autosomal dominant disorder. The patients survived into adolescence upon which the seizure syndrome appeared. In contrast, the only homozygous missense mutation discovered causes more serious symptoms, severe brain pathology and death in infancy. Whether the disease results from loss or gain of function of these mutant alleles is yet to be determined.

VII. EFHC1 protein family

The human EFHC1 gene encodes a conserved protein containing three tandem DM10 domain of unknown function and a predicted EF-hand motif at the C terminus(King, 2006). Homologs have been identified in a variety of organisms from unicellular ciliates, like *Tetrahymena*, throughout the higher vertebrates, like *Xenopus*, mouse and human. The DM10 domain contains nearby 105 amino acids and is predicted to have a secondary structure mainly consisting of beta sheet. So far this domain has only been identified in two types of proteins. The first class is the nm23-H7 class of nucleoside diphosphate kinase (NDK) that comprises a single copy of DM10 domain at the N-terminal and two catalytic NDK modules(Ikeda, 2010). This NDK protein is associated with the axoneme of cilia in several organisms and thought to regulate GTP recycling in cilia motility. The second class of protein containing the DM 10 domain is EFHC1 with three copies. One noticeable feature is there is more homology shared across the species within the 3 individual DM10 domains than there is within a particular organism. As mentioned above the gene is linked to JME in humans; most of the mutations discovered in JME patients are clustered within a small region from the end of the first DM10 domain to the start of the second DM10 domain(King, 2006). A large percentage of these altered residues are identical or highly conserved in other organisms based on pair-wise comparison. However, the pathological mechanism is still unclear. Recently, an EFHC1 paralogue, EFHC2 has been implicated as another susceptible locus related to JME, as well as fear recognition and harm avoidance pathologies (Gu et al., 2005). EFHC2 is widely expressed in brain tissue and the protein contains the same structural features as EFHC1, three repeat DM10

domain and EF-hand motif at the C-terminal end. Similarly to human, an EFHC1 paralogue is also identified in other organisms, like mouse, flies and *Tetrahymena*. One exception is *Xenopus. laveis*, where only one EFHC1-like gene is

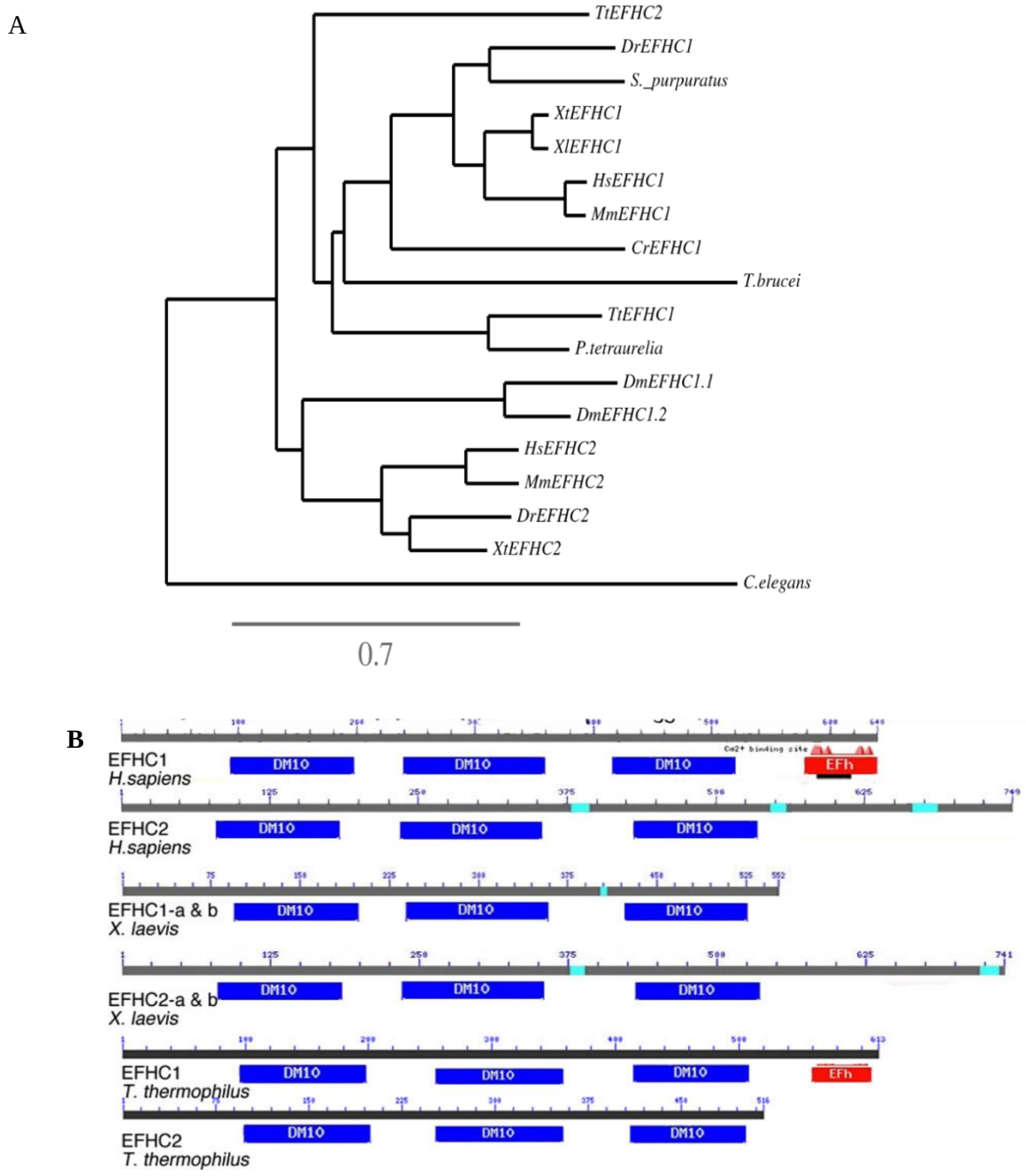

Figure1-5. Phylogenetic analysis and sequence alignment of *EFHC* family. (A) Phylogenetic tree of EFHC1 and EFHC2 protein families cross different species. Known or predicted sequences from blast to human EFHC1 were used. The tree was built by using Phylogeny.fr (Dereeper, Guignon et al. 2008)

(B) Schematic showing the protein domains and motifs within EFHC1. (C) Sequence alignment of human EFHC1, human EFHC2, *X.laveis* EFHC1(b) *Chlamydomanos* Rib72 and EFHC1-like genes identified from Tetrahymena genome. Red , blue and grey color indicates highest, moderate and lowest homology respectively. Red arrows and block boxes indicate the affected residues from EFHC1 gene mutants associated with JME patients

C

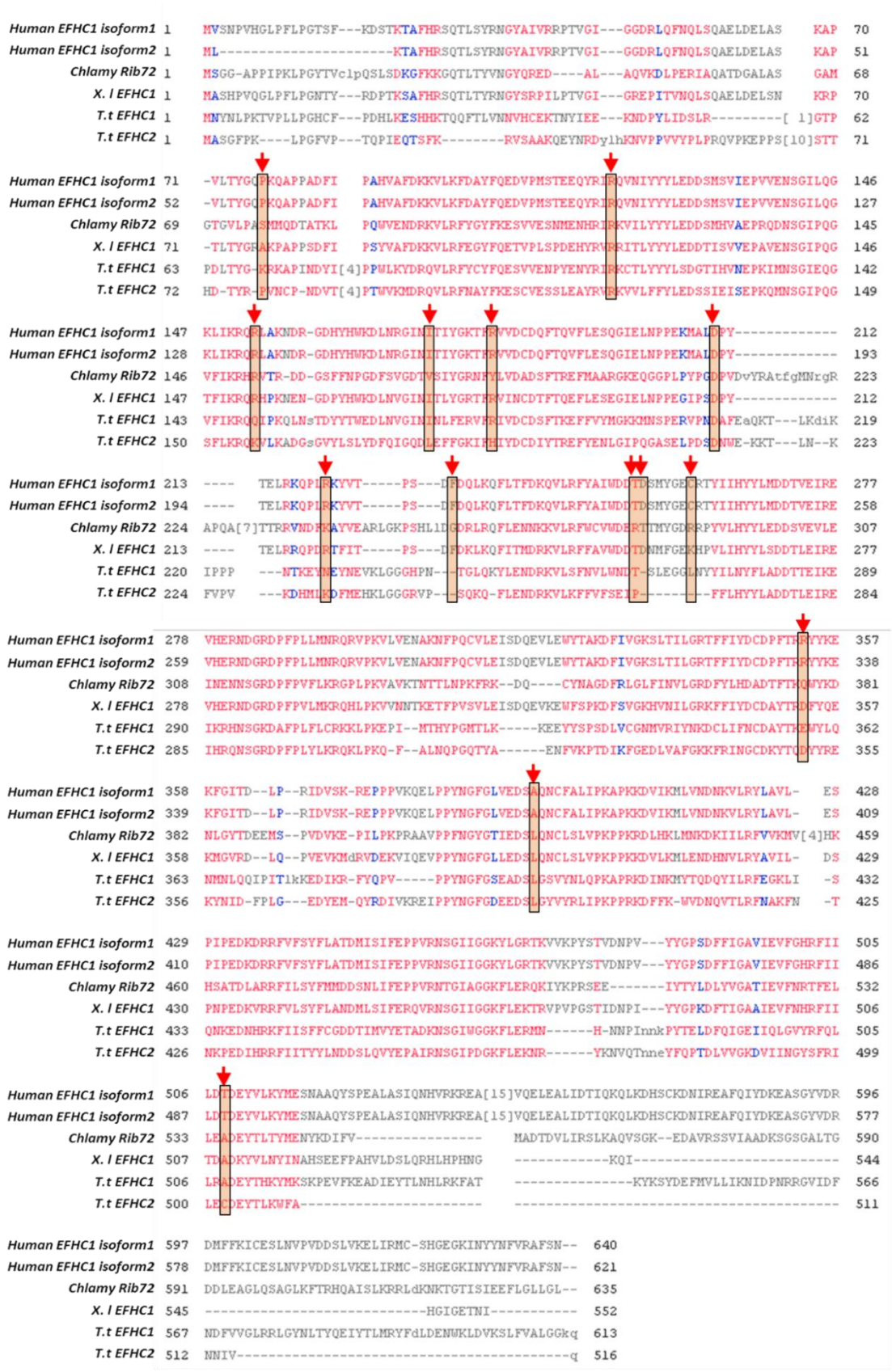
Human EFHC1 isoform1
Human EFHC1 isoform2
Chlamy Rib72
X. l EFHC1
T.t EFHC1
T.t EFHC2

found in the genome. However, recently, the updated genome of *X.laveis* showed that there are also two EFHC1-like genes by sequence. EFHC1a and EFHC1b, although it is not known whether EFHC1a is expressed.

VIII. EFHC1 function

Beyond its causal relationship with JME, strong evidence supports EFHC1 as a ciliary component. Phylogenetic analysis reveals orthologs of EFHC1 are present in many organisms containing cilia, while no relative has been recognized in the genomes of higher plants, which do not contain cilia (Fig1-5A). Moreover, northern analysis detected a vast amount of EFHC1 transcript present in multiple highly ciliated tissues in mouse and human, including testis, lung and oviduct, and brain; in addition, up-regulated EFHC1 expression was observed during ciliogenesis in mouse embryonic development(Conte et al., 2009; Ikeda et al., 2005). Immunofluorescence data further demonstrated the EFHC1 protein present in the cilia of tracheal epithelia and in the sperm flagella(Ikeda et al., 2005; Suzuki et al., 2008).

The first homolog, Rib72/EFHC1, was reported in 2003 as a structural component of flagella axenomes in *Chlamydomonas,* functioning in axoneme assembly and flagella motility(Ikeda et al., 2003). Later in 2004, a group discovered a EFHC1 gene association in JME patients(Suzuki et al., 2004). Ever since then, researchers have tried to address the following questions with a variety of model systems: What is the cellular and physiological function of EFHC1 and what is its link to the pathological mechanism of JME? Successive studies uncovered multiple unexpected functions of this protein and therefore three distinct models were proposed for onset of EFHC1 linked epilepsy disease(Ganesh, 2010). After it was first identified as an axoneme component, a study broadened EFHC1 association with microtubule-based structures to centrosomes and mitotic spindles in mammalian cells, suggesting EFHC1 is a microtubule associated protein(de Nijs et al., 2006). It was demonstrated that the N-terminal region of EFHC1 interacts with α-tubulin directly by the same group later(de Nijs et al., 2009). Based on this finding, it was not surprising to find out EFHC1 plays a role in cell cycle regulation. EFHC1 loss of

function impaired mitotic spindle organization, M phase progression and apoptosis in HEK293 cells. The observation was extended to the rat developing neocortex, indicating EFHC1 is essential for mitotic progression and cell cycle of cortex progenitors. The radial migration of projection neurons was affected during EFHC1 knockdown cortex development, probably due to failure to exit the cell cycle and mitotic proliferation. A similar analysis was carried out on EFHC1 mutants associated with JME(de Nijs et al., 2012). While the subcellular localization of these mutants is not changed, they also cause disrupted radial migration. Moreover, the EFHC1 mutants led to disrupted tangential migration of interneurons and impaired morphology of radial glia and projection neurons. A study on the *Drosophilia* homolog of EFHC1 confirmed it is a microtubule-associated protein. Elimination of *Defhc1.1* caused elevated spontaneous neurotransmitter release and overgrowth of the dendritic arbor(Rossetto et al., 2011). Treatment with an inhibitor of microtubule dynamics rescued the phenotype. Taken together these data suggested EFHC1 is a cell cycle regulator and affects neuronal migration and these roles are manifested by finely tuning the microtubule cytoskeleton dynamics. This is one proposed model for the EFHC1 role in JME(Ganesh, 2010).

A second hypothesis of EFHC1 in JME is based on its role in apoptosis. During the development of the central nervous system, programmed cell death is critical to eliminate particular subgroups of neurons at various embryonic stages(De Zio et al., 2005). Ectopic overexpression of EFHC1 in mouse hippocampal neurons induced apoptosis. Intriguingly, EFHC1 mutations significantly rescued this abnormal apoptosis(Suzuki et al., 2004). As EFHC1 contains a predicted calcium binding motif and voltage-dependent Ca^{2+} channels have been linked to other epilepsy(Murai et al., 2008), researchers tested whether the EFHC1-induced cell death is associated with any calcium channels. Indeed they found EFHC1 specifically increases R-type voltage-dependent calcium channel current. An antagonist of this $Ca_v2.3$ channel suppressed the induced apoptosis. A different in vitro study showed EFHC1 interacted with the Ca^{2+}-permeable cation channel TRPM2(Katano et al., 2012). EFHC1 enhanced the

TRAP2 channel activity and TRAP2 dependent cell death, which can be altered by EFHC1 mutations. Altogether, these observations suggested EFHC1 as a pro-apoptotic protein and a regulator of calcium channels(Ganesh, 2010). Thus EFHC1 mutations associated with JME may increase neuron density by failing to remove the unwanted neurons at right time and right places. This, together with impaired calcium homoeostasis likely induced in the patients with the disease may result in epilepsy seizures(Wallace, 2005).

The third model of EFHC1 in JME is related to its ciliary function. After the discovery of EFHC1 association with axoneme in *Chlamydomonas*(Ikeda et al., 2003), Myoclonin1/EFHC1, the murine homologue, was found to localize to the cilia in tracheal epithelia and the sperm flagella(Conte et al., 2009; Ikeda et al., 2005), suggesting EFHC1 is also involved in ciliary function in mammalian cells. There is a known connection between the brain development and the function of cilia(Ibañez-Tallon et al., 2003). In the brain, there is the epithelia-like lining of the ventricular system called ependymal, which is made up of ependymal cells. These cells are covered with a layer of long motile cilia, which help to circulate the cerebrospinal fluid around the central nervous system. Impairment of the cilia function on ependymal cells leads to a developmental abnormal hydrocephalus, which is observed in some ciliopathies. This evidence suggests a defect in ependymal cilia motility may affect neuronal development directly. Indeed, EFHC1 was demonstrated to be expressed in ependymal cells and localize to cilia(Suzuki et al., 2008). EFHC1 deficient mice were generated and carefully characterized(Suzuki et al., 2009). Although the ciliary structure was unaffected, the ciliary beating frequency was significantly decreased in the null mutants. What's more, the Efhc1 null mutant mice displayed frequent spontaneous myoclonus with reduced threshold of seizures. Taken together, this suggested the loss of function of EFHC1 impaired the ciliary function, which may be the biological basis for epilepsy.

Despite all the studies of EFHC1 described above, we still do not understand its exact cellular function and the mechanism of EFHC1 dysfunction causing JME. There are a number of questions arising

from that. For example, the three proposed functions of EFHC1 do not seem to be connected. Does it mean the protein has multiple functions in various biological process or there is cellular mechanism linking them together? If ciliary function is the underlying biological basis for JME, why are no ciliopathies observed either with JME patients or observed in the Efhc1 null mice? Is it true that Efhc1 is only associated with motile cilia? What about its role in basal bodies and primary cilia? During my thesis research, I sought to address questions about EFHC1 function by using two different model systems *Tetrahymena thermophila* and *Xenopus laveis.*

Chapter 2. Localization of four conserved basal body component proteins

I. Introduction

Basal bodies and centrioles are conserved structures (500nm in length and 250nm in diameter) that are composed of nine-fold symmetric microtubule triplets (Pearson and Winey, 2009). They are important microtubule organizing centers involved in multiple cellular functions, which include nucleating cilia at the apical surface of cells, regulating mitotic progression and determining organelle position. Impairment of basal body and centriole components has been linked to the onset of a variety of human diseases, such as cancer and ciliopathies(Ferkol and Leigh, 2012). Despite the established knowledge on the morphology of basal bodies and centrioles since early 1960s, a large percentage of individual building blocks remains unknown as it's predicted that there are approximately 200~300 molecules that made up this structure(Dutcher, 1995). Determining the composition of these structures has been a goal for decades and recently tools with the combination of genomics and proteomics analysis were applied to this field. Comparative genomics was applied with the available genomes among different organisms and the evolutionary assumption, that absence of organelles was associated with the absence of genes required for building those structures(Avidor-Reiss et al., 2004; Broadhead et al., 2006; Li et al., 2004). Specifically, for the case of basal bodies and centrioles, many genes have been predicted to participate in building the two structures by comparing the genome of organisms with or without cilia structure. An example is from Li et al, where they reported that the flagellar and basal body proteome in *Chlamydomonas* is made up of 688 genes. In contrast, the proteomic studies provide more straightforward evidence by isolating these complex structures and identifying the proteins directly by mass spectrometry(Andersen et al., 2003; Keller et al., 2005; Pazour et al., 2005). A representative among these studies came from the first centriole proteome in *Chlamydomonas*, 195 centriole proteins

were discovered by mass spectrometry using purified centrioles(Keller et al., 2005). Although these two methods are powerful in identifying novel composition in large scale, caveats still exist. False positives occur in both of the analyses. Genes involved in basal body and cilia function can be missed in genomics studies if they have roles in other cellular functions in non-cilia organisms. Contamination during isolation of basal bodies and centrioles give rise in proteomic analysis to proteins that do not actually belong to these structures. So validation is required following the initial identification of potential candidates. Beyond that, an arising question is what should we do with this long list of basal body and centriole proteins? As these successive studies assist our understanding of the molecular architecture of basal bodies and centrioles, investigation on the function of newly discovered individual components is required for gaining insights on how basal bodies and centrioles carry out their functions.

In the Winey lab, we use *Tetrahymena thermophila* to study the function and composition of basal bodies(Pearson et al., 2009; Stemm-Wolf et al., 2013; Vonderfecht et al., 2012). *Tetrahymena* is a free-living ciliated protozoan, found in freshwater worldwide(Frankel, 2000). This unicellular eukaryote exhibits nuclear dimorphism, a typical feature of ciliates. The two nuclei, the germline micronucleus and the somatic macronucleus function differently. The micronucleus is diploid and the genes of the micronucleus are transcriptionally inactive during the vegetative cell cycle(Cassidy-Hanley, 2012). The macronucleus is polyploid and the genes are actively expressed. When encountering food deficiency and starvation, *Tetrahymena* cells undergo conjugation between two different mating types. During this process, the cell pair exchanges their gamete nuclei and both the new micronucleus and macronucleus are built in the progeny. In this way, the DNA information is passed from one sexual generation to another. The boost of advanced sequencing techniques makes it plausible to use *Tetrahymena* as a model to study gene functions. Both of the nuclei have been sequenced and more than 35,000 genes have been identified in the macronucleus. The annotated genome information can be extracted from the *Tetrahymena Genome Database* (http://ciliate.org/index.php/home/welcome).

As a free swimming ciliate, *Tetrahymena* cells each possess hundreds of basal bodies and cilia (Wloga and Frankel, 2012). The basal bodies are organized into approximately 17~21 longitudinal cortical

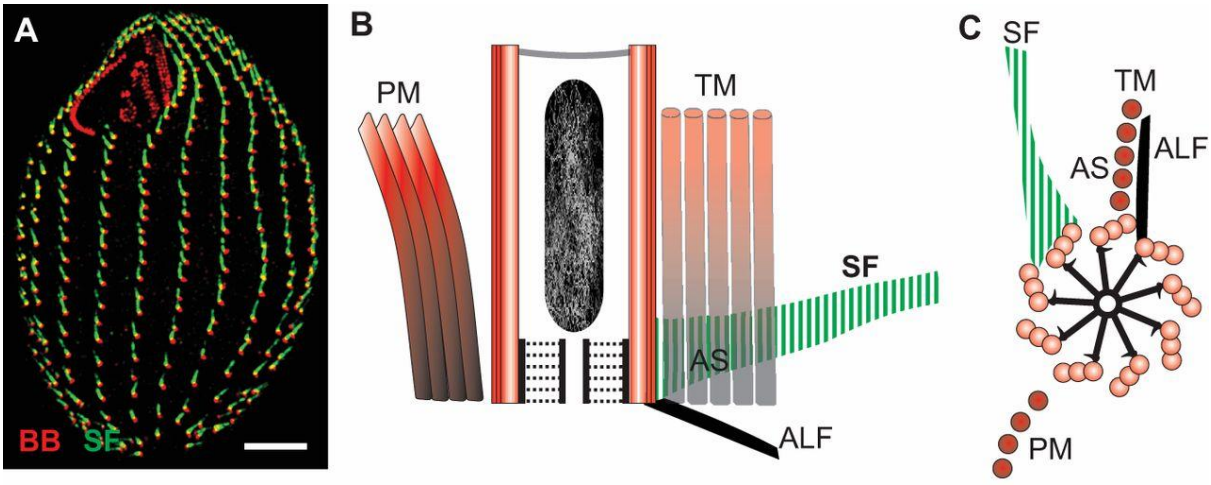

Figure2-1. *Tetrahymena* basal body organization. (A) A *Tetrahymena* cell showing basal bodies stained with centrin (red) and striated fibers (green) scale bar: 5µm. (B) longitudinal and (C) cross section schematic cartoon of a single *Tetrahymena* basal body and its associated structures. BB, basal body; PM, post-ciliary microtubules; TM, transverse microtubules; SF, striated fiber (i.e.*Tetrahymena* kinetodesmal fiber); AS, new basal body assembly site; ALF, anterior left filament. Adapted from "Choosing sides – asymmetric centriole and basal body assembly" Pearson C G. 2014

rows and also in a specialized feeding organelle termed the oral apparatus (Fig2). The later structure is composed of four strips of basal body clusters and some membranelles, accounting for nearly 150 out of ~800 total basal bodies per cell. The *Tetrahymena* basal body and cilia are conserved both morphologically and compositionally. Like in human cells, both of the organelles (basal bodies and cilia) exhibit the nine-fold symmetry of microtubule arrays. Recent genomic and proteomic analysis have identified bulk homology of the building blocks and regulators in the *Tetrahymena* genome and homologous proteins within the basal bodies and cilia structure. Together, these facts demonstrate *Tetrahymena* is an excellent organism to illustrate the function of basal body and cilia.

Additionally, advanced molecular tools and techniques make *Tetrahymena* a powerful model system(Cassidy-Hanley, 2012). The feature of homologous recombination in the *Tetrahymena* genome makes the genetic manipulation plausible. A list of the methods includes the somatic and germline knockout, epitope tagging, targeted mutations and inducible allele of any genes of interest. Moreover, *Tetrahymena* cell has a large size of approximately 30X50um, which enables the resolution of the subcellular structures by both live and fixed whole cell imaging. A careful characterization of basal body and cilia ultrastructure in *Tetrahymena* exists by electron microscopy, enabling the identification of any subtle structural defects(Giddings et al., 2010). Furthermore, phenotypic assays have been developed in *Tetrahymena*, providing a platform to study basal body assembly and maintenance as well as ciliary functions, like cilia motility and signal sensing(Hennessey and Lampert, 2012). Within the last ten years, work in the Winey lab defined a *Tetrahymena* basal body proteome of 355 proteins, in which they identified 24 novel basal body components and localized 19 of them inside basal bodies(Kilburn et al., 2007a). This validation shortened the list of new basal body proteins and made it a good start point for further studies on the functions of these individual molecules. Among the 19 proteins that shown localized to basal bodies, two criteria were used to determine which candidate was the highest priority

to study. First of all, the candidate had to be conserved and a human homologue had to exist. Secondly, it was important that orthologues had been reported as basal body or centriole proteins from other genomics or proteomics analysis in organisms other than *Tetrahymena*. Based on these criteria, 4 candidates stood out from the list of 19 proteins: BBC31, BBC52, BBC57 and BBC73.

In the Kilburn et al. study, localization of these proteins at basal bodies was determined using exogenous GFP fusions in wild-type cells, which may be affected by overexpression (Kilburn et al., 2007a). So first the basal body localization of the four proteins needed to be validated at an endogenous protein level before any further functional analysis. Moreover, since all of the four genes have homologues in human, it was worth determining whether the gene products was associated with basal body or centriole structures in human cells, which may suggest the orthologue has conserved functions across species, more specifically, from *Tetrahymena* to human. To answer these questions, in this chapter, a combination of fluorescence microscopy and gene manipulation to construct endogenous mCherry fusions were used to reveal the subcellular localization of the four candidates in *Tetrahymena* cells. GFP-fusion proteins were used in determining the localization of human homologues in U2OS cells. The results of the experiments revealed that these proteins are not only localized to basal bodies, but also are associated with other microtubule-based structures. Additionally, not all human homologues were shown to be centriole components. The data provided guidance in determining which particular protein should be chosen for my future study.

II. Material and method

Tetrahymena stains and culture conditions

Tetrahymena thermophile strain B2086 (*Tetrahymena* Stock Center, Cornell University) was used in this study as wild-type control and to generate the transgenic cell lines. All cell lines were growing in 2% SPP media (2% proteose peptone, 0.1% yeast extract, 0.2% glucose and 0.003% FeEDTA) at 30°C. For

experiments with MTT promoter, protein expression was induced with 500ng/ml $CdCl_2$ in 2% SPP media for 3hrs at 30°C. Cells were starved in 10mM Tris pH7.4.

Mammalian cell culture and transfection

Human U2Os cells were gifted from Pearson Lab. The cells were cultured in DMEM with 10% fetal bovine serum at 37 °C in incubator supplemented with 5% CO_2. EGFP fusion DNA construct was transfected into U2OS cells using Lipofectamine 2000 (Life Technologies) according to the manufacturer's instruction. Transfected cells were subjected to immune fluorescence analysis 24hr after transfection.

Plasmid construction

mCherry fusion constructs (BBC31-mcherry, BBC52-mcherry, BBC57-mcherry and BBC73-mcherry, BBC60-mCherry) were built from the vector pmCherry-LAP-NEO2 by cloning 1kb upstream sequence of desired genes to the mCherryLAP tag and 1kb downstream sequence of desired genes to the NEO2 cassette. The flanking regions were amplified by PCR from genomic DNA of B2086 with Phusion DNA polymerase. By homologous recombination, the constructs integrated into the locus of targeted genes with a C-terminus mCherry tag under the endogenous promoter and paromomycin resistance from NEO2 cassette. BBC31 null construct was made by engineering P4T21 plasmid, that NEO2 cassette was flanked by the 3' and 5' sequence of BBC31 amplified by PCR from genomic DNA. MTT inducible GFP-Bbc73 construct were made in pBS-MTT-GFP-gtw. BBC73 cDNA was amplified from DNase treated wild-type mRNA by RT reaction with SuperScriptII reverse transcriptase (Invitrogen, Grand Island, NY) and followed by PCR reaction with Phusion DNA polymerase. The coding sequence was cloned into pENTR4 Gateway Enter vector and then cloned into pBS-MTT-GFP-gtw by recombination with the LR recombinase in the Gateway clonging systems (Invitrogen). Caspl-EGFP construct was built from PEGFP-N2 plasmid by cloning the cDNA of CAPSL into it. CAPSL cDNA was amplified from Hela cell mRNA by RT reaction and then followed by PCR reaction with Phusion DNA polymerase.

***Tetrahymena* strain construction**

Constructs encoding the mCherry fusions and BBC31 deletion were transformed into the macronuclear of specific *Tetrahymena* strains by biolistic bombardment as described before. Briefly, cells were grown in 2% SPP to log phase at 2.5X10^5cells/ml, then starved for 18~24hours in 10mM Tris pH7.4. Starved cells were bombarded with linearized plasmids and recovered in 2% SPP at room temperature overnight. Desired transformants were selected by paromomycin resistance at a final concentration of 120ug/ml. For BBC31 somatic knockout strain, phenotypic assortment was carried out by increasing paromomycin concentration until cells no longer survived. The final concentration of paromomycin achieved was 120ug/ul. Constructs encodes N-terminal GFP fusions were transformed in the same way, except that the transformants were selected with cycloheximide at a final concentration of 15ug/ml.

Fluorescence microscopy

All images were acquired at room temperature using an Eclipse Ti inverted microscope (Nikon, Japan) fitted with a CFI Plan Apo VC 60× H numerical aperture 1.4 objective (Nikon, Japan) and a CoolSNAP HQ2 charge-coupled device camera (Photometrics, Tuscon, AZ). MetaMorph Imaging software (Molecular Devices, Sunnyvale, CA) was used to collect images and generate the projection images. For live cell imaging, cells were grown in SPP media with $CdCl_2$ induction, washed once with 10 mM Tris-HCl, pH 7.4, pelleted, and placed on microscope slides (VWR, Radnor, PA). For immunofluorescence, *Tetrahymena* cells were fixed either by 3%formadhyde or 70% ethanol and then placed on poly-L-lysin treated slides. Both the centrin1 antibody 20H5 and anti-mouse Alexa488 were diluted at 1:1000 in PBS+1% BSA. Human U2OS cells cultured on cover poly-L-lysin treated coverslips were fixed in -20°C methonal. Then cells were permeabilized with PBS+0.05% Triton X-100 for 5 min, followed by PBS washes and then blocked in PBS+1% BSA for 30 min at RT. ɣ-tubulin antibody was diluted at 1:1000 in PBS +1% BSA. Primary antibody incubation was done at 4°C overnight and secondary antibody incubation was 1hour at room temperature. 1ug/ml DAPI in PBS was used to stain nuclei at

room temperature for 5min. Cells were washed in PBS+ 0.1%BSA five times after each incubation. Finally, cells were mounted in Citifluor (Ted Pella, Inc., Redding, CA).

III. Results

Bbc31 localizes to accessory structures of basal bodies

Gene identification and descriptions of BBC31 were obtained from a query of the *Tetrahymena Genome Database wiki,* including Information about gene sequence, protein sequence and domains in the gene product. The *Tetrahymena* ID for this gene is TTHERM_00161270 and two features were predicted in the protein. One is DUF1024, a domain of unknown function. The second is a possible calponin homology (CH) domain at the N-terminal end, widely present in cytoskeleton and signaling transduction proteins (Korenbaum and Rivero, 2002)(Table2-1). The putative protein sequence was used in BLASTp search against a human database to identify the human homologue. The top hit from this search was sperm flagellar protein1 (Spef1), also called c20orf28 or CLAMP, displaying 34% identity and 55% similarity to Bbc31. 227 total residues were aligned with only 21 gaps in the whole alignment. Moreover, Spef1 also contains predicted DUF1024 and CH domains near its amino-terminus. Additionally, by searching through previous reported basal body and cilium proteome, this gene was found as a basal body or cilia component in other eukaryotes, like *Trypanosome* and *Chlamydomonas* (Table2-1). A mouse orthologue was demonstrated to be present in mouse sperm flagellar using a specific antibody(Chan et al., 2005).

Previously, overexpressed GFP-Bbc31 fusion has been shown to localize to basal bodies in *Tetrahymena* cells(Kilburn et al., 2007a). Since no antibody is available for Bbc31, an endogenous C-terminal mCherry fusion was made in this study to confirm its localization pattern. The mCherry tag was inserted right before the stop codon of BBC31 gene, so the intact fusion was expressed under the endogenous promoter of BBC31. Live cell imaging indicated that Bbc31-mCherry localized to the basal

	Domain	Human ortholog	Proteome and genomic study on Cilia/centrosome/basal body
Bbc31	DUF1042 CH	sperm flagellar 1 (SPEF1) or CLAMP	*Trypanosoma, Chlamydomonas, Tetrahymena*
Bbc52	EF hand	calcyphosin-like protein (CAPSL) C15orf26 protein	*Trypanosoma, Chlamydomonas, Tetrahymena*
Bbc57	EF hand	calcyphosin-like protein (CAPSL) C15orf26 protein	*Trypanosoma, Chlamydomonas, Tetrahymena*
Bbc73	EF hand DM10	EF-hand domain-containing protein 1 isoform 1 (EFHC1)	*Trypanosoma, Chlamydomonas, Tetrahymena*

Table 2-1. The four BBC protein candidates are conserved. The chart showing their conserved domains, human orthologs and homologs identified in other species(Broadhead et al., 2006; Kilburn et al., 2007a; Li et al., 2004).

body, as well as other structures in *Tetrahymena* cells. Specifically, there are two populations of Bbc31 clustered at or around the basal bodies in cortical rows. Signal of Bbc31 was also found at the deep fiber of oral apparatus and contractile vacuole pores (Fig2-1A). The former structure is a mixture of microtubular filamentous network, while the latter one is an organelle decorated strongly with antibodies to γ-tubulin and tubulin post-translational modifications. To dissect the precise localization pattern of Bbc31 along the cortical row basal bodies, Bbc31-mCherry was immuno-analyzed with two basal body markers separately. Sas6a and Cen1 are basal body components, whose localization within basal bodies is well established (Culver et al., 2009; Vonderfecht et al., 2012).Sas6a is restricted to the proximal end of microtubule wall, while Cen1 has a broader distribution inside the core structure of basal body and the site of new basal body assembly. *Tetrahymena* cells expressing Bbc31-mCherry were fixed and stained with Sas6a and Cen1 antibodies generated previously. With basal bodies labeled by Sas6a and Cen1, it is clear that Bbc31-mCherry is not associated with the microtubular core structure; instead, it is present at two accessory structures, postciliary microtubule and transverse microtubule (Fig2-1B). Signal was absent from the oral primordium, in which the developing basal bodies lack the

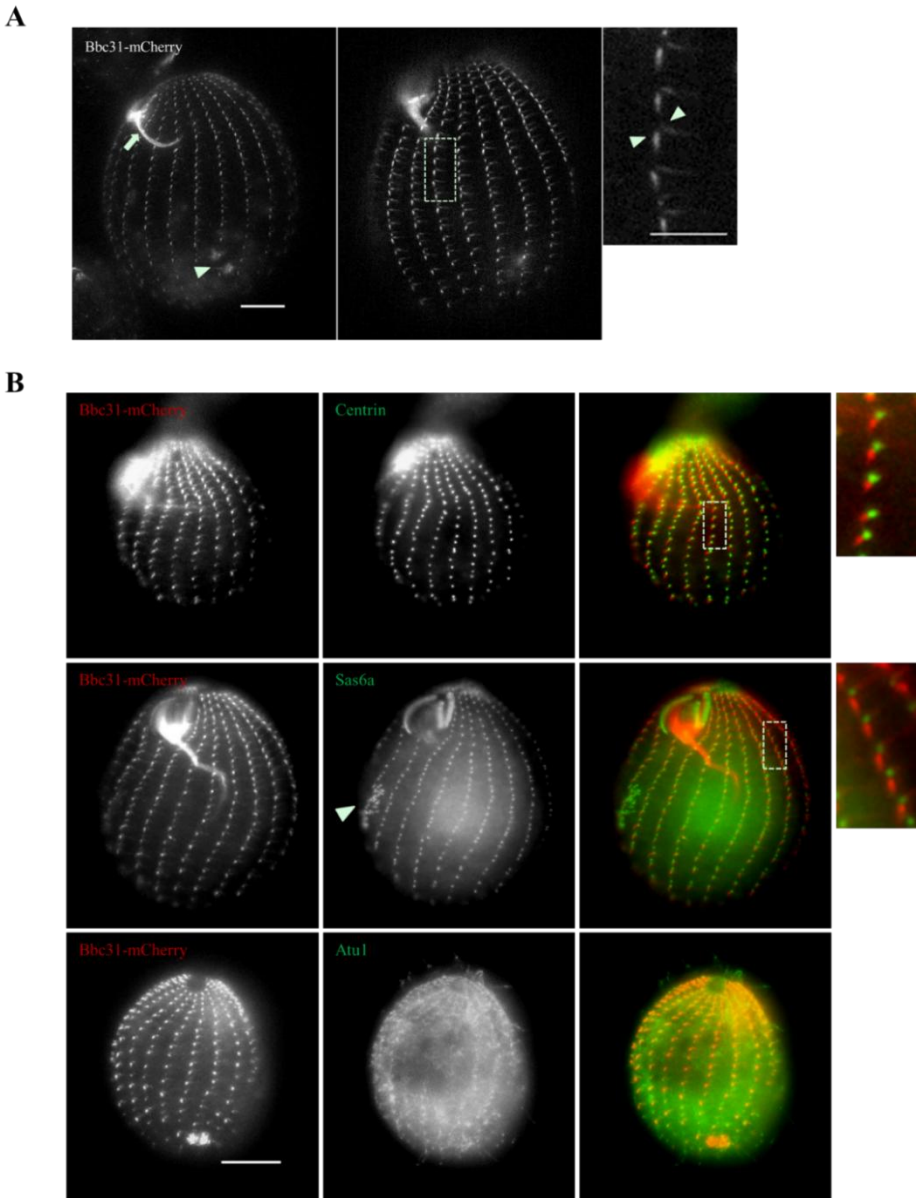

Figure2-2. Bbc31 is associated with the accessory structures of basal bodies. (A) Bbc31-mCherry localizes to microtubule-based structures. Live cell image of Bbc31-mCherry expressing cells. mCherry fluorescence was seen at microtubule based structures. Left panel: the arrow indicates the deep fiber at the oral apparatus and the arrow head shows the pair of contractile vacuole pores. Right panel: a second Bbc31-mCherry expressing cell with the arrowhead in the insert showing the post ciliary microtubule and transverse microtubule. (B) Bbc31 does not co-localize with Cen1 and Sas6a. Fixed Bbc31-mCherry (red) expressing cells were labeled with antibodies to Cen1, Sas6a and Atu1 (green). Cen1 and Sas6a are basal body components and Atu1 is associated with not only basal bodies, but also cilia and other microtubule structures. Bbc31-mCherry fluorescence signal did not overlap with Cen1 and Sas6a. Arrowhead labels the developing oral primordium. No Bbc31 was found there. Scale bar: 10µm

accessory structure. Postciliary microtubule originates posterior to the basal body and extends toward the posterior of the cell(Wloga and Frankel, 2012). Transverse microtubule arises anterior to the basal body and continues horizontally toward the left side basal body cortical row. The assembly and regulation of these cortical microtubule arrays remain obscure, but they are thought to function in basal body stability and orientation. Localization of Bbc31-mCherry (post ciliary microtubule, transverse microtubule and contractile vacuole pores) suggested it is a microtubule-associated protein and it may play a role in microtubule stability and ensuring basal body orientation.

To better understand the function of Bbc31, a somatic knockout strain was generated and characterized. *bbc31* null cells had the BBC31 gene replaced at *BBC31* locus by NEO2 cassette that conferred resistance to paramomycin. Phenotypic assortment was carried out by constantly increasing the drug concentration to increase the loss of wild-type BBC31 copies in macronucleus. The resulting strain was viable, but grew slower than wild-type cells. Cells were fixed and immunostained with Cen1 antibody to visualize the basal bodies. Loss of Bbc31 resulted in disrupted cortical basal body rows compared with the well- aligned ones in wild-type cells (Fig2-3). Evidence of basal bodies clusters diverged from cortical rows was observed in bbc31 null cells. Taken together, this data suggested Bbc31 is required for basal body orientation.

Bbc52 and Bbc57 localize to both basal bodies and cilia

Bbc52 (TTHERM_00219350) and Bbc57 (TTHERM_00155380) were found in the *Tetrahymena* basal body proteome(Kilburn et al., 2007a). Fluorescence localization data demonstrated the overexpressed GFP fusions were associated with both basal bodies and cilia. Both of the proteins have been identified in *Chlamydomonas* cilia and centriole proteomes, and comparative genomics indicated they are basal body and cilia proteins in *Trypanosome*(Broadhead et al., 2006; Li et al., 2004). The two proteins share 34% identity and 58% similarity with 4% gap based on alignment of 490 amino acids, which is 98% coverage of the total length of the proteins. Moreover, they have similar expression profile

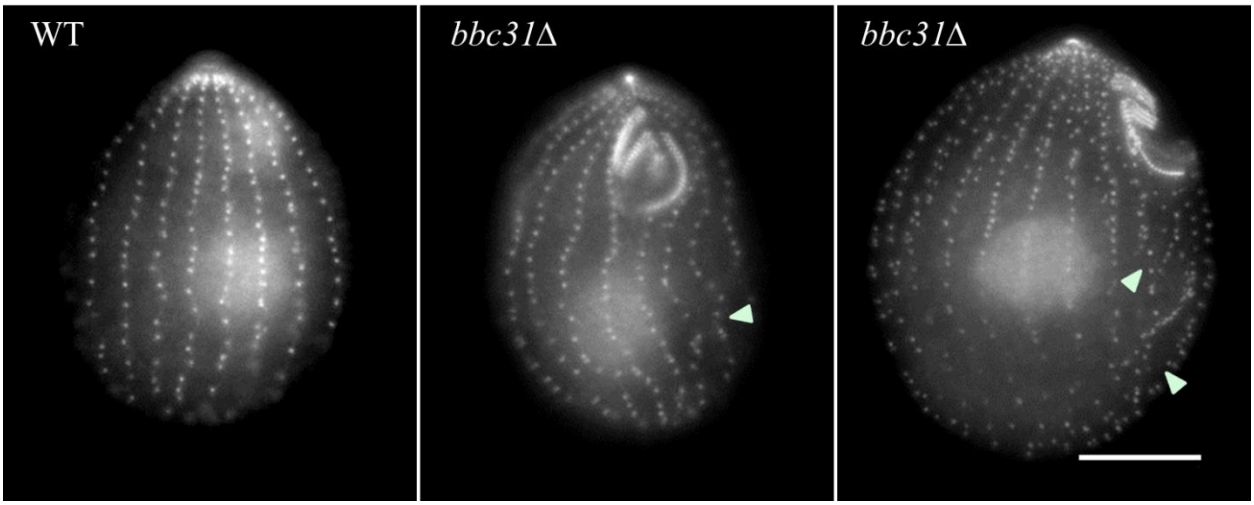

Figure2-3. Bbc31 is required for maintaining the cortical row alignment. Immuno-fluorescent micrographs of fixed cells labeled with antibody to Cen1. The arrowhead shows examples of disrupted cortical rows of basal bodies in *bbc31* null cells. Scale bar: 10µm.

during the cell cycle (*Tetrahymena Genome Database*). A structural feature, EF hand motif, was predicted near the C-terminal end of both proteins (Table2-1). The EF hand motif is a Ca^{2+} binding domain found in many proteins associated with basal bodies and cilia(Vonderfecht et al., 2012). A good example is centrin, a small basal body protein with four EF hand motifs. By searching through the human database of non-redundant protein sequences, two human proteins were identified as orthologues of Bbc52 and Bbc57. They are CAPSL (calcyphosine-like protein) and C15orf26, the functions of which are poorly understood. C15orf26 aligned well with the N-terminal half of Bbc52 and Bbc57, displaying approximately 31% identity and 50% similarity. In contrast, CAPSL showed high homology to the C-terminal half of Bbc52 and Bbc57 with nearly 30% identity and 47% similarity. A reciprocal blast against *Tetrahymena* database was carried out. The top two hits against C15orf26 are Bbc52 and Bbc57, while for CAPSL Bbc52 and Bbc57 are still ranked as top hits but not with the highest scores.

Transgenic *Tetrahymena* strains expressing Bbc52-mCherry and Bbc57-mCherry chimera were generated in order to determine where these proteins are localized. These fusions were constitutively expressed under the endogenous promoters of BBC52 and BBC57. Live cell imaging revealed the two proteins have a similar localization pattern: both of them are associated with basal bodies and cilia. The fluorescence signal was present in all three populations of basal bodies, including basal bodies at cortical rows, oral apparatus and oral primordium (Fig2-4A, Fig2-5A). To confirm this result, BBC52-mCherry and BBBC57-mCherry were transformed into strains expressing GFP-Cen1 and GFP-Sas6a. Unlike Bbc31-mCherry, the resulting cells have Bbc52 and Bbc57 signal overlapped with GFP-Cen1 and GFP-Sas6a at basal bodies (Fig2-4B, Fig2-5B), indicating the two proteins are components of the basal body core structure. In *Tetrahymena*, new basal body assembly happens at the proximal end of existing ones. During maturation, the daughter migrates anterior to the mother and stay along the cortical rows. Once matured, the basal body can form a cilium from its distal end. The mother and daughter can be

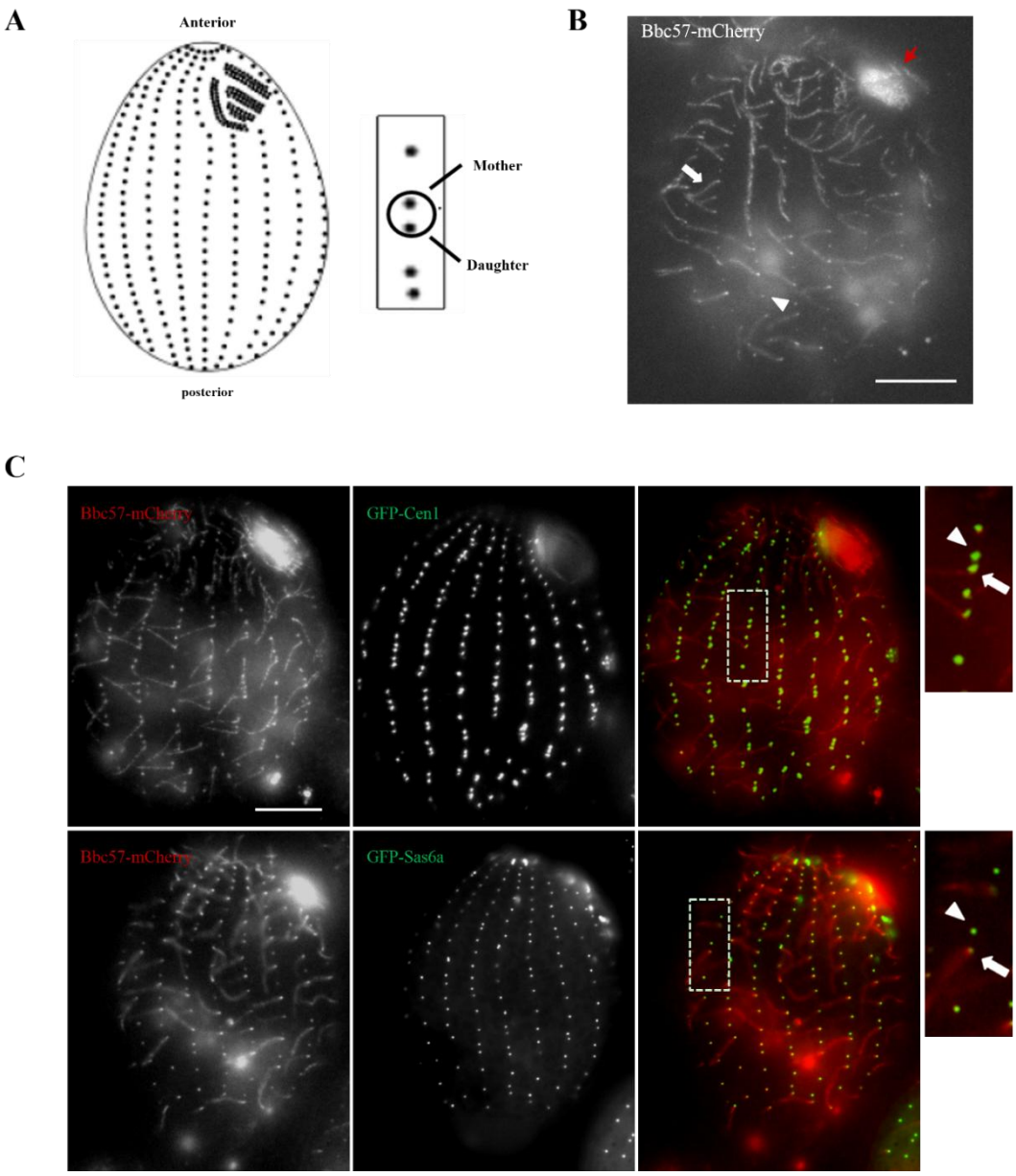

Figure2-4. Bbc57 localizes to both basal bodies and cilia. (A) Schematic of basal body cortical organization in a *Tetrahymena* cell. Daughter basal bodies assembles anterior to the mother basal bodies. (B) Bbc57-mCherry localizes to both basal bodies and cilia. Live cell image of Bbc57-mCherry expressing cells. mCherry fluorescence was seen at basal bodies and cilia at the cortical rows and oral apparatus. White arrow indicates the mCherry signal at a cilium and white arrowhead points to a basal body labeled with mCherry. Red arrow shows the oral apparatus. (C) Bbc57 co-localizes with Cen1 and Sas6a. Live cell images showing mCherry tagged Bbc57 with GFP tagged basal body markers. Expression of GFP fusion was induced with 300ng/ml Cd^{2+} for 3hrs. Upper panel: cells expressing Bbc52-mCherry and GFP-centrin1. Lower panel: cells expressing Bbc57-mCherry and GFP-Sas6a. Arrowheads point to the posterior mother basal bodies with cilia. Arrows point to the anterior daughter basal bodies. Scale bar: 10μm.

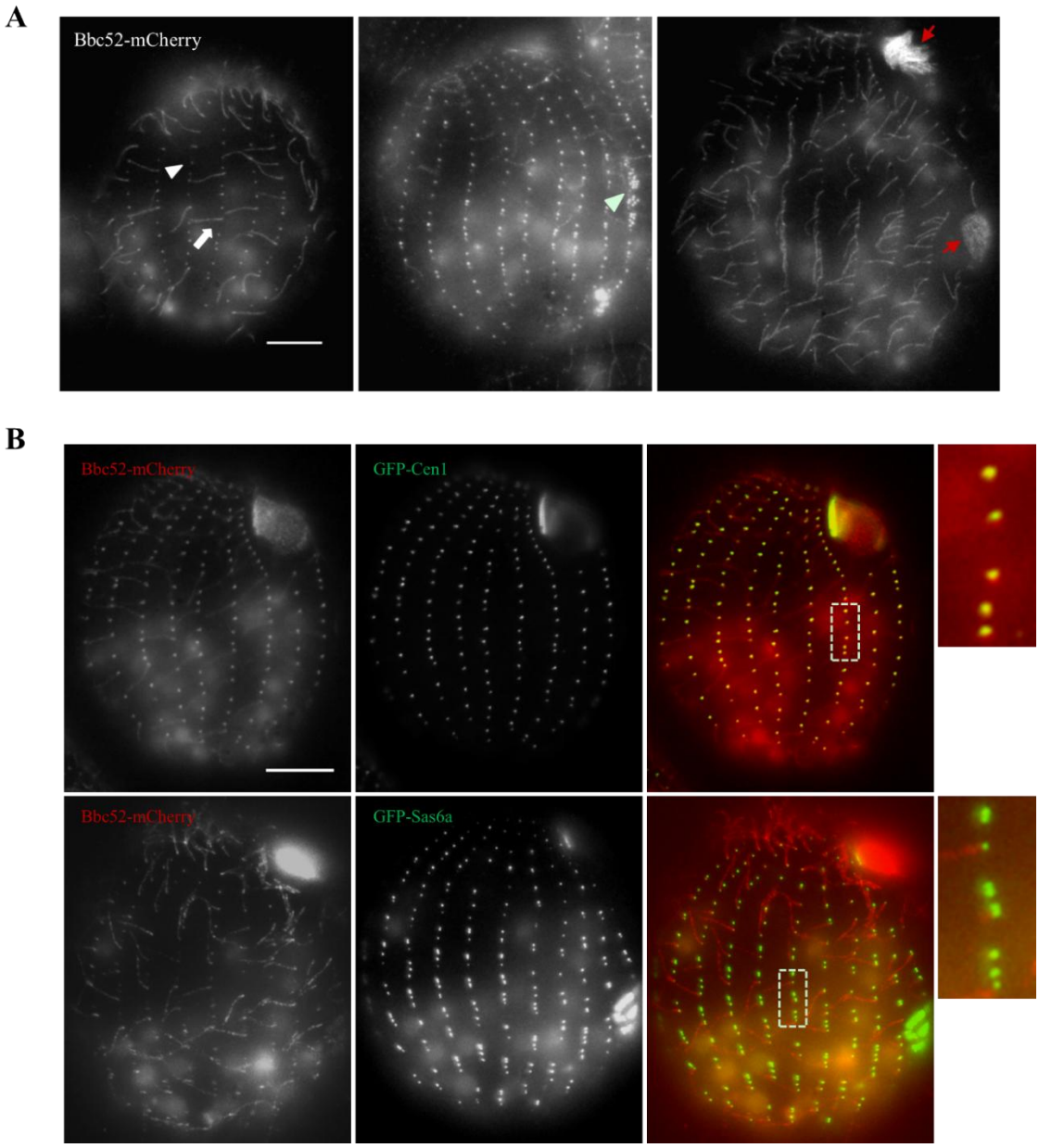

Figure2-5. Bbc52 is associated with both basal bodies and cilia. (A) Bbc52-mCherry localizes to both basal bodies and cilia. Live cell image of Bbc52-mCherry expressing cells. mCherry fluorescence was seen at basal bodies and cilia at the cortical rows and oral apparatus. Left panel: a non-dividing cell; white arrow points to a cilium and white arrowhead points to a basal body. Middle panel: a dividing cell with the arrowhead labels developing primordium. Where no cilia formed from the basal bodies yet. Right panel: a dividing cell with the red arrow label the mature and the newly formed apparatus, both of which have cilia developed already. (B) Bbc52 co-localizes with Cen1 and Sas6a. Live cell images showing mCherry tagged Bbc52 with GFP tagged basal body markers. Expression of GFP fusion was induced with 500ng/ml Cd2+ for 3hrs. Upper panel: cells expressing Bbc52-mCherry and GFP-centrin1. Lower panel: cells expressing Bbc52-mCherry and GFP-Sas6a. Scale bar: 10μm.

recognized as a basal body pair close to each other. Sas6a is required in this process to form the initial assembly platform, the cartwheel(Culver et al., 2009). Exploring the colocalization data with Sas6a in more detail, Bbc52-mCherry and Bbc57-mCherry signal were found enriched at the mother basal bodies compared to the daughters, which was the opposite of the Sas6a signal (Fig2-4B, Fig2-5B). This observation suggested the Bbc57 has different protein dynamics at the basal bodies and it is more likely to function in basal body maintenance and later stage of ciliogenosis.

Human Bbc52 is not a centrosome component

Since there is no literature available describing whether the human homologue of Bbc52 and Bbc57 are basal body or ciliary proteins, I studied the localization of them in human tissue culture cells. In the absence of an antibody for CAPSL (human Bbc52), a Capsl-EGFP construct was made and transiently transfected into U2OS cells. Cells were fixed and probed with antibody against γ-tubulin and DAPI to visualize the centrosome and nuclei respectively. Different from γ-tubulin, accumulated at the centrosome, Capsl-EGFP was diffuse in the cytoplasm, indicating this protein is not centriole specific in human cells (Fig2-6). Although some nuclei signal was observed, the amount was comparable to the empty vector EGFP-alone, indicating this nuclei localization was non-specific and might be due to overexpression.

Identification of Bbc73 homologs in human and *Tetrahymena*

Bbc73 (TTHERM_00143690) was reported to localize to both basal bodies and cilia(Kilburn et al., 2007a). The gene call from Tetrahymena Genome Database Wiki describes Bbc73 as a microtubule protofilament ribbon protein containing two predicted structural domains. One is three tandem repeats of DM10 domains (a domain of unknown function). The second is a EF hand motif that resides at the C-terminal end of the protein. Both of the domains have been discovered in proteins associated with basal bodies and cilia(King, 2006). Bbc73 is conserved in a wide range of model organisms and homologues were reported in cilia and centriole proteomes in *Chlamydomonas*(Keller et al., 2005; Li et al., 2004). In

mouse, this protein was present in cilia in tracheal epithelia and the sperm flagella(Ikeda et al., 2005). By searching against the human genome with Bbc73 sequence, two human homologues were identified:

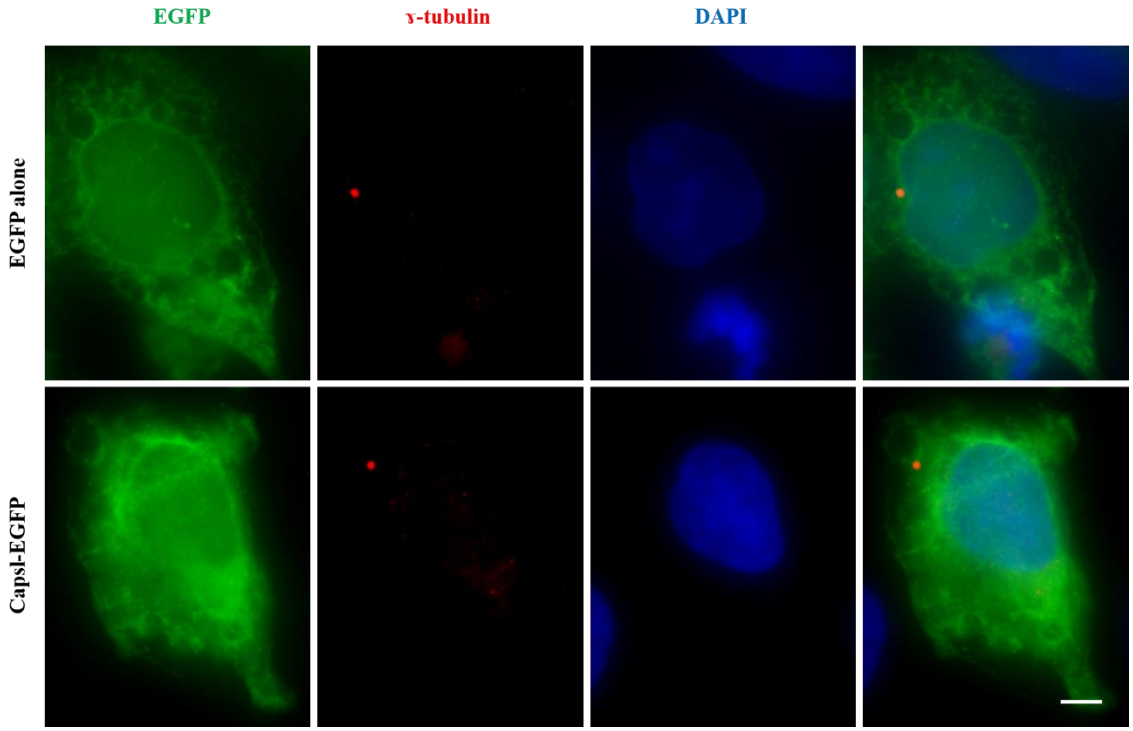

Figure2-6. Capsl does not localizes to the centrosome. Immuno-fluorescence analysis of U2OS cells transiently transfected with EGFP alone or Capsl-EGFP plasmid. Cells were fixed and stained with antibody against centrosome marker r-tubulin and DAPI for DNA. Scale bar: 5μm.

EFHC1 (EF hand domain containing1) and EFHC2 (EF hand domain containing2). Bbc73 sequence shares 35% identity and 55% similarity with EFHC1 for 86% query cover and 32% identity and 48%similarity with EFHC2 for 98% query cover (Fig1-7). EFHC1 and EFHC2 were thought to be orthologous in human and both genes were linked to human diseases(Blaya et al., 2009; Gu et al., 2005; Suzuki et al., 2004, 2006). EFHC1 is made up of 640 amino acids while EFHC2 has 749 residues. 36% sequences of EFHC1 and EFHC2 are the same and 52% are similar. Similar to Bbc73, EFHC1 has a predicted EF hand motif at the C terminal end of the protein; that is missing in EFHC2. Mutations of EFHC1 and EFHC2 are associated with JME and mutations in EFHC2 alone are linked to pathologies of fear recognition and harm avoidance. EFHC1 was previously demonstrated to associated with centrosome and mitotic spindle during cell cycle in Hela cells(de Nijs et al., 2009) and *Chlamydomonas* homologue was found as a cilia ribbon component(Ikeda et al., 2003). In contrast, no literature is available on EFHC2 subcellular localization. As there are two Bbc73-like genes in the human genome, it was of interest to check whether a second gene also exists in *Tetrahymena*. Not surprisingly, searching using the Bbc73 sequence, as well as reciprocal blasts by EFHC1 and EFHC2 against *Tetrahymena* protein database all resulted in identifying TTHERM_00584850 as the top hit. Moreover, data from *Tetrahymena* Gene Network suggested BBC73 and TTHERM_0058 have a similar expression profile (Fig2-8A). The protein product of TTHERM_00584850 has the common feature of three DM10 domains of this family but lacking the EF hand motif, similar to EFHC2 (Fig2-8A). Intriguingly, this protein was not reported in *Tetrahymena* basal body proteome(Kilburn et al., 2007).

Bbc73 is associated with both basal bodies and cilia

A mCherry fusion to Bbc73 and TTHERM_00584850 was generated and transformed into wild-type *Tetrahymena* cells to determine the subcellular localization of these proteins. Consistent with the previous study, Bbc73-mCherry localized to both basal bodies and cilia. The signal was found at basal

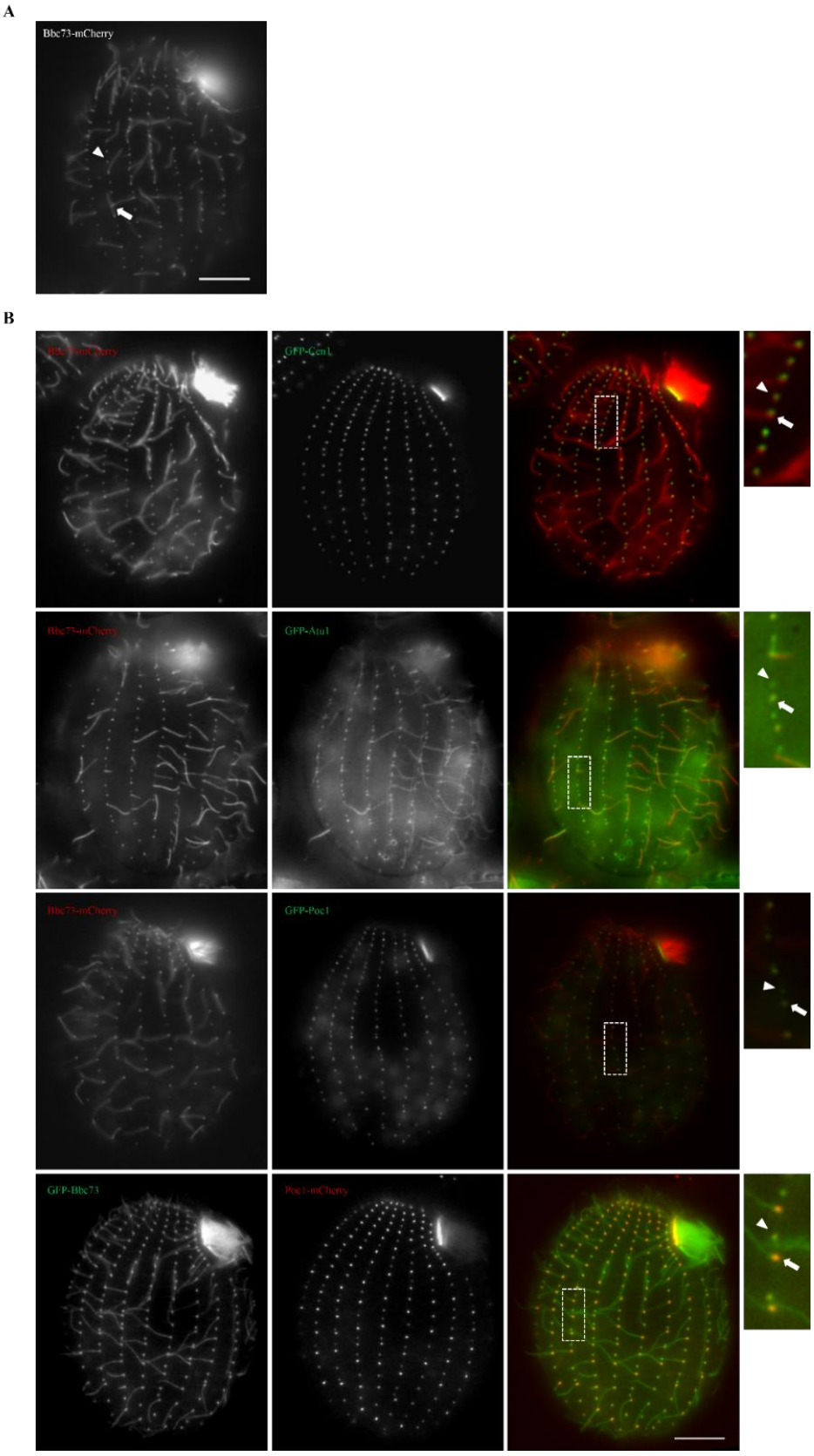
A
Bbc73-mCherry
B
GFP-Cen1
GFP-Atu1
GFP-Poc1
GFP-Bbc73
Poc1-mCherry

Figure2-7. Bbc73 is associated with both basal bodies and cilia. (A) Bbc73-mCherry localizes to both basal bodies and cilia. Live cell image of Bbc73-mCherry expressing cells. Arrow pointing the cilium and the arrowhead pointing the basal body. (B) Bbc73 co-localizes with Cen1, Atu1 and Poc1 at basal bodies and cilia respectively. Live cell images showing mCherry tagged Bbc73 with GFP tagged basal body markers. Expression of GFP fusion was induced with 500ng/ml Cd2+ for 3hrs. First panel: cells expressing Bbc73-mCherry and GFP-centrin1. Second panel: cells expressing Bbc72-mCherry and GFP-Atu1. Third panel: Cells expressing Bbc72-mCherry and GFP-Poc1. Last panel: cells expressing GFP-Bbc73 and Poc1-mCherry. Arrowheads point to the posterior mother basal bodies with cilia. Arrows point to the anterior daughter basal bodies. Scale bar: 10μm.

bodies in cortical rows and in the oral apparatus (Fig2-7A). A novel discovery is that this protein was also enriched at contractile vacuole pores. To confirm this result, Bbc73-mCherry was co-expressed with GFP-Poc1, GFP-Cen1 and GFP-a-tubulin respectively. Poc1 and Cen1 are known basal body markers and a-tubulin labels both basal bodies and cilia. Bbc73-mCherry partially overlapped with GFP-Cen1 as the mCherry signal was posterior to GFP-Cen1. Previously, Cen1 has been described as present not only at the basal body microtubule cylinder, but also at the site of new basal body assembly, which is anterior to the mother basal body(Vonderfecht et al., 2012). This data suggested localization of Bbc73 is restricted to the basal body core structure and it may not function in basal body assembly. In contrast, Bbc73-mCherry fully overlapped with GFP-Poc1 at the basal bodies. However within mother and daughter pairs, more mCherry signal was found at the mother basal body (Fig2-7B). Poc1 is not associated with the site of new basal body assembly and protein dynamics assay revealed it is stably associated with the mature mother basal body(Pearson et al., 2009). Here, GFP-Poc1 was equally distributed to the mother and daughter pair probably due to an over expression effect. So, transgenic *Tetrahymena* strain expression of endogenous Poc1-mCherry and exogenous GFP-Bbc73 was generated. Now the weaker Poc1 signal at daughter basal bodies were observed. Induced GFP-Bbc73 was still localized to both basal bodies and cilia. However, the predominate Bbc73 signal at the mother was diminished, probably due to the artificial effect of over expression. Bbc73 cilia signal is co-localized with α-tubulin at cilia (Fig2-7B).

Bbc60 is also a basal body and cilia component

To study the function of the paralog of EFHC1 (Bbc60) in *Tetrahymena*, I first determine the localization of protein. Using the same strategy, endogenous TTHERM_00584850 was engineered with a C-terminal mCherry tag. Live cell imaging on this transgenic *Tetrahymena* cells indicated TTHERM_00584850 was similar to Bbc73, associated with both basal bodies and cilia (Fig2-8B). To compare localization pattern of the two proteins more carefully, GFP-Bbc73 and TTHERM_00584850-

mCherry were co-expressed and examined in *Tetrahymena* cells (Fig2-8C). Both of the tagged proteins were found present in individual basal bodies and cilia. Taken together, these data demonstrated Bbc73 was a basal body and cilia component and also enriched in contract vacuole pores. A second BBC73 ortholog, *TTHERM_00584850* was identified in *Tetrahymena* genome. As with Bbc73, this protein is also associated with microtubule based structures including basal bodies and cilia. Bbc73 and TTHERM_00584850 may function together and redundantly in basal body and cilium assembly and regulation. I have renamed *TTHERM_00584850* as *BBC60* following the rule in the *Tetrahymena* basal body proteome study, where BBC stands for basal body component and 60 is the molecular weight of its protein product.

IV. Discussion

The previous report of localization of the four basal body components considered here relied on overexpressed GFP fusions (Kilburn et al., 2007b). This may lead to artifacts not representing the true localization pattern at endogenous protein level. In this study, mCherry fusions under endogenous promoter were used to reanalyze the precise localization of these proteins with other basal body markers. Not surprisingly, despite some overlap in the localization patterns with the two methods, there were some new discoveries in my work.

BBC31

Bbc31 was described to localize approximately to basal bodies(Kilburn et al., 2007a). However, the data obtained from endogenous Bbc31-mCherry revealed its association with basal bodies, deep fiber and contractile vacuole pores (Fig2-2A). More specifically, even within the basal body, Bbc31 is not present at the core structure mainly made of microtubule wall; instead, the protein sits in accessory structures of transverse microtubule and postciliary microtubule. This localization pattern was confirmed by a lack of colocalization with Sas6a and Cen1 (Fig2-2B). The broader distribution of

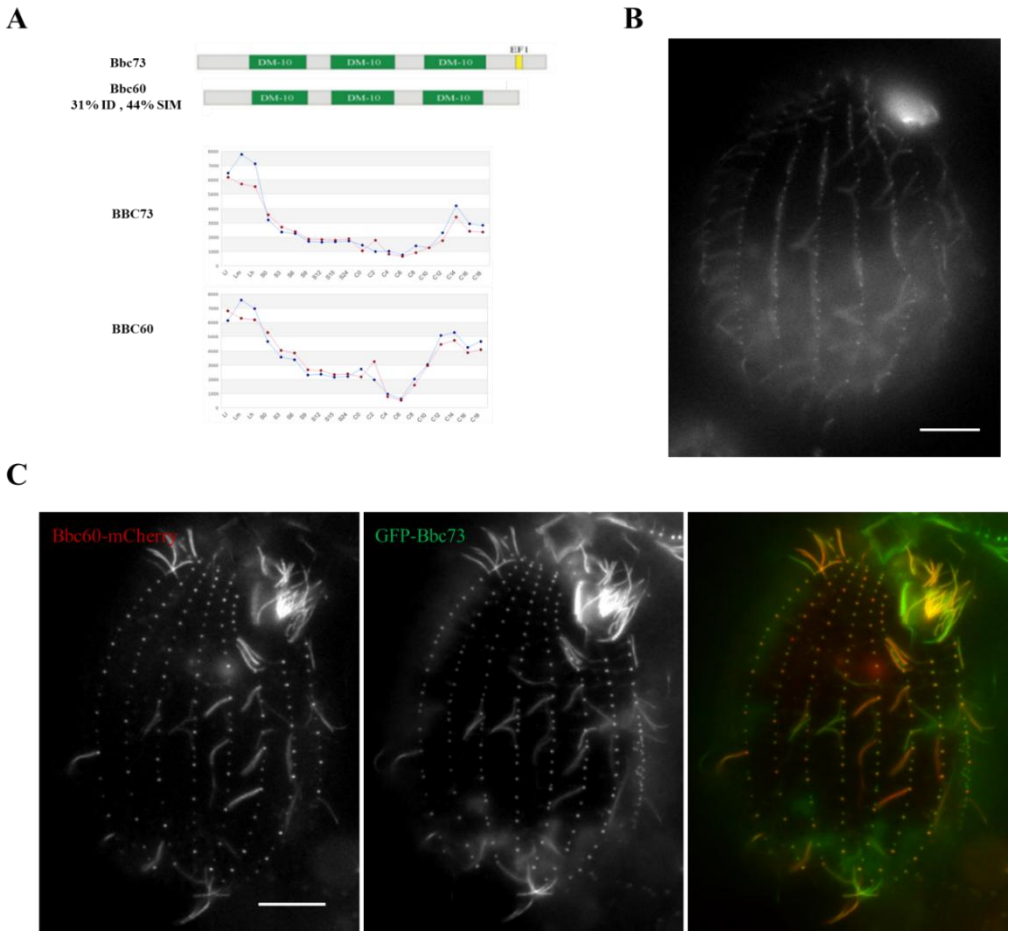

Figure2-8. Bbc60, the homolog of Bbc73, exhibits the similar localization pattern to Bbc73 in *Tetrahymena*. (A) Comparison of Bbc73 and Bbc60. The schematic showing the alignment of protein domains and the identity and similarity of sequence alignment. The charts are the expression profile of BBC73 and BBC60 during different stages of the cell cycle. Adapted from *Tetrahymena Genome Database*. (B) Bbc60-mCherry localizes to both basal bodies and cilia. Live cell image of Bbc60-mCherry expressing cell. (C) Bbc60 co-localizes with Bbc73. Live cell images showing mCherry tagged Bbc60 with GFP tagged Bbc73. Expression of GFP-Bbc73 was induced with 500ng/ml Cd^{2+} for 3hrs.

Bbc31 suggested it may be a microtubule interacting protein. This idea is supported by the presence of CH domain similar to EB protein family(Dougherty et al., 2005). Additionally, a study demonstrated mouse CLAMP, the mammalian homolog of Bbc31, localized to the well- organized microtubule bundles inside pillar cells, showing this aspect of Bbc31 is conserved in mammals. A somatic knockout strain was made to study the function of Bbc31. Bbc31 null cells displayed short basal body strings arising from existing longitudinal cortical rows, indicating Bbc31 may function in stabilizing general cortical row organization and orientating individual basal bodies (Fig2-3). Researchers found Myc-CLAMP in Cos-7 cells induced microtubule bundling and stabilized microtubule against depolymerization(Dougherty et al., 2005).Considering both basal bodies and cilia are built on stable microtubule bundles, with my preliminary data and other study, it would be worthwhile to build a complete knockout (both micronucleus and macronuleus) to study the role of Bbc31 in basal body and cilia function more carefully.

BBC52 and BBC57

Bbc52 and Bbc57 are *Tetrahymena* paralogs based on their sequence alignment, predicted structure domain and expression profiles during cell cycle. In this study, I found they shared the same localization pattern and were associated with both basal bodies and cilia. mCherry fusion signal was present in basal body populations of cortical rows, oral apparatus and oral primordium. Distinguished from Bbc31-mCherry, co-localization with Sas6a and Cen1 indicated the two proteins reside within basal body core structure. Moreover, Bbc52-mCherry and Bbc57-mCherry localized preferentially in the mother basal bodies. This asymmetry between the mother and daughter basal body is not uncommon and is believed coincident with functions in basal body maturation and cilia formation. Researchers had shown that Cep164 was enriched at the mother centriole and was required for the initiation of early ciliogenesis(Schmidt et al., 2012). The asymmetric localization between mother and daughter along with the ciliary association suggests that Bbc52 and Bbc57 are recruited to the basal body at late stage during

assembly and may play a role in ciliogensis. This idea was further supported by the immuno-EM data in Kilburn et al study. Using overexpressed GFP-Bbc52, the protein was revealed predominant localized to the transition zone, which is a critical compartment for cilia formation(Kilburn et al., 2007a). To further illustrate this finding, in a future study, it would be worth repeating the immuno-EM analysis with the endogenous mCherry fusion and generating knockout strains to examine whether loss of function of the proteins results in any ciliogenesis defects. Based on the blast searching, Bbc52 and Bbc57 seem to be homologues of both CAPSL and C15orf26. CAPSL has been linked to type I diabetes disease, although the underlying mechanism remains unknown(Santiago et al., 2008). So far, no functional study of Capsl is available other than the sequencing analysis in patients. My data demonstrated Capsl was not enriched in centrioles, instead, it localized to the entire cytoplasm. However, it will be interesting to study if the protein is associated with a subset of cytoskeleton and whether its localization is dynamic during cell cycle. Pursuing with this direction may contribute to understand how mutations in CAPSL cause type I diabetes. Similar to CASPL, C15orf26 was identified in a locus associated with Primary ciliary dyskinesia in a sequencing study (Geremek et al., 2008). Recently, a study described that knockdown of C15orf26 in *Zebrafish* leads to a ciliopathy-like phenotype with defective cilia structure and impaired cilia motility(Austin-Tse et al., 2013). However, the authors did not report the underlying basis of the defect. Further study of *Tetrahymena* Bbc52 and Bbc57 may provide unique perspectives on the function of this gene family and shed light on the foundation of that human disease.

BBC73 and BBC60

In this study, Bbc73-mcherry was used to understand the localization of this protein. Consistent with previous work, Bbc73 localizes in both basal bodies and cilia(Kilburn et al., 2007a). Co-expression of GFP-Poc1, GFP-Cen1 and GFP-a-tubulin confirmed this result. Additionally, the protein was also found present at contractile vacuole pores, another microtubule-based organelle. A second BBC73-like gene BBC60 was identified in *Tetrahymena* genome. Although Bbc60 has approximately 120 fewer residues

than Bbc73, it has the similar protein structure of three DM10 domains. Like the localization pattern of Bbc73, Bbc60 was associated with cilia and basal bodies at cortical rows and oral apparatus. The similarity shared between the two proteins suggested they may cooperate redundantly in basal body and cilia function. EFHC1 and EFHC2 were recognized as human homologues of Bbc73 by Blastp search. I present functional analysis of Bbc73 and Bbc60 in the next chapter.

Chapter 3. Genetic analysis of *BBC73* in *Tetrahymena thermophila*

I. Introduction

EFHC1 is a highly conserved but poorly understood protein across eukaryotes containing cellular organelles of centrosomes or basal bodies and cilia. Mutations in *EFHC1* have been associated with juvenile myoclonic epilepsy, the most frequent form of genetic epilepsy in humans(Suzuki et al., 2004). In human, a paralog of *EFHC1*, *EFHC2* is present and has tentatively been associated with juvenile myoclonic epilepsy (Gu et al. 2005) and neurological syndromes such as autism(Blaya et al., 2009; Weiss et al., 2007). Similarly, two EFHC1-like genes were identified in *Tetrahymena*: *BBC73* and *BBC60*. There is high sequence identity among *Tetrahymena* Bbc73, Bbc60, human EFHC1 and EFHC2 (Fig1-5).

EFHC1/Rib72 was first reported as a component of the axonemal ribbon in *Chlamydomanos* and is thought to be a major component of the doublet microtubules (Ikeda et al. 2003). The mouse homolog has been shown to be present in sperm flagella and tracheal cilia (Suzuki et al. 2008). Despite their wide spread occurrence, the exact ciliary function of EFHC1 genes remains unknown. Human EFHC1 is reported to be a microtubule associated protein that localizes to mitotic spindle and centrosomes in HeLa cells(de Nijs et al., 2009) and the N-terminal end of EFHC1 is the domain required for its localization(de Nijs et al., 2006). The Drosophila homolog of EFHC1, Defhc1.1 appears to regulate microtubule stability at neuromuscular junctions (Rossetto et al. 2011); no function has yet been assigned to a second EFHC paralog, CG11048. Homozygous EFHC1 null mice are viable and fertile, but display hydrocephalus as well as a number of ciliopathy-associated phenotypes, including a seizure disorder (Suzuki et al. 2009). Cilia are still present in EFHC1 null mice but their motility appears to be reduced (Narita et al. 2012). However, in this study, the author did not report the cause of the reduced motility and if there are any ciliary structure defects in the *efhc1*$^{-/-}$ mice.

I sought to use *Tetrahymena* to investigate the role of Bbc73 and Bbc60 in basal body and cilia biogenesis to better understand the function of EFHC1 proteins. The large number of basal bodies and

cilia in *Tetrahymena* (over 700 basal bodies per cell) makes it a powerful system in which to study ciliary structure and function (Pearson and Winey 2009). I previously showed that Bbc73 and Bbc60 are associated with the cilia, but also with the basal bodies and some other microtubule based structures (Chapter 2). I have gone on to conduct immuno-electron microcopy to determine whether Bbc73 is a true basal body component and where it localizes within these intracellular organelles. I have carried out domain mapping to ask whether the N-terminus of Bbc73 is the localization determinant as the sequences of that region are less conserved in EFHC1 family across species (Fig1-5). Finally, I carried out genetic analysis of *BBC73* by deleting the *BBC73* gene from *Tetrahymena* genome and applying phenotypic assays developed in our lab and cryo-electron microscopy from our collaborators to characterize the potential structurally defects within the cilia from the null cells. I have shown that Bbc73 and Bbc60 have similar expression profiles and that they colocalize at basal bodies and cilia. It is reasonable to ask whether the two proteins are redundant in their cellular function. I have attempted to produce a double Bbc73 and Bbc60 null strain for this analysis.

II. Material and Method

Tetrahymena stains and culture conditions

Tetrahymena thermophile strain B2086, CU428, CU427, SB1969, B*VI and B*VII (*Tetrahymena* Stock Center, Cornell University) were used in this study as wild-type controls and to generate the transgenic cell lines. All cell lines were growing in 2% SPP media (2% proteose peptone, 0.1% yeast extract, 0.2% glucose and 0.003% FeEDTA) at 30°C or 38°C. For experiments with MTT promoter, protein expression was induced with 500ng/ml $CdCl_2$ in 2% SPP media for 3hrs at 30°C. Cells were starved in 10mM Tris pH7.4.

Plasmid construction

mCherry fusion *BBC60* with paromomycin resistance was built from the vector pmCherry-LAP-NEO2 by cloning 1kb sequence of 3'end of *BBC60* to the mCherryLAP tag and 1kb downstream sequence

of *BBC60* to the *NEO2* cassette. By homologous recombination, the linearized construct was integrated into the locus of *BBC60* gene with a C-terminus mCherry tag under the endogenous promoter. mCherry fusions with cycloheximide resistance were built on vector p4T21-mCherry HHF-CHX (Which has a mCherry followed by HHF promoter and *RPL38A* homologue). Similarly, the 1kb of the 3'end of the gene was cloned next to mCherry while the 1kb of the 3' of downstream was cloned adjacent to RPL38A homologue. The expression of *RPL38A* homologue gives rise to the cycloheximide resistance. BBC73-GFP used in immune-electron microscopy was generated from p4T21-NEO2-GFP vector. The flanking regions were amplified by PCR from genomic DNA of B2086 with Phusion DNA polymerase. Exogenous N-terminal GFP fusions (*BBC73* full length and truncation mutants) were made in pBS-MTT-GFP-gtw. cDNA was amplified from DNase treated wild-type mRNA by RT reaction with SuperScriptII reverse transcriptase (Invitrogen, Grand Island, NY) and followed by PCR reaction with Phusion DNA polymerase. The coding sequence was cloned into pENTR4 Gateway Enter vector and then cloned into pBS-MTT-GFP-gtw by recombination with the LR recombinase in the Gateway clonging systems (Invitrogen). Rescue strains for cryo-EM were made based on pBS-MTT-GFP-*BBC73*. Luciferase was amplified from plasmid P and cloned between GFP and *BBC73* or adjacent to 5' end of *BBC73*, which results in luciferase tag at either N-terminal or C-terminal end of *BBC73*. Similarly, mCherry was amplified from plasmid mCherry-LAP-NEO2 and cloned into the same position of pBS-MTT-GFP-BBC73. Rescue strains for *BBC60* were built by replacing *BBC73* sequence with *BBC60* sequence in the above rescue strains. The *BBC73* null construct was made by engineering P4T21 plasmid, in which *NEO2* cassette was flanked by the 1kb upstream before the start codon and 1kb downstream sequences after the stop codon of *BBC73*. By homologous recombination, *BBC73* was replaced by the *NEO2* cassette at *BBC73* locus. Flanked regions were amplified by PCR from genomic DNA.

***Tetrahymena* strain construction**

Constructs encodes the mCherry fusions and GFP fusions were transformed into the macronuclear of specific *Tetrahymena* strains by biolistic bombardment as described before. Briefly, cells were grown in 2% SPP to log phase at 2.5X10^5cells/ml, then starved for 18~24hours in 10mM Tris pH7.4. Starved cells were bombarded with linearized plasmids and recovered in 2% SPP at room temperature overnight. Desired transformants were selected by paromomycin resistance at a final concentration of 120ug/ml or cycloheximide resistance at a final concentration of 15ug/ml.

Generation of *BBC73* germline knockout strains

The *BBC73* null strain was generated as described previously (Bruns and Cassidy-Hanley, 1999) with some modification. Two micronuclear knockout heterokaryons of different mating types were built first. The wild-type B2086 and CU428 strains were used and engineered by integrating frame shift *NEO* gene at the RPL29 locus in the macronucleus, which is suggested to prevent DNA elimination of the selectable marker (Mochizuki et al., 2002; Yao et al., 2003). *BBC73* null construct was transformed into the micronuclear of mating engineered B2086 and CU427 conjugation by bombardment (PDS 1000 from Biorad). Then cells were allowed to finish conjugation in Tris-HCl, pH 7.4 until next day prior to introduction of media. Germline heterozygous strains for the *NEO2* cassette of different mating types were made homozygous for the *NEO2* cassette at the micronucleus by mating to star strains with defective micronuclei (B*VI and B*VII). Once micronuclear knockout heterokaryons were generated (Hai et al., 1999), strains with different mating types were mated to each other to build a new macronucleus with *BBC73* replaced by the *NEO2* cassette at *BBC73* locus. The *BBC73 null* cells were selected for resistance to paromomycin at final concentration of 120µg/ml. Total genomic DNA was isolated by phenol: chloroform: isoamyl alcohol extraction and isopropyl alcohol precipitation (Gaertig et al., 1994) and complete loss of wild-type *BBC73* was confirmed by PCR.

Fluorescence microscopy

All images were acquired at room temperature using an Eclipse Ti inverted microscope (Nikon, Japan) equipped with a CFI Plan Apo VC 60× H numerical aperture 1.4 objective (Nikon, Japan) and a CoolSNAP HQ2 charge-coupled device camera (Photometrics, Tuscon, AZ). MetaMorph Imaging software (Molecular Devices, Sunnyvale, CA) was used to collect images and generate the projection images. For live cell imaging, cells were grown in SPP media with $CdCl_2$ induction, washed once with 10 mM Tris-HCl, pH 7.4, pelleted, and placed on microscope slides (VWR, Radnor, PA). For immunofluorescence, cells were fixed either by 3% formaldehyde or70% ethanol and then placed on poly-L-lysin treated slides. Both the centrin1 antibody 20H5 and anti-mouse Alexa488 were diluted at 1:1000 in PBS+1% BSA. Primary antibody incubation was done at 4°C overnight and secondary antibody incubation was done for 1hour at room temperature. Cells were washed in PBS+ 0.1%BSA five times after each antibody incubation. Finally, cells were mounted in Citifluor (Ted Pella, Inc., Redding, CA).

Immuno-electronic microscopy

Tetrahymena cells were high pressure frozen and subjected to freeze substitution as described before(Giddings et al., 2010; Meehl et al., 2009). Cells were pelleted into a protective solution made of 15% dextran and 5% BSA in 2% SPP media. A Bal-Tec HPM-010 (Leica Microsystems, Wetzlar, Germany) high pressure freezer was used to freeze the loose cell pellet on specimen carriers, and then the cells were freeze-substituted in 0.25% glutaraldehyde and 0.1% uranyl acetate in acetone and embedded in Lowicryl HM20. Nickel grids containing serial 70-nm-thick sections were incubated in blocking solution (2% nonfat dry milk in PBS with Tween 20) and then in blocking solution containing the rabbit polyclonal GFP antibody (the gift of Chad Pearson) diluted 1:200. After rinsing with PBST, the grids were incubated in 15 nm gold-conjugated anti-rabbit secondary antibody diluted 1:20 in blocking solution (Ted Pella, Redding, CA). Grids were stained with 2% uranyl acetate and lead citrate. Images were collected with a Philips CM 100 transmission electron microscope equipped with an AMT V600 digital camera (Advanced Microscopy Techniques, Danvers MA). Images of serial sections of 11 total cells were viewed and gold

particles on each image were counted and matched on a map of basal body domains identified before(Kilburn et al., 2007).

Chemo-attractant assay

The method used here is two-phase assay based on reported study(Koppelhus et al., 1994)with some modification. Log phase (~2.5X10^5cells/ml) cells were starved for 48hrs at 30°C. Chemoattratant solution was made by dissolving 1%PP in 3% histodenz instead of 5% solution of metrizamide. 1.5ml starved cells were loaded carefully on top of the 1ml chemoattractant solution in a cuvette. OD_{600} of the lower histodenz phase was measured every minute for 30min period and then following equation was used to calculate the percentage of the cells moved to the lower phase. The assay was done at room temperature.

$$\frac{OD600\ of\ the\ lower\ phase}{1.5X(OD600\ of\ the\ original\ cell\ suspension\ used)}X100\%$$

Swimming assay

Cells were grown to mid log phase, and washed in 10mM Tris pH7.4. Then cells were incubated in the same starvation solution for 30min at 30°C. 7ul of cell suspension was loaded on to microscope slides (VWR, Radnor, PA). Images were taken at room temperature by using an Eclipse Ti inverted microscope (Nikon, Japan) fitted with a Plan Apo 10× numerical aperture 0.45 objective (Nikon, Japan) and a CoolSNAP HQ2 charge-coupled device camera (Photometrics, Tuscon, AZ). MetaMorph Imaging software (Molecular Devices, Sunnyvale, CA) was used to collect images at 0.02s intervals for 0.2s cell swimming trace images were generated by stacking multiple frames in MetaMorph Imaging software. Distance of swimming was measured in ImageJ. Swimming speed was calculated by dividing the swimming distance by 0.2s. 35 cells for each strain were counted.

Western blot analysis

Cells growing to mid-log phase were pelleted, lysed in buffer and centrifuged at 4°C. The supernatant was saved and boiled for 5min with sample buffer (20% glycerol, 2% SDS, 125 mM Tris, pH 6.8, 5% β-mercaptoethanol). Whole cell lysate was loaded on SDS-PAGE gel for electrophoresis. Proteins were transferred to PVDF membrane (Millipore, Billerica, MA). Membranes were blocked in TBST (TBS+0.05% Tween) +2%BSA for 1hr at room temperature prior to antibody incubation. Primary antibody (monoclonal mouse anti- GFP) was diluted 1:5000 and the incubation was carried out at 4°C overnight. Secondary antibodies (anti–rabbit IR800 and anti–mouse IR680 [LI-COR Biosciences, Lincoln, NE]) were diluted 1:10,000 and the incubation was done for 1hr at room temperature. Three washes with TBST were performed after each incubation. A LI-COR Odyssey scanner was used to visualize the blot and take images.

III. Results

Ultrastructural localization of Bbc73

It has been shown that Bbc73 is associated with basal bodies and cilia by fluorescence microscopy (Chapter2), however, where the protein is within these structures remains obscure. To address this question, immuno-electron microscopy was applied to determine the ultrastructural localization of Bbc73 within the basal bodies. *Tetrahymena* basal bodies are made of several distinct substructure domains as described previously(Kilburn et al., 2007). The core structure of basal body is the microtubule cylinder wall containing three recognizable domains aligned longitudinally: the cartwheel at the proximal end, the transition zone at the distal end and the electron densed lumen in the middle region. Besides that, there are accessory structures around this center feature, including postciliary microtubule, transverse microtubule and kinetodesmal fiber. Previously, overexpressed GFP-Bbc73 was found predominantly at microtubule scaffold and transition zone(Kilburn et al., 2007). As no Bbc73 antibody is available, transgenic cells constantly expressing Bbc73-GFP at endogenous level were used. Here live cell imaging indicated this Bbc73-GFP fusion localized to both basal bodies and cilia as

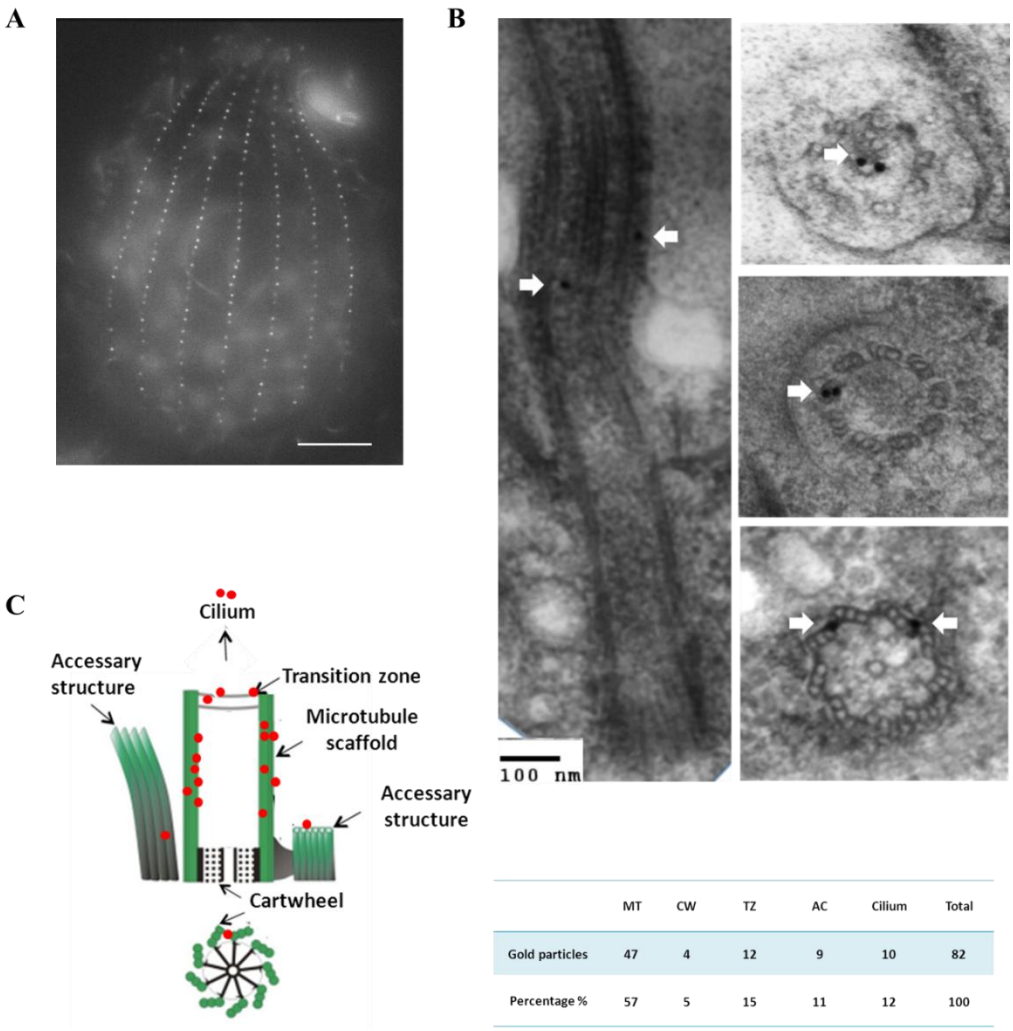

	MT	CW	TZ	AC	Cilium	Total
Gold particles	47	4	12	9	10	82
Percentage %	57	5	15	11	12	100

Figure3-1. Ultrastructural localization of Bbc73-GFP. (A) Bbc73-GFP localizes to both basal bodies and cilia. Live cell image shows the GFP signal from endogenous C-terminal tagged chimera has the similar localization pattern of Bbc73-mCherry. Scale bar: 10 µm. (B) Bbc73 localizes to subdomains within the basal bodies and cilia. *Tetrahymena* cells were labeled with GFP antibody. The localization of the protein was identified by 25nm gold particle conjugated secondary antibody. Left panel: longitudinal view of the basal body and its adjacent cilium. Arrowhead indicates two gold particles at the axoneme of the cilium. Right upper panel: cross section view of the cilium. Arrow head shows the localization to the central pair microtubules of axoneme. Right middle panel: cross section view of the distal end of basal body. Arrowhead shows two gold particles in the triplet microtubule at the transition zone. Right lower panel: cross section view of the proximal end of basal body. Arrowhead shows two gold particles in the triplet microtubule at the cartwheel. (C) Schematic shows the individual basal body subdomain and the distribution of gold particles within them. The chart lists the frequency gold particles were observed at each domain. A whole serial section of 15 basal bodies from 7 cells were counted.

was Bbc73-mCherry (Fig3-1A). Immuno-electron microscopy revealed that like the overexpression GFP tagged counterpart, Bbc73-GFP localized to the microtubule wall and transition zone. The new finding is that Bbc73 is also found at the cartwheel and accessory structures. Moreover, within the cilia, this protein was identified at both central pair microtubule and the doublet microtubule walls (Fig3-1B). The numbers of gold particles belonging to each domain were counted and shown in a table (Fig3-1C). It is obvious that the majority of the protein is present at the microtubule scaffold along the longitudinal length from the proximal end of basal bodies into cilia. These data suggest that Bbc73 may be a microtubule associated protein and play a role in basal body and cilia assembly.

Generation and analysis of *BBC73* knockout cells

To understand the function of Bbc73 protein, I generated *BBC73* null cells (Fig3-2A). *BBC73* is not an essential gene as mating two *BBC73* knockout heterokaryons produced viable progeny in which the cells have a complete knockout of *BBC73* in both somatic and germline nuclei. PCR data confirmed the absence of wild type *BBC73* allele in the null cells (Fig3-2A). The null strain underwent normal cell division as no growth defect was identified. Growth curves of null and wild type strains were measured at both permissive and restrictive temperatures. No significant difference was observed (Fig3-2B).

Although *BBC73* is not essential, it is worth asking whether there are any basal body or cilia related phenotypes with these knockout cells. Therefore, the *BBC73* null cells were first examined by immune-fluorescence microscopy with Cen1 antibody as a basal body marker. DAPI was used to stain the nuclei. For cells growing at both 30˚C and 38˚C, no obvious basal body defects were seen. Like wild type cells, *bbc73* null strains had normal cortical organization, the basal bodies aligned along the anterior to posterior axis. The oral apparatus in null cells was correctly positioned and its morphology was normal too (Fig3-3).

Since Bbc73 is also associated with cilia, I wanted to detect whether there were any ciliary defects in *bbc73* null cells. Motile cilia in *Tetrahymena* are responsible for cell locomotion and enable

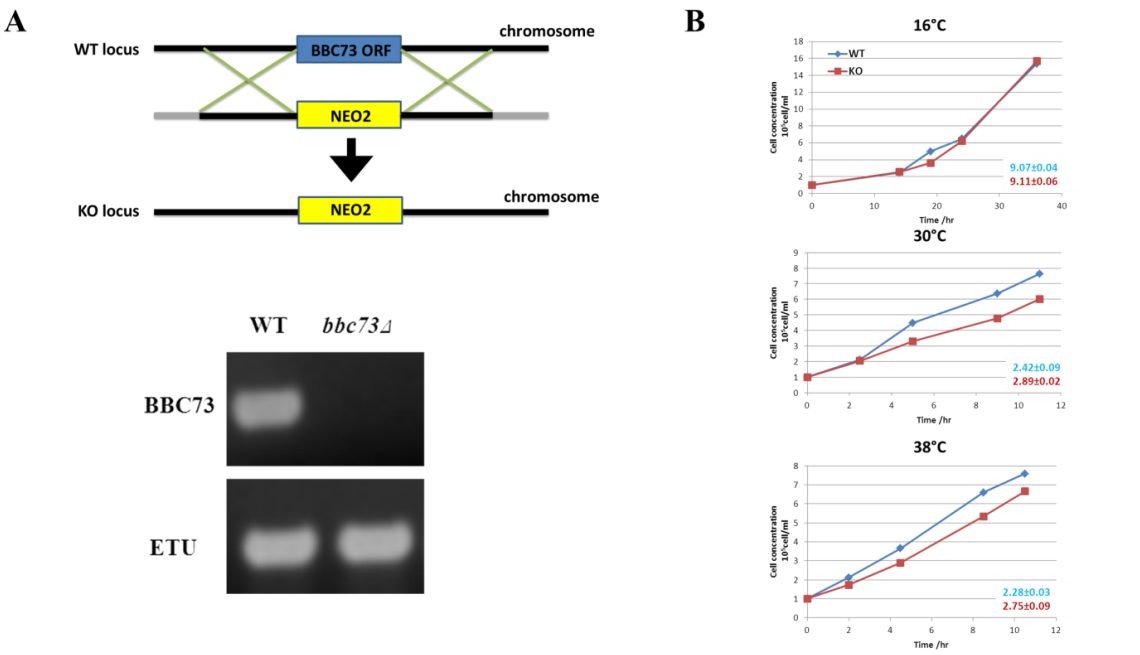

Figure3-2. *BBC73* is not an essential gene in *Tetrahymena*. (A) *BBC73* locus is completely eliminated from complete null. Schematic shows the WT locus was replaced by *NEO2*, which give rise to paromomycin resistance. PCR indicates no WT gene was found in *bbc73Δ* cells. *ETU* is Epsilon Tubulin as a control. (B) *bbc73Δ* cells are viable and the growth rate of the null is similar to WT. The charts are growth curves under three different temperatures. The numbers at the right corner of each chart is the corresponding doubling time. No significant difference was observed between WT and null. Blue color represents WT and red color represents *bbc73Δ.*

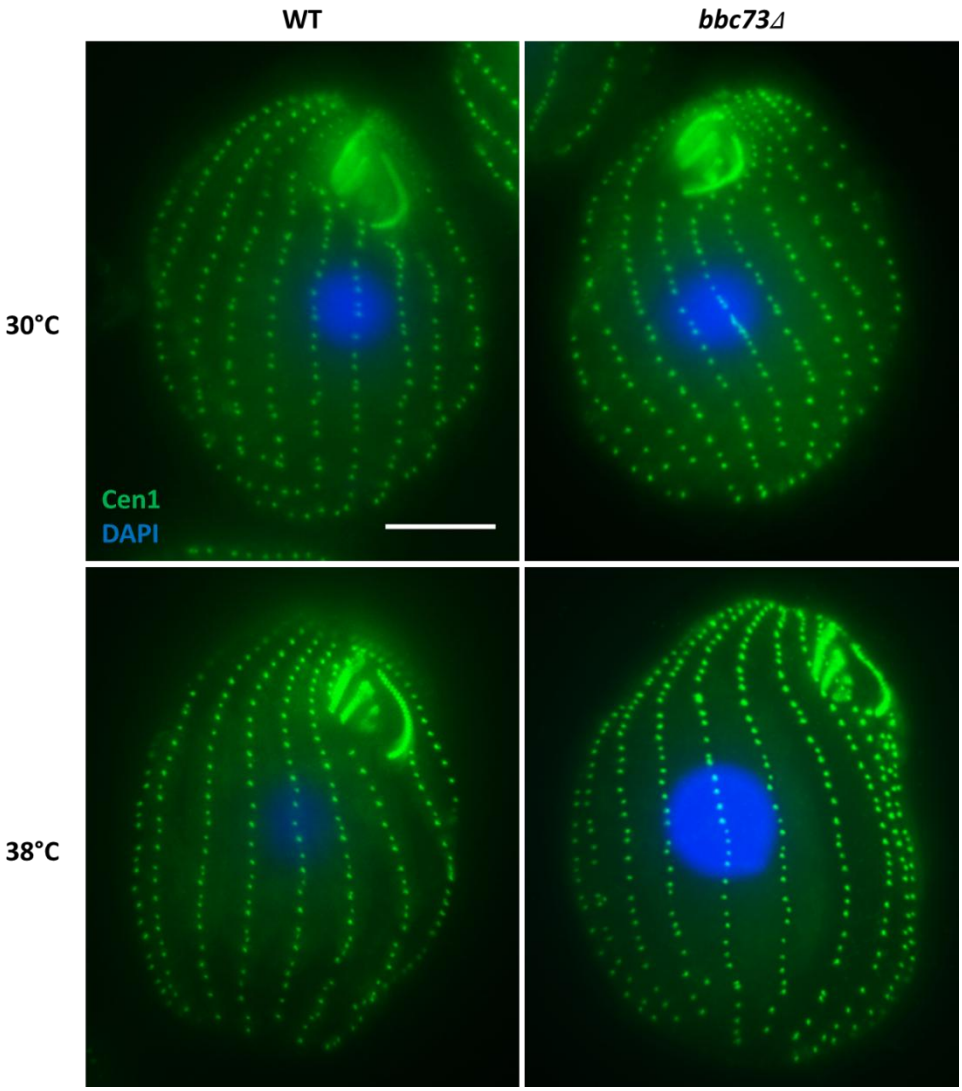

Figure3-3. Bbc73 is not required for overall cortical organization and basal body assembly or maintenance. Immuno-fluorescent micrographs of fixed cells labeled with antibody to Cen1 (green) and DAPI for DNA (blue). Both of the WT and *bbc73Δ* cells were growing at 30° and 38° respectively. Scale bar: 10μm.

cell swimming and directed movement. Swimming behaviors can be used to estimate ciliary function. First, the basal swimming rate was measured, which indicates whether ciliary beating frequency and waveform are altered. Knockout and wild type cells were grown to the same concentration and were monitored under the microscope. Only cells swimming in straight passes were counted. The result showed that the swimming speed was slightly decreased in the *BBC73* knockout cells (Fig3-4A). However, when the forward swim speed was stimulated by incubating cells with 1.0mM IBMX, no significant difference was observed between the wild type and *bbc73* null cells, suggesting that both of them can accelerate accordingly to the proper stimuli (Fig3-4C). A second chemoattractant assay was used to determine how cells respond to positive food stimuli. In this experiment, *bbc73Δ* cells were actually more reactive than wild type cells to the attractants (Fig3-4B). *Tetrahymena* cells use cilia over the cell surface to sense and respond to environment stimuli. Ion channels are clustered on the cilia membrane and initiate membrane action potential to properly direct cell locomotion. The outcome of these complicated physiological states also can be indicated by swimming behaviors of the cells(Hennessey and Lampert, 2012). More specifically, voltage-dependent inward calcium current causes ciliary reversal once it reaches the calcium concentration threshold. This ciliary reversal leads to measureable avoidance reactions and backward swimming. As Bbc73 has an EF-hand motif at the C-terminal end, it is plausible that this protein functions in calcium binding or through some iron channel on the ciliary membrane. To test this hypothesis, swim paths of *Tetrahymena* cells were captured by digital camera under different buffer conditions. 0.5mM Ba^{2+} was used to stimulate avoidance reaction and 20mM K^{+} was applied as a stronger stimulus to cause backward swimming. Both the wild type cells and *BBC73* knockout mutants had the same ability to show ciliary reversal and backward swimming (Fig3-4C).

Loss of *BBC73* affects ciliary axoneme structure

Axonemes of *bbc73* mutant cells were isolated, frozen and subjected to cryo-EM to examine the

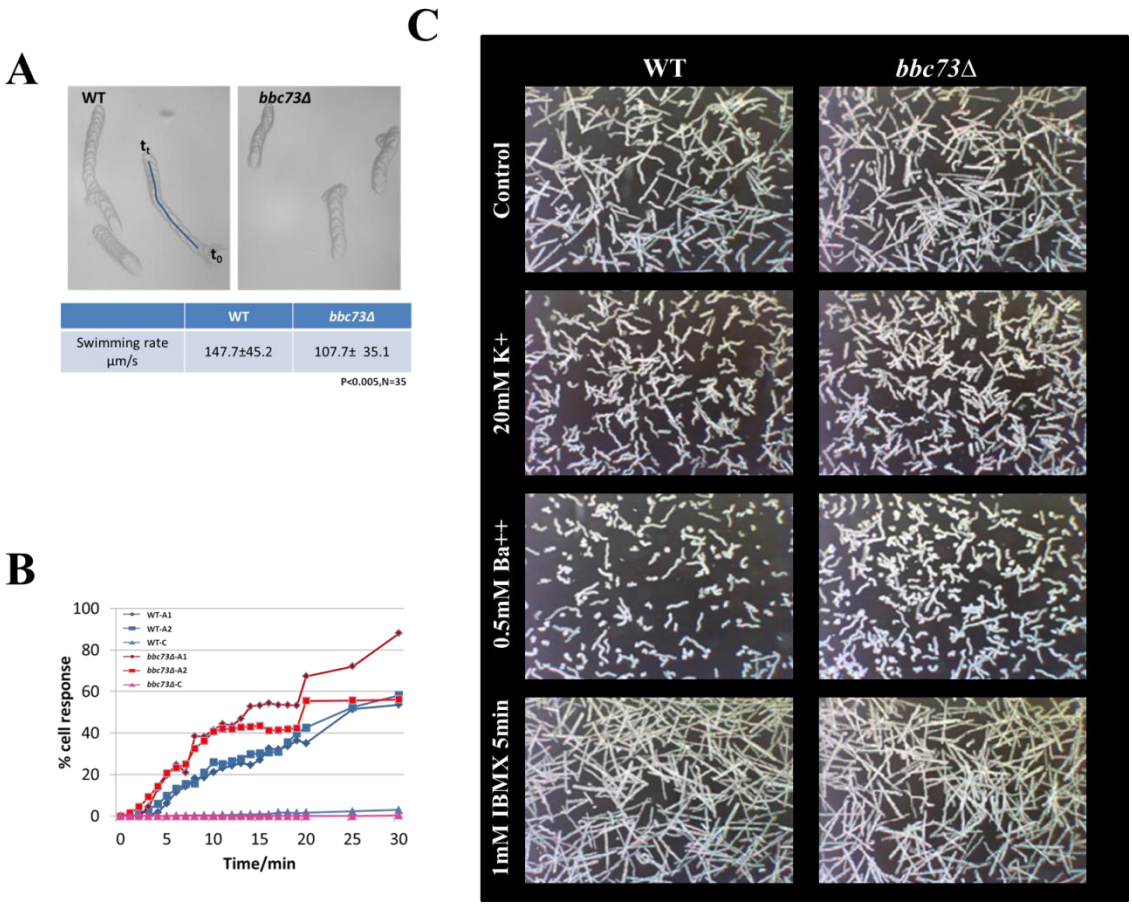

Figure3-4. Loss of *BBC73* leads to subtle behavior defects. (A) *bbc73Δ* cells displays decreased forward swimming rates. (B) *BBC73* null mutant cells are more hyperreactive to chemoattractant than the wild type cells. Color curves indicate the percentage of cells respond to the food stimuli. Red curves refer to the *BBC73* null mutant and blues curves refer to the wild type cells. Two independent measurements were done for each strain. C. Depletion of Bbc73 does not influence backward swimming and avoiding reaction in *Tetrahymena* cells. Digital images of cell swimming paths with incubation of various salt conditions. The experiments in C was done by Prof. Todd Hennessey in University of Buffalo.

detailed structure. In general, the overall 9+2 structure of the cilia was unaffected in *bbc73* null cells (Fig3-5A). Recently, application of cryo-EM has identified various structures in the microtubule lumen. One of them is microtubule inside protein (MIP) complex. Based on the relevant localization to the protofilament, so far, four distinct MIP complexes have been identified although the functions and the compositions of MIPs remain unknown(Nicastro et al., 2011). A close look at the doublet microtubules of *bbc73Δ* cells revealed defective structures; MIP1a, as well as a second density (unnamed MIP) were missing close to protofilaments A2-3 at the bottom of the A tubule (Fig3-5B, C, D). Besides MIP1a and the unnamed MIP, no other MIPs and axonemal structures, such as dynein arms were affected. This data suggested Bbc73 may be a molecular component or regulator of this novel structure.

To address whether Bbc73 is a component or a regulator of MIPs, Bbc73 constructs were built with various tags to enlarge the protein such that the additional mass could be detected by cryo-electron tomography. Luciferase tag is commonly used in electron-microscopy for distinguishing whether a protein itself is part of a structure by additional density. Here I designed the *BBC73* alleles under the inducible MTT promoter with both luciferase and GFP tags. In this way, I can control the expression of the fusion protein with Cd^{2+} in the growth media. Moreover, by monitoring GFP signal, I can determine whether the fusion is expressed and binds along the whole axoneme similar to wildtype Bbc73. The fusion proteins were expressed, which is confirmed by western blot (Fig3-6A). The first strain was built with GFP and luciferase tags at N and C terminus of Bbc73 respectively. GFP-*BBC73*-luciferase construct was transformed into *BBC73* mutant and wild type cells. 250ng/ml and 500ng/ml of Cd^{2+} was used to induce the fusion protein expression for different time series. Live cell imaging showed that only limited number of cilia harbored the GFP signal for both strains under all the induction conditions (Fig3-6B). In contrast, GFP-Bbc73 has been demonstrated to distribute robustly into almost every single cilium. Since sub tomogram of cryo-electron tomography needs to average multiple axoneme images,

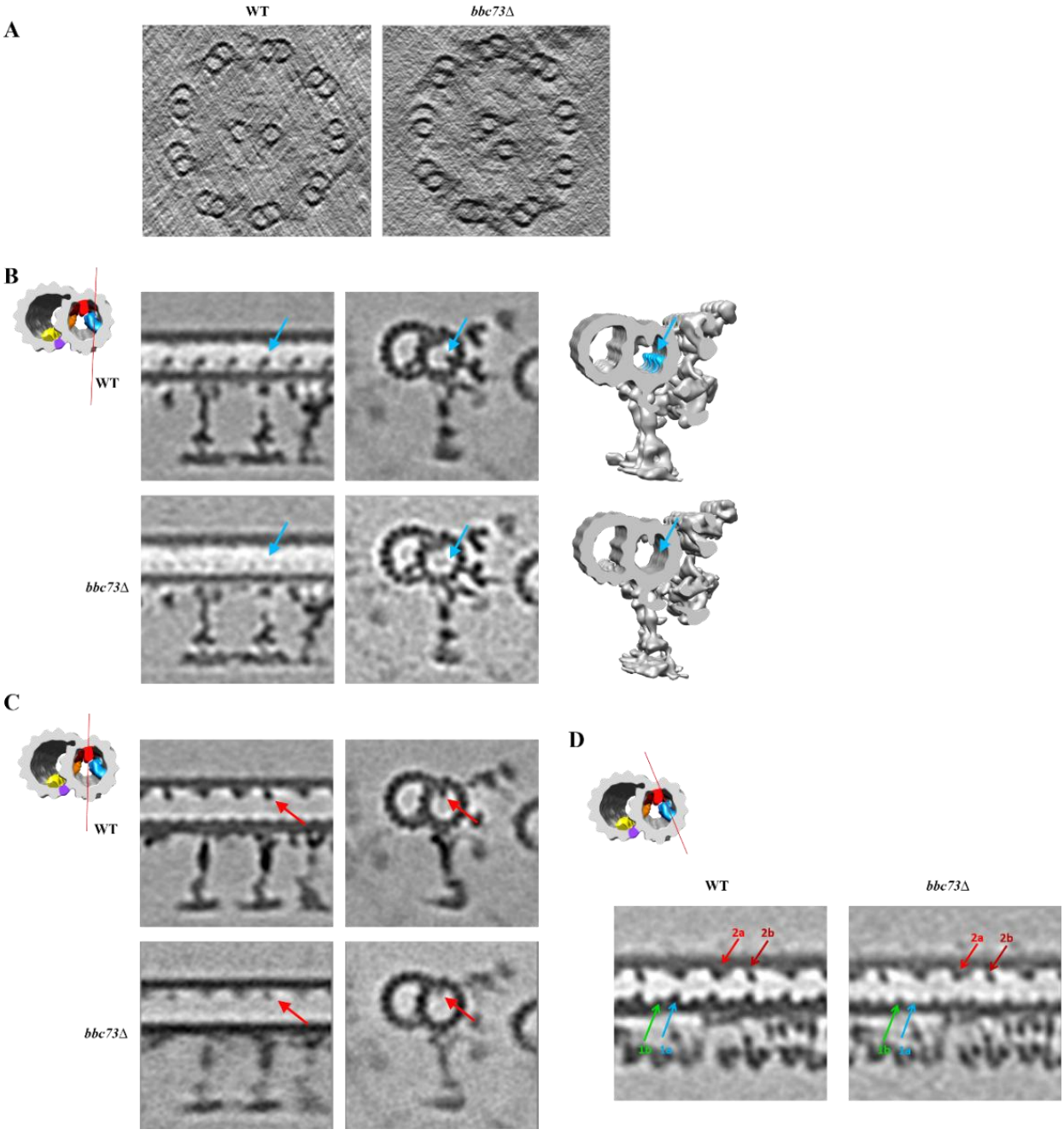
A
WT
bbc73Δ
B
WT
bbc73Δ
C
WT
bbc73Δ
D
WT
bbc73Δ
2a
2b
1b
1a

Figure3-5. *bbc73Δ* cells has MIP defect. (A) Cross-sectional overview of 9+2 axoneme for both WT and *bbc73Δ*. (B) MIP1a is missing from the axoneme in *bbc73Δ*. Tomographic slice of an averaged axonemal 96 nm repeat from both WT and *bbc73Δ* cells, viewed in cross-section from the proximal side and in longitudinal section, showing the arrangement of axonemal dyneins and MIP1a. 3D isosurface renderings of averaged cross sectional axoneme doublet. Blue color represents MIP1a as arrows in tomographic slice and electronic density in isosurface renderings respectively. (C) MIP2 is still present in *bbc73Δ* cells. Tomographic slice of an averaged axonemal 96 nm repeat from both WT and *bbc73Δ* cells, viewed in cross and longitudinal section. Red arrows points to the density structure of MIP2. (D) Tomographic slice of longitudinal view of an averaged axonemal repeat from both WT and *bbc73Δ* cells, showing all four subunits of MIP1 and MIP2. The arrows pointing toward the MIPs are color-coded: MIP1a and MIP1b (blue and green, respectively), MIP2a and MIP2b (light and dark red, respectively). The experiments in this figure were done by Daniel Stoddard in Nicastro Lab.

this non-uniform expression of the rescue fusion is not appropriate for this application. One possible explanation for this result is that a relative large tag at the C-terminal end interferes with protein folding. To rule out that possibility, the luciferase tag was moved to the N-terminal between the GFP tag and *BBC73*. However, this new fusion GFP-luciferase-Bbc73 had the same inefficient expression pattern as the previous chimera (Fig3-6C). Neither high Cd^{2+} concentration nor longer induction time improved the ciliary expression. As indicated by the images, apparently both chimeras were present at the majority of the basal bodies, but not the cilia. It is known that turnover rate of ciliary protein can influence its incorporation into the axoneme(Marshall and Rosenbaum, 2001; Stephens, 1997; Stephens and Lemieux, 1999). If this is the case for GFP-luciferase-Bbc73 fusion, deciliation and reciliation with Cd^{2+} induction could solve the problem. However, no improvement was observed upon reciliation for ciliary association of either GFP luciferase fusions. An alternative explanation is that the fusion protein is too large to incorporate into the microtubule lumen. Moreover, the luciferase tag has 51% GC content and it is not codon optimized for *Tetrahymena*.

To overcome these potential issues, I decided to replace the luciferase tag with codon-optimized mCherry. Previously I had great success with this mCherry fusion expressed in *Tetrahymena*, such as Bbc73-mCherry. Furthermore, the molecular weight of GFP plus mCherry exceeds the single luciferase tag, which fulfils the requirement for our cryo-electron tomography application. GFP-mCherry-BBC73 construct was generated and transformed into wild type and *bbc73* null cells. PCR was used to prove this fusion allele was integrated into the correct locus. Transformants were imaged after 3hr of induction with 500ng/ml Cd^{2+}. The data revealed that GFP-mCherry-Bbc73 fusion was localized to high percentage of cilia in *bbc73* null cells, comparable to GFP-Bbc73. Signals of both GFP and mCherry were detected at the basal bodies and cilia (Fig3-7). The strain was sent to our collaborator for cryo-EM analysis. I am waiting for the result of this experiment. In contrast, in the presence of wild type of Bbc73, only a small

portion of cilia had the double fluorescence signal, suggesting the GFP mCherry fusion failed to associate with most of the cilia. One reasonable explanation is that the chimera was out-competed by wild type Bbc73.

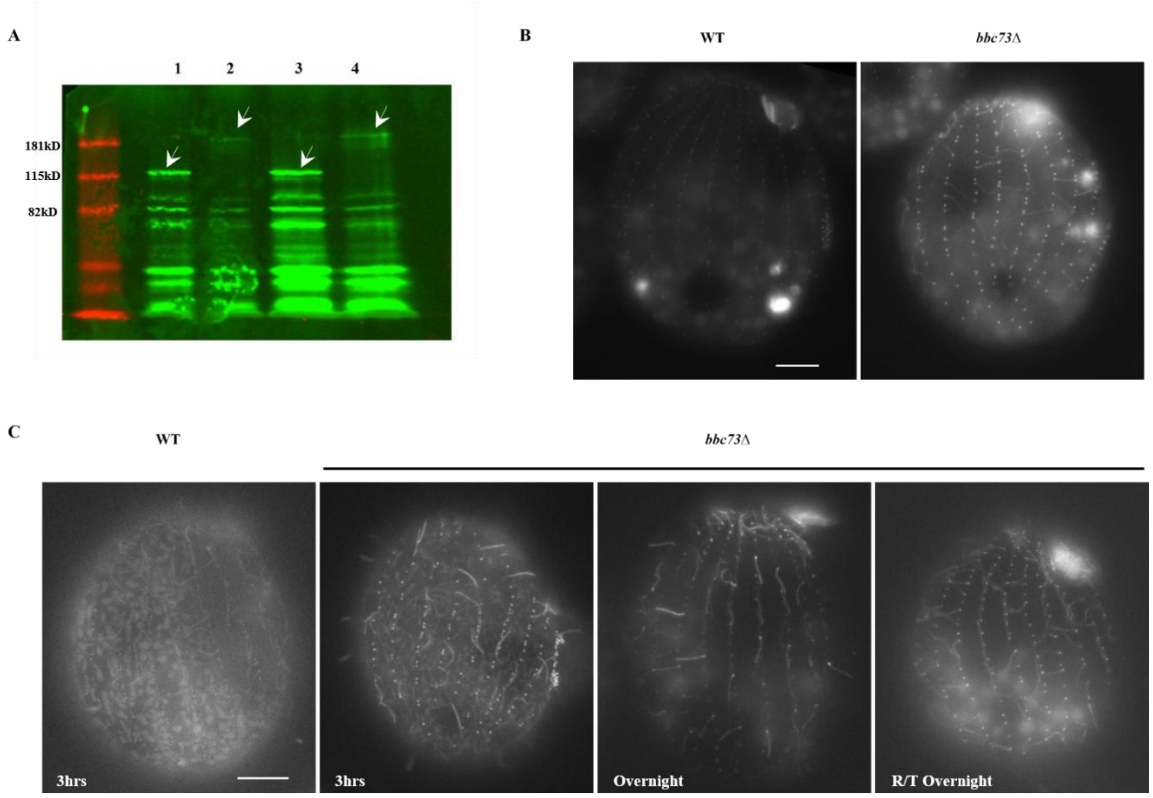

Figure3-6. Localization of GFP-luciferase-Bbc73 fusions. (A) Western blot of cell extracts from WT/GFP-*BBC73* (1), WT/GFP-*BBC73*-luciferase (2), *bbc73Δ*/GFP-*BBC73* (3) and WT/GFP-luciferase-*BBC73* (4). Probed with GFP antibody. (B) Localization of GFP-Bbc73-luciferase. (C) Localization of GFP-luciferase-Bbc73. Different Cd^{2+} induction conditions were tested. Scale bar: 10 µm.

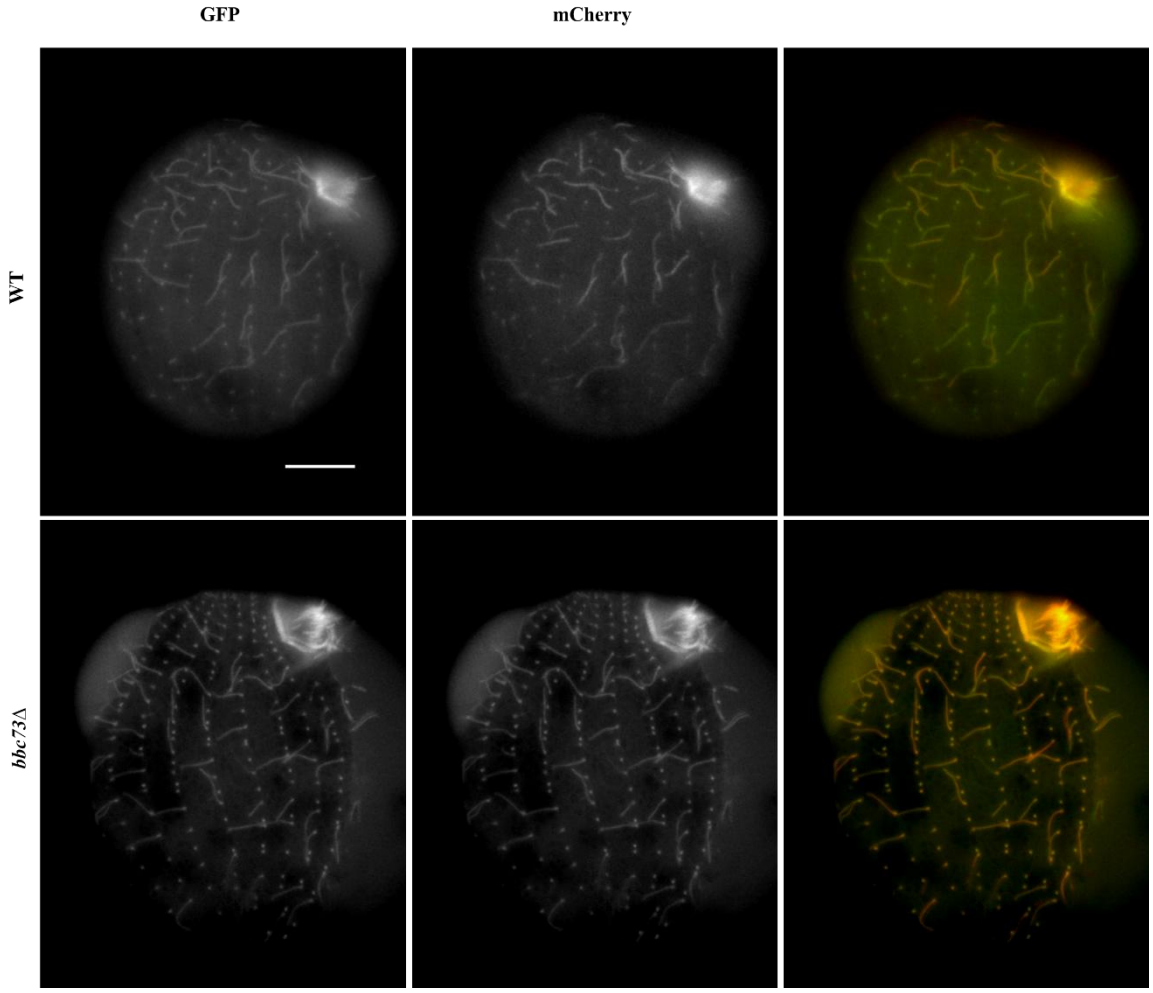

Figure3-7. Localization of GFP-mCherry-Bbc73 fusions. Upper panel: Wild type cells. Lower panel: *bbc73Δ* cells. Expression of the fusion protein was induced with 500ng/ml Cd^{2+} for 3hrs at 30˚C. Scale bar: 10 µm.

Localization determinants of *BBC73* mutants

Bbc73 contains two recognizable structural domains. One is the EF hand, a calcium binding motif present in a variety of proteins such as Centrin and Calmodulin, required for conducting their cellular functions. The second is the DM10 domain, the function of which is unknown. To understand which region of Bbc73 is responsible for its basal body and ciliary localization, three truncation mutants tagged with GFP were generated and used for fluorescence localization analysis. Previously, N-terminal end of EFHC1 has been shown required for its localization in Hela cells(de Nijs et al., 2006). To test whether it is the case in *Tetrahymena*, mutations were designed lacking or only containing the N-terminus as ΔN and N88 (Fig3-8A). The third mutant, DM10Δ was made without the last DM10 domain and the EF hand motif. A schematic cartoon illustrates which portions of Bbc73 were retained in various alleles (Fig3-8A). Surprisingly, fluorescence microscopy showed that all of the mutants were still associated with the basal bodies and cilia (Fig3-8B). However, distinct patterns did exist in these mutants compared with wild type GFP-Bbc73. The specific signal of N88 at basal bodies and cilia was much weaker than wild type protein and there was an increased cytoplasmic pool of this mutant protein, suggesting this truncation protein may be less competitive than wild type Bbc73 for recruitment to the correct location. In contrast, the intensity of DM10Δ signal is similar to the full length protein at both the basal bodies and cilia. ΔN mutant accumulated at basal bodies but the ciliary localization was affected, as only a few cilia retained the GFP signal and the signal was quite low. Taken together, the data on these mutants indicated that the N-terminus itself of Bbc73 was sufficient for its basal body and cilia localization, similar to human EFHC1. Additionally, this small fragment may contain the ciliary specific signal that results in cilia localization of Bbc73. Moreover, there may be a second localization signal outside the N-terminal domain in Bbc73 that assists the recruitment of the protein to basal bodies. Alternatively, since the experiments were done with the presence of wild type Bbc73, it is possible that the mutants can form

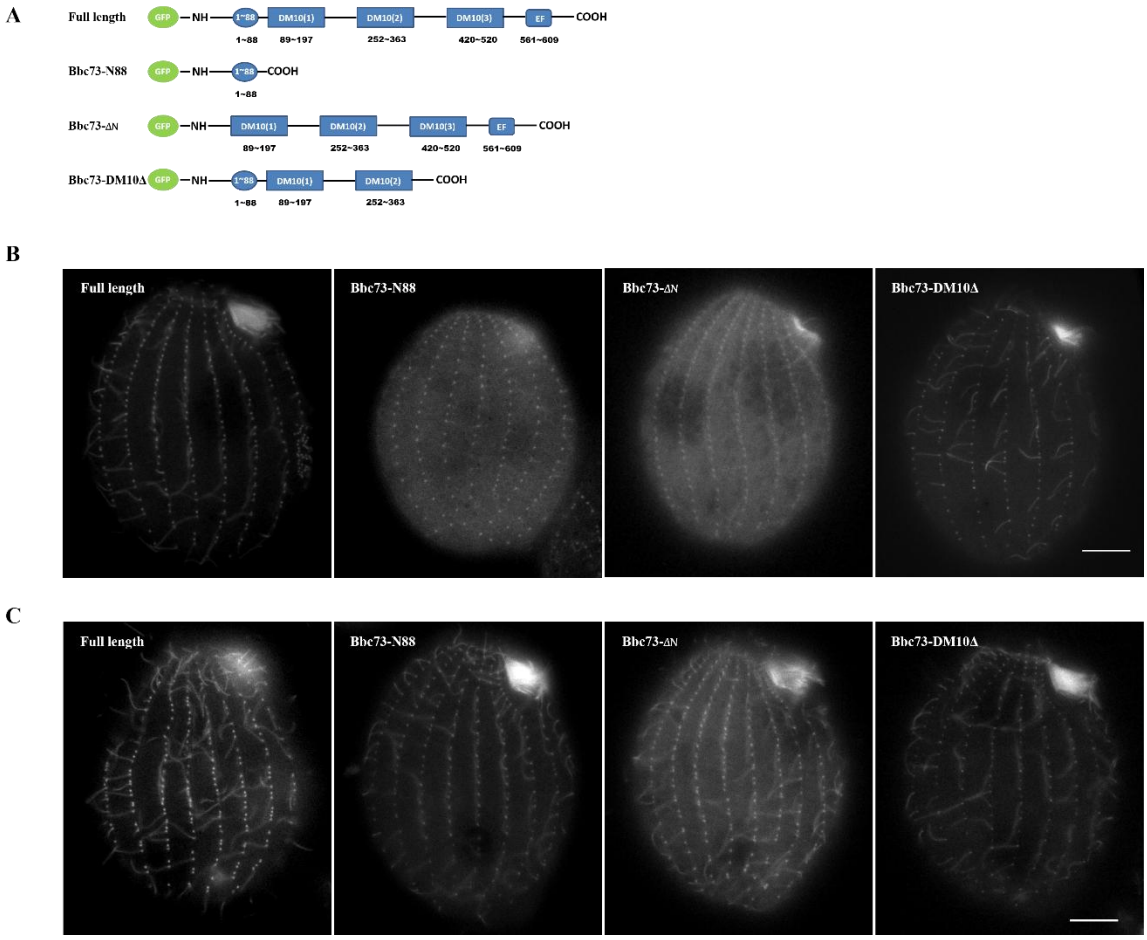

Figure3-8. The N-terminus of Bbc73 is sufficient but not required for its basal body and ciliary localization. (A) Schematic of Bbc73 protein domains and the truncation mutants designed for the localization analysis. (B) All of the three mutants localizes to the basal bodies and cilia in WT. Live cell images of GFP tagged full length Bbc73 and its truncations with the presence of wild type Bbc73. (C) the mutants still localizes to basal bodies and cilia in *bbc73Δ* cells. Live cell images of GFP tagged full length Bbc73 and its truncations without the presence of wild type Bbc73. Scale bar: 10 μm.

protein dimers with the wild type and then be recruited to the cilia. This would explain how Bbc73 DM10Δ-GFP was found at basal bodies and cilia.

To test the dependency on wild-type Bbc73, the localization of Bbc73 mutants was determined in *bbc73* null cells that lack wild type Bbc73 protein. The data clearly shows that even without the wild type Bbc73, all the three GFP fusions of Bbc73 truncation still associated with both basal bodies and cilia (Fig3-8C). Moreover, the signal of N88 is stronger in the cilia when wild type Bbc73 was absent, suggesting this mutant was out-competed by full length Bbc73 in wild type cells. This data supports the idea that two domains exist in Bbc73 for its localization and either of them alone is sufficient for the basal body and ciliary localization of Bbc73.

Bbc60 is also required for intact MIPs structure

It has been shown that Bbc73 and Bbc60 have similar localization patterns at both basal bodies and cilia. So they may share some redundancy in function, which may explain why I did not observe much defect in *bbc73* null strain. By personal communication, Jacek Gaertig (University of Georgia) has informed us that he has generated a *bbc60* null mutant. Similar to *bbc73*Δ cells, *bbc60*Δ cells have no obvious phenotype. This evidence further supports the idea that the two proteins are redundant. As we saw MIP1a missing in *bbc73* null, we went on to determine whether Bbc60 also functions in axoneme structure. Axonemes of *bbc60Δ* cells were isolated, purified and subjected to cryo-EM analysis. Not surprisingly, we found the subtomogram average suggested the overall axoneme structure was unaffected, like *bbcΔ73* cells. The *bbc60Δ* assembled normal 9+2 microtubule organization with intact dynein arms and other adjacent structures. Slices from a different angle through the doublet clearly showed that MIP2 and MIP3 remained intact in *bbc60Δ*. The only defect was the absence MIP1a and the unnamed MIP inside the microtubules while MIP1b remained. This result is the same as with the *bbc73* mutant (Fig3-9A). Isosurface renderings of cross-sectional view of these subtomograms show the MIPs inside the microtubules, and the only diminished density in the mutant is MIP1a (Fig3-9B). Additionally,

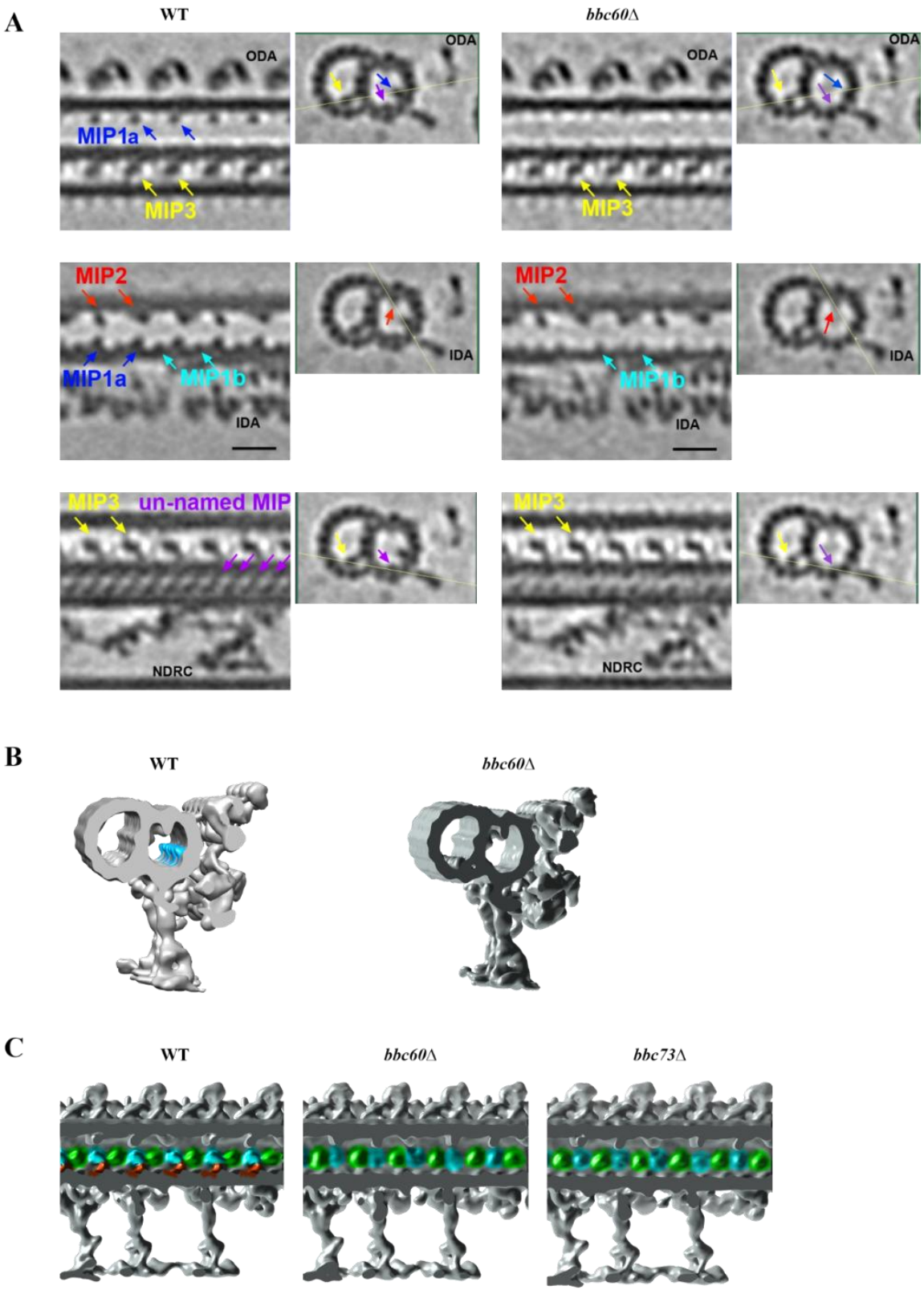
A
WT
bbc60Δ
ODA
MIP1a
MIP3
MIP2
MIP1b
IDA
un-named MIP
NDRC
B
WT
bbc60Δ
C
WT
bbc60Δ
bbc73Δ

Figure3-9. *bbc60Δ* cells has MIP defect. (A) Tomographic slice of an averaged axonemal 96 nm repeat from both WT and *bbc60Δ* cells, in cross-sectionial and longitudinal view. The arrows pointing toward the MIPs are color-coded: MIP1a and MIP1b (dark and light blue, respectively), MIP2 (red), MIP3 (yellow), new unnamed MIP (purple). IDA: Inner Dynein Arm, ODA: Outer Dynein Arm. NDRC: Nexin-Dynein Regulatory Complex. Scale bar: 15 nm. (B) Isosurface renderings of averaged axonemal repeats in cross sectional view. The electron densities for MIP1a is in blue. (C) Isosurface renderings of averaged axonemal repeats in longitudinal view for WT, *bbc60Δ* and *bbc73Δ*. The electron densities for MIPs are color-coded: MIP1a (blue), MIP1b (green) and unnamed MIP (orange). The experiments in this figure was done by Daniel Stoddard in Nicastro Lab.

isosurface renderings of longitudinal view of averaged axoneme repeats from WT, *bbc73Δ* and *bbc60Δ* were also compared, which makes it clear that MIP1a and the unnamed MIP are missing from both null strains (Fig3-9C). This data provides strong evidence that Bbc73 and Bbc60 may function cooperatively in assembling and /or maintaining MIPs structure.

Similar to the case of *bbc73* null, a rescue strain expressing a GFP-luciferase-Bbc60 was generated. However, as GFP-luciferase-Bbc73, this Bbc60 chimera predominantly localized to the basal bodies with very weak ciliary GFP signal (Fig3-10). Again, I thought the high GC content luciferase may be problematic. I would like to switch to GFP and mCherry tag for the fusion if it turns out that the dual tag fusion of Bbc73 works for cryo-EM.

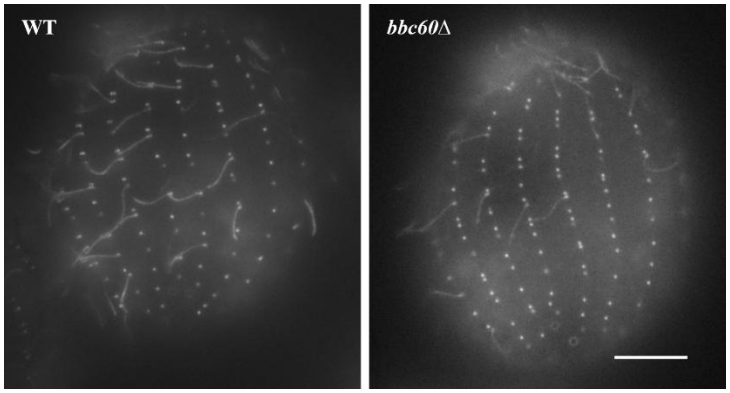

Figure3-10. Localization of GFP-luciferase-Bbc60 rescue fusion in wild type cells and *bbc60Δ* cells. Expression of the fusion protein was induced with 500ng/ml Cd^{2+} for 3hrs at 30˚C. Scale bar: 10 µm.

Localization of Bbc73 and Bbc60 are independent from each other

One question raised by my work is whether the localization of these two proteins is interdependent. To address this potential dependency, localization of Bbc73 and Bbc60 was examined in the *BBC060* and *BBC73* knockout cells separately. First, the GFP-Bbc73 chimera was expressed in *bbc60* null cells by Cd^{2+} induction. Live cell microscopy revealed that the GFP-Bbc73 signal was abundantly

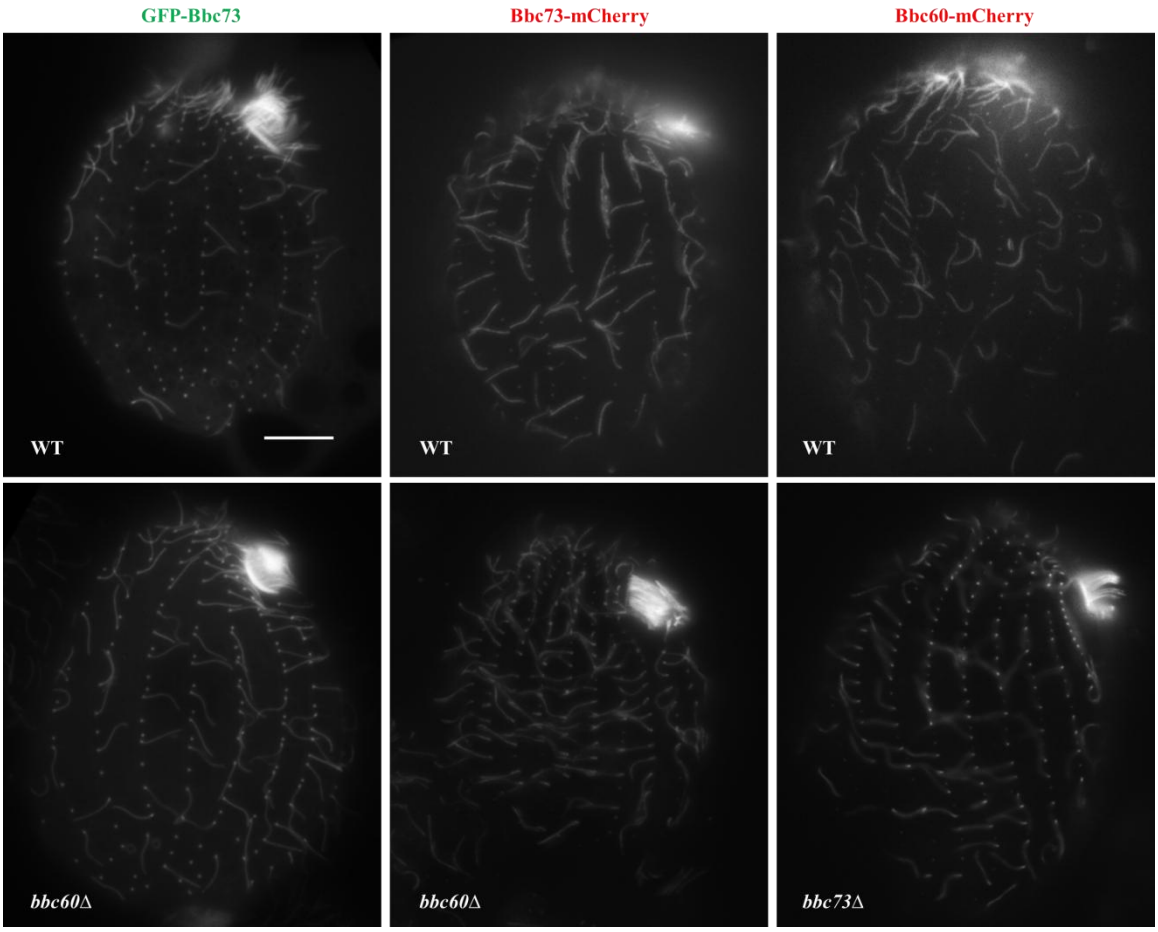

Figure3-11. Localization of Bbc73 and Bbc60 are independent on each other. Live cell images of GFP or mCherry Bbc73 and Bbc60 fusions. Left panel: WT and *bbc60*Δ cells expressing GFP-Bbc73. The GFP fusion was induced with 500ng/ml Cd2+ for 3hrs. Middle panel: WT and *bbc60*Δ cells expressing endogenous Bbc73-mCherry. Right panel: WT and *bbc73*Δ cells expressing endogenous Bbc60-mCherry. Scale bar: 10µm.

associated with both basal bodies and cilia, just like the localization of GFP-Bbc73 in the wild type cells, where both wild type Bbc73 and Bbc60 were present (Fig3-11). Thus this data demonstrated the basal body and ciliary localization of Bbc73 is independent of Bbc60. Since this chimera was overexpressed under MTT promoter, its localization may have an artifactual component. To get a more conclusive result, a new Bbc73 fusion was designed with a mCherry tag and cyh resistant (HHF) selectable marker. Upon successful homologous recombination, the *BBC73*-HHF-mCherry allele was integrated into *BBC73* locus where it was expressed by the endogenous *BBC73* promoter. The localization of Bbc73-mCherry was seen robustly at both basal bodies and cilia in *bbc60* mutants, the same as within the wild type cells (Fig3-11). Together, both the localization GFP-Bbc73 and Bbc73-mCherry in *bbc60* null cells indicated that presence of Bbc60 is not required for the basal body and ciliary association of Bbc73.

To determine whether localization of Bbc60 relies on Bbc73, similar experiments were carried out. Bbc60-mCherry construct was transformed into bbc73 mutant along with wild type *Tetrahymena* cells as control. This Bbc60 fusion was also controlled by its endogenous promoter and expressed continuously. As the case for Bbc73, Bbc60-mCherry was present at both cilia and basal bodies in *bbc73* null cells (Fig3-11). No difference in localization pattern was noticed between the wild type and *BBC73* knockout cells. In summary, although Bbc73 and Bbc60 share a similar localization pattern and seem to function together to maintain the axonemal structure intact, they do not require each other for their individual basal body and ciliary localization.

IV. Discussion:

Previously, EFHC1 has been identified as a component of flagella, cilia and basal body or centrosomes in different organisms. In *Chlamydamonas*, Rib72 was recognized by the antibody only at the flagella. No basal body signal was observed(Ikeda et al., 2003).Two EFHC1-like polypeptides were co-fractionated with loosely bound tubulin in echinoderm flagella(Setter et al., 2006). Mouse EFHC1/Myoclonin was found at the motile cilia and the flagella(Ikeda et al., 2005). Overexpression of

GFP tagged human EFHC1 was not only associated with centrosome, but also found at the mitotic spindle and cytoplasm in Hela cells(de Nijs et al., 2009). The above studies used overexpression that may lead to artifacts and antibodies were demonstrated not reliable. Here my study has clearly established that Bbc73 is both a basal body and cilia component by endogenous tagging of Bbc73 (Fig3-1). There is not much of a cytoplasmic pool in the transgenic cells. Additionally, the protein was found at the contractile vacuolar pores, another microtubule system in *Tetrahymena* (Chapter2). Moreover, When GFP-Bbc73 is overexpressed, the fusion protein is associated with cortical longitudinal microtubule arrays. These bundles of microtubule extend parallel and to the left of the cortical basal body rows. On average, 7~12 partly overlapping microtubules make up the longitudinal microtubule arrays(Allen, 1967). The observed broad distribution of Bbc73 at the variety microtubule arrays strongly suggests this protein is a microtubule associated protein. This idea was further supported by the ultrastructure localization of Bbc73-GFP. The majority of the protein recognized by immuno-gold reagents is associated with microtubule scaffold along the wall of triplet microtubule inside basal bodies and the doublet microtubules in ciliary axoneme (Fig3-1). One remarkable feature of cortical microtubules is that they are post-translationally modified and highly stable(Gaertig et al., 1995; Wloga and Gaertig, 2010; Xia et al., 2000). The observation that Bbc73 is preferably localized to the cortical microtubules indicates it may function to stabilize these microtubule arrays.

I created a knockout *Tetrahymena* strain to study the function of *BBC73*. Depletion of *BBC73* does not influence the viability of cells (Fig3-2B). *bbc73Δ* cells grew and divided normally compared to the wild type cells. Interestingly, loss of *BBC73* did not disrupt the basal body biogenesis and the general cortical organization although abundant Bbc73 was found at these structures in wild type cells (Fig3-3). Cilia of $Efhc^{-/-}$ mice displayed reduced ciliary beating frequency (Suzukit et al., 2009). Initially, I thought *BBC73* deficiency would affect the ciliary motility of the cells. However, in swimming behavior assays, only subtle variance was captured in *bbc73Δ* cells (Fig3-4). When cells were exposed to food after

starvation, they were stimulated to swim toward the attractant. During this process, *bbc73Δ* cells are slightly more hyperactive than the wild type cells in the two-phase assay with SPP as the attractants (Fig3-4B). However, when starved cells were incubated in a second chemoattractants IBMX, no difference of the swimming was recognized between the null and the wild type by comparing the swimming paths captured by digital camera (Fig3-4C). This discrepancy may be caused by the property of the attractants and the limit of resolution power of the two methods. Similarly, both the avoiding reactions and backward swimming in *BBC73* depletion were unaffected (Fig3-4C).

In the past decade, the technology advances that have substantially improved the resolution of cryo-EM that enables the discovery detailed microtubule structures. A good example is the observation of the electron-dense MIPs. These structures were described in axonemal microtubules, including the insect sperms(Romano Dallai, 2005), *Chlamydomonas* flagella and sea urchin sperm(Nicastro et al., 2006, 2011). Meanwhile, other studies also identified the presence of MIPs in cytoplasmic microtubules in stem cells, neuron and brain tissues (Garvalov et al., 2006). The electron-dense material appears to be periodically attached to the axonemal microtubule walls, whereas cytoplasmic particles seem to be suspended within the microtubule lumen without strong interactions with the microtubule walls. So far, four MIPs have been discovered inside the axonemal microtubule walls and they are composed of globular small and large subunits arranged in 16 and/or 48nm periodicity(Nicastro et al., 2011). Among these four, MIP1, MIP2 and MIP4 bind to the inner wall of A-tubule and MIP3 is associated with the microtubule walls of B-tubule. Despite the well-established structural and morphological descriptions of these MIP material, there is not any functional study on MIPs in the literature. Up to this point, no molecular component or regulator for MIPs has been identified. My study on Bbc73 and Bbc60 shed light on this biological question. Analysis on *bbc73Δ* revealed that loss of *BBC73* resulted loss of MIP1a and of a small electron-density attached to the protofilament A3. We call it a newly discovered unnamed MIP (Fig3-5). Other MIP complexes, MIP2, 3 and 4 and the other structures remained intact in

bbc73Δ cells (Fig3-5). The elimination of the same MIPs was also seen in *bbc60Δ* axonemes (Fig3-9). Together, the data provided the first connection between a gene and the MIPs. This raises the question, do Bbc73 and Bbc60 encode the proteins MIP1a and the unnamed MIP or are they regulators for assembly and maintenance of MIPs? To address these questions, I generated a strain expressing GFP-mCherry-Bbc73 fusion (Fig3-7). The strength of this transgenic cell is that the chimeric protein will not only restore the MIPs but also increase the electron density of them if Bbc73 is a component of these structures. Alternatively, if Bbc73 is a regulator, the MIPs will remain their regular size. This structural labeling strategy has been applied successfully in electron microscopy to position a specific molecule in a protein complex. Recently, a biotin-streptavidin system and cryo-ET has been shown as a powerful related tool for this application. The biotinylation-tagged IC2 of *Chlamydomonas* axoneme was labeled by streptavidin and visualized by subtomogram averaging(Oda and Kikkawa, 2013). Extra density was observed at outer-inner dynein linker where IC2 locates due to the bound streptavidin. However, I decided this system likely will not work for our MIPs molecular candidates as they are inside the MT. Streptavidin may not get access to the biotin tag. Instead, as described, I initially attempted to use a luciferase tag for this experiment. Our collaborator has had success with a luciferase tag in *Chlamydomonas*. Unfortunately, neither GFP-Bbc73-Luciferase nor GFP-luciferase-Bbc73 were able to localize to the cilia robustly as endogenous Bbc73-mCherry (Fig3-6). Since GFP-Bbc73 localized normally to cilia (Fig2-7), the problem most likely is caused by the newly introduced luciferase tag. The luciferase tag I used originated from fireflies with approximate 50% GC content. In contrast, the average GC content of *Tetrahymena* genome is around 33%. I have noticed that high GC content exogenous genes are not expressed well in *Tetrahymena* cells. The western blot further supported this idea (Fig3-6). On the other hand, we have no knowledge on how Bbc73 is incorporated into the microtubules and no knowledge of its turn-over dynamics at the cilia. This relative large tag may inhibit incorporation or turnover. A single GFP was not identifiable in previous study as a protein density in a GFP fusion to wild

type. (Nicastro. D et al., 2011). Therefore, I added two fluorescent proteins. A *Tetrahymena* codon optimized mCherry tag adds the molecular weight of the tags equally to single luciferase tag and rules out the potential expression issue. Indeed, GFP-mCherry-Bbc73 mimicked the location of Bbc73-mCherry (Fig3-7). Abundant GFP-mCherry signal was captured at the cilia in both WT and *bbc73Δ*. The strains were sent to Nicastro lab for cryo-ET analysis. This system is not ideal. The globular domains of mCherry and GFP are flexibly linked so that each tag may not be detected in subtomogram averages. If this is the case, I will codon optimize the luciferase sequence for*Tetrahymena* or switch to another labeling technique.

Before this study, nothing was known about the composition and function of MIPs. Knowledge was limited to their relative localization to protofilament and their periodic arrangement. Based on that, researchers proposed that MIPs may facilitate the anchoring of other axonemal complexes to the doublet microtubule walls(Nicastro et al., 2011). The cryo-ET data I showed here seems to disprove this hypothesis. All the critical axoneme complexes (IDA, ODA, RS and NRDC) persist in *bbc73Δ* and *bbc60Δ* cells (Fig3-5, Fig3-9). However, it is plausible that the other MIPs are able to compensate for the missing MIP1a. Future work to identify more MIP components should resolve this problem. I expected the structural defect would be reflected functionally in swimming behaviors, which, apparently is not the case. One explanation is that our behavior assays are not sensitive enough to capture the subtle changes caused by the deficiency in MIPs.

Mutational analysis of Bbc73 domains revealed that the N-terminus is sufficient for its ciliary and basal body localization. This is consistent with previous study on human EFHC1 in Hela cells. The N-terminal domain of human EFHC1 enabled recruitment to the centrosome(de Nijs et al., 2006). The authors further demonstrated a new motif in that region that interacted with α-tubulin. However, I uncovered a second domain outside the first 88 amino acids that also enabled the localization to the basal bodies and cilia. This suggests the N-terminal domain is not required for Bbc73 localization in

Tetrahymena, which is different from human EFHC1. The same analysis in *bbc73Δ* ruled out the possibility that mutants associated with basal body and cilia by forming dimers with wild type Bbc73 (Fig3-8). Further work to identify the second minimum localization motif may help to better understand the recruitment of Bbc73 to these microtubule structures.

So far, I have identified two EFHC1-like genes in *Tetrahymena* genome, *BBC73* and *BBC60*. Both of the genes encode protein products containing three DM10 domains and in the case of EFHC1 also an EF hand motif at the C terminus (similar to the human gene). From the Tetrahymena functional genomic database, the expression profiles of *BBC73* and *BBC60* are quite similar during the whole vegetative and sexual cell cycles (Fig2-7). Moreover, the two proteins shared similar localization pattern at the basal bodies, cilia and contractile vacuole pores. Occasionally, association with cortical longitudinal microtubule arrays was observed. By analysis of the individual knockout strains, I discovered that the mutants had the same defects in MIP1a and the unnamed MIP structures (Fig3-5, Fig3-9). Thereafter, it is reasonable to propose that the two proteins function together in these MIPs. Actually, this phenomenon is not uncommon for ciliary components. It has been shown that mutations in *Chlamydomonas* MIA1 and MIA2 displayed the same slow swimming and low flagellar beat frequency defects respectively(Yamamoto et al., 2013). The polypeptides encoded by MIA1 and MIA2 interacted with each other and formed the modifier of inner arms in flagella. Simultaneous mutations of both genes in *Chlamydomonas* did not make the defect worse. Generating and analyzing the double knockout of *BBC73* and *BBC60* will extend our understanding on how EFHC1 family members function together. This is an ongoing project as elimination of two genes in *Tetrahymen* is time consuming and not easy to achieve. I suspect that the *BBC73* and *BBC60* genes are redundant and that the double null *Tetrahymena* strain may reveal a strong phenotype. Indeed, since each of the single mutant strain loses the same structure, it is also possible that the structure itself is not essential so the double would not be worse growing.

Like the case for MIA complex, I asked whether Bbc73 and Bbc60 also interacted with each other and whether they required the presence of each other to correctly localize. Surprisingly, my data revealed that the basal body and ciliary localization of Bbc73 and Bbc60 are independent of each other (Fig3-11). This evidence does not diminish the possibility that the two proteins cooperatively form a complex. In the future it is still worth investigating whether there is physical interaction between the Bbc73 and Bbc60.

Although it is apparent that Bbc73 and Bbc60 are required for MIP integrity, it is still unknown how they carry out the function. Currently, there are only limited number of proteins identified that physically interact with EFHC1, including α-tubulin and Tektin(Linck et al., 2014; de Nijs et al., 2006). Both of them are molecular components of protofiliaments. Identifying more components and building a functional module for MIP complexes will help to elucidate how the EFHC1 family is involved in MIPs structure.

My study on the EFHC1 family in *Tetrahymena* provides the groundwork for future analysis on the molecular assembly of MIPs, how the axonemal doublet microtubule is stabilized, how specific periodicities in the doublet microtubules are achieved.

Chapter 4. Functional analysis of EFHC1 in *Xenopus* embryos

This work is a collaboration with Dr. Jianli Shi and Prof. Michael Klymkowsky

I. Introduction

Cilia are complex intracellular organelles involved in various cellular processes. Within the past decade, they have come into the spotlight as studies reveal their relation with intracellular signaling. The hedgehog signaling pathway is the best studied, and it depends on the primary cilia integrity (Huangfu and Anderson, 2005). Recently, Wnt signaling has also been reported to be dependent on cilia. However, the basis of these processes are still unclear and there is some controversy in the literature. Depletion of ciliary protein, BBS4, in Zebrafish leads to elevated wnt signaling(Gerdes et al., 2007). But mutants of cilia components, Ift88 and Ift172, in mouse did not exhibit any Wnt signaling related defects(Ocbina et al., 2009). Both the hedgehog and Wnt signaling pathways have proved to be critical for vertebrate developmental processes, such as cell differentiation and tissue patterning(Basten and Giles, 2013).

In Chapter 3, I showed that both EFHC1 and EFHC2 in *Tetrahymena* are critical for maintaining the MIP structures in the doublet microtubule lumen. This discovery reveals a new structural role of EFHC1 proteins in ciliary axoneme. However, it does not explain why the human orthologues are involved in JME. Recently, studies suggest the physiological mechanisms of EFHC1 mutant alleles causing JME are more complicated than previous thought as some of the mutations are tolerated in healthy individuals (Subaran et al., 2015). Currently, one hypothesis for the linkage of EFHC1 and the pathologic mechanisms to JME is that the biological basis for epilepsy is the impaired cilia function(Ganesh, 2010). EFHC1 null mice exhibit defects in their brain development(de Nijs et al., 2012).The authors did not report whether this defect is caused by altered signaling. Moreover, not much ciliary deficiency is observed in EFHC1 null mice. *Tetrahymena*, a sing free swimming ciliate, powerful for basal body and cilium research, but is not useful for developmental and signaling studies because they lack the cellular machineries only present in vertebrates.

To better understand the function of EFHC1, I choose to use *Xenopus laveis* as a model to study its roles during vertebrate development. *Xenopus laveis*, commonly known as the African clawed frog, is an outstanding tool for biological research. This organism is used to study vertebrate embryonic development, basic cell and molecular biology, and as a neurobiology model for human diseases. *Xenopus* is relatively close evolutionary to humans and it offers invaluable experimental tractability. The genome of *X.laveis* has been sequenced, exhibiting significant similarity with the human genome. Although *X.laveis* is allotetraploid, which makes it infeasible to directly manipulate the genome, alternative tools have been developed. Loss of function and gain of function studies can be carried out by microinjection, when a variety of materials, such as RNA, plasmid DNA and morpholino oligonucleotides are delivered into the embryos to manipulate gene function. Additionally, *X.laveis* has a relatively short life cycle. It only takes a couple days to go from a fertilized oocyte to a tadpole with functional organs, allowing for quick assessment of any experimental outcome. Furthermore, its known cell fate, the large size and high tolerance for manipulation of embryos make *Xenopus* ideal for microsurgery, so that given tissue types or signaling centers can be studied extensively and exclusively through grafting.

In recent years, intensive studies have demonstrated *X.laveis* is a powerful model to explore the development of the ciliated cell and the dynamics of cilia function. *Xenopus* embryos utilize the two types of cilia to conduct a range of cellular functions during development procession. The *Xenopus* embryos are covered with epidermis, which has a punctuat pattern of ciliated cells surrounding by non-cilia cells. These motile cilia function to generate directed fluid flow across the embryo skin surface. This process is critical for *Xenopus* embryos because they use their skin to respire. The second motile cilia in *Xenopus* embryos is the motile monocilia on the gastrocoel roof plate, an analogous tissue of ventral node in mammals. Like the nodal cilia in humans, the GRP cilia play a role in driving the leftward extracellular flow to establish the left-right asymmetry in the body. Dysfunction in these cilia of *Xenopus*

causes noticeable *situs inversus*, like heart looping. Beside the motile cilia, there are primary cilia present in the neural tube of *Xenopus* tadpoles. When the primary cilia function is impaired, abnormal embryonic development will happen due to the disrupted signaling transduction. Finally, the development of cutting-edge confocal microscopy empowers visualizing these diverse types of cilia in the context of *Xenopus* embryo tissue.

In this Chapter, I present the findings of EFHC1's cellular and developmental roles in ciliogenesis, tissue patterning, gene expression and Wnt signaling by using *Xenopus* embryos and explants.

II. Material and Methods

Embryos manipulation

X. laevis embryos were staged, and explants were generated, following standard procedures (Nieuwkoop and Faber 1967)(Sive et al. 2000)(Shi et al. 2011). Capped mRNAs were transcribed from linearized plasmid templates using mMessage mMachine kits (Ambion) following manufacturer's instructions. At the two-cell stage embryo injections were directed equatorially; for explant studies injections were targeted to the animal hemisphere region. All the injection was done by Dr. Jianli Shi. As an injection tracer, we routinely included RNAs (150 pgs/embryo) encoding either β-galactosidase, green fluorescent protein (GFP) or GFP-CAAX, which is membrane-associated. In the case of GFP/GFP-CAAX RNA injection, embryos were examined by fluorescent microscopy to confirm the accuracy of injection. Animal caps were isolated from stage 8-9 blastula embryos in 0.5 MMR (Sive et al. 2000)(Shi et al. 2011), transferred into wells on an 2% agarose coated plate and harvested when siblings reached stage 18. Neural crest explants were carried out as described previously (Carl et al. 1999).

Molecular analysis

RT-PCR and qPCR analyses were carried out as described previously (Zhang et al. 2003)(Zhang et al. 2006). cDNA synthesis was performed using 1 µg purified RNA and a Verso cDNA kit (Thermo Scientific) following manufacturer's directions. Real-time (quantitative) PCR was carried out using a

Mastercycler Epgradient Realplex device (Eppendorf). PCR reactions were set up using DyNAmo SYBR Green qPCR kits (Finnzymes). Each sample was normalized to the expression level of ornithine decarboxylase (ODC). The cycling conditions used were: 95°C for 5 minutes; then 40 cycles of 95°C for 15 seconds, 56°C for 15 seconds, 60°C for 30 seconds. The ΔΔCT method was used to calculate real-time PCR results. The primers used for RT-PCR analysis were Ornithine decarboxylase (ODC) [U 5'-CAG CTA GCT GTG GTG TGG-3' D 5'-CAA CAT GGA AAC TCA CAC-3']; Wnt8a [U 5'-TGA TGC CTT CAC TTC TGT GG-3' D 5'-TCC TGC AGC TTC TTC TCT CC -3']; BMP4 [U 5'-TGG TGG ATT AGT CTC GTG TCC -3' D 5'-TCA ACC TCA GCA GCA TTC C -3']; Noggin [U 5'-AGT TGC AGA TGT GGC TCT -3' D 5'-AGT CCA AGA GTC TCA GCA -3']; FGF8 [U 5'-tgg tga ccg acc aac taa gc D 5'-cga tta act tgg cgt gtg g]; TUBB2B [U 5'-CCA GGC TTT GCC CCA TTA AC D 5'-GCT ACT GTG AGG TAG CGT CC].

Morpholinos and plasmids

The EFHC1 morpholino was designed by and purchased from Gene Tools, Inc. Control morpholino has been described previously (Zhang et al. 2006; Zhang and Klymkowsky 2009). We generated plasmids that encode EFHC1-GFP chimeras that either perfectly match (pCS2-EFHC1-GFP-match) or maximally mismatch (pCS2-EFHC1-GFP-rescue) the EFHC1 morpholino. Other plasmids used encode membrane-bound GFP, GFP-CAAX, supplied by Kristen Kwan (U. Utah), ΔG-β-catenin (Merriam et al. 1997), Dickkopf-1 (Glinka et al. 1998), SFRP2 (Bradley et al. 2000). The details of the TOPFLASH/FOPFLASH assay have been described previously (Zhang et al. 2006). Statistical analysis were based on values expressed as mean ± standard deviation. Comparisons between EFHC1 MO alone or together with rescue RNA versus control MO were analyzed by unpaired student's t-test. $p<0.05$ was considered as significant in all analyses.

***In situ* hybridization**

For in situ hybridization studies, anti-sense probes for Sox9, Twist1, Krox20, En2, and Tubb2b RNAs were synthesized using digoxigenin-UTP following standard methods. Generally, embryos were co-

injected with β-galactosidase RNA (50 pg/embryo) and β-galactosidase activity was visualized in fixed embryos using a brief Red-Gal (Research Organics) reaction.

Immunocytochemistry and confocal microscopy

Whole-mount immunocytochemistry was carried as described by Dent et al., (Dent et al. 1989). To image gastrocoele roof plate cilia or primary cilia in the neural tube, control morpholino or EFHC1 morpholino (together with RNA encoding membrane-bound GFP as a lineage tracer) were injected alone or together with rescuing RNAs into dorsal blastomeres at the 4-cell stage. To examine gastrocoele roof plate cilia cilia, gastrocoel roof plates were dissected from stage 19 embryos and fixed in MEMFA and prepared for immunohistochemistry as described by Chung et al (Chung et al. 2012). To examine neural tube primary cilia, embryos at stage 26 were fixed in MEMFA and embedded in 2% agarose and 300μm sections were generated using a Leica VT1000S Vibratome. Images were collected using a Zeiss 510 Confocal Laser Scanning Microscope. The mouse monoclonal anti-acetylated α-tubulin antibody 6-B-11 was used to visualized ciliated cells (Chu and Klymkowsky 1989). Rabbit anti-Xenopus centrin was supplied by Sergei Sokol (Kim et al. 2012). In situ hybridization images were captured using a Nikon D5000 camera on a Wild microscope. Immunoblot analysis was carried out as described previously in Zhang et al (Zhang et al. 2003) using an anti-GFP antibody, for immunocytochemistry, a chicken anti-GFP antibody was used (Immunology Consultants Lab, Inc.). The quantification of basal body density and the ciliated cell density were done with automated image processing algorithms described before using the ImageJ(Shi et al., 2014). The algorithms were optimized using the antibody staining and confocal acquisition settings.

III. Results:

X. laevis is allotetraploid and often contains –a and –b alloalleles of genes present in single copies in the diploid species *X. tropicalis* (Hellsten et al. 2007). A BLAST search of the latest (7.1) version of the *X. laevis* genome using the previously identified *X. laevis* EFHC1 coding region reveals two

chromosomal scaffolds; one contains originally annotated EFHC1-like gene, termed EFHC1b. The coding region of the second scaffold has yet to be annotated and its putative start site remains to be identified. We tentatively identify this gene as EFHC1a. Originally no EFHC2 gene had been identified in *X. laevis*, but a BLAST search of 7.1 version of the *X. laevis* genome using the *X. tropicalis* EFHC2 coding region sequence revealed two likely EFHC2 genes in *X. laevis*. In contrast to mouse, human, and *Tetrahymena* EFHC1 proteins, the Xenopus EFCH1 polypeptides appear to be missing the C-terminal EF-hand domain. This part of my thesis work is focused on the *X. laevis* EFHC1b gene and I will use EFHC1 for the rest of this chapter.

To study the function of EFHC1 gene, I first detected the temporal and spatial expression of EFHC1. RT-PCR analyses, along with the data from Yanai et al showed that EFHC1 RNA was supplied maternally at low level and increase dramatically around the time right after the onset of gastrulation. The RNA level remained high to late stages (Fig4-1A). Spatially, In situ hybridization studies revealed that EFHC1 RNA was highly expressed in the multiciliated cells of the epidermis in neurula stage embryos. In later stage embryos, robust EFHC1 RNA was found in a variety of tissues including eye, neural crest and neural tube (Fig4-1B). This data indicated EFHC1 may play a role in cilia and neural system function in *X.laveis*.

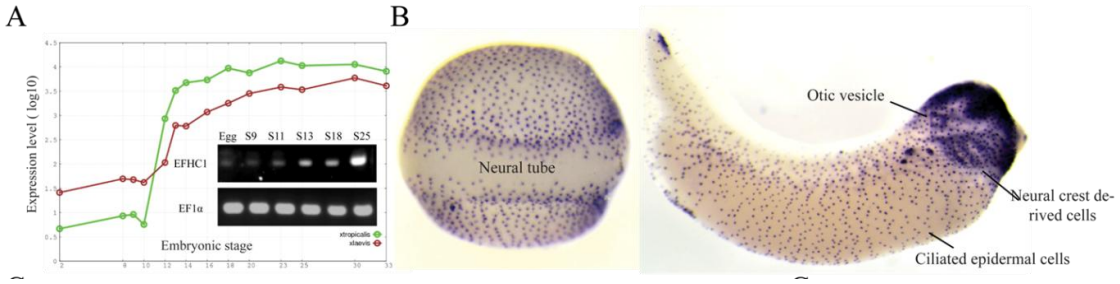

Figure4-1. Expression of *EFHC1* RNA in *Xenopus* embryos. (A) RT-PCR analysis in *X. laevis* of *EFHC1* RNA at various developmental stages using *EF1α* RNA as the internal control. The chart of EFHC1 log expression level is adapted from Xenbase. (B) *In situ* hybridization studies indicated that *EFHC1* is expressed at various tissues in *Xenopus* embryos.

EFHC1 is associated with both motile and immotile cilia

EFHC1 has been shown as a ciliary component in *Chlamydomonas* and associated with centrosome and mitotic spindle in HeLa cells (Ikeda et al., 2003; de Nijs et al., 2006). My data for *Tetrahymena* Bbc73 extended our understanding that EFHC1 is not only a ciliary protein but also a basal body component. To determine the cellular localization of EFHC1 in *X. laevis*, we expressed a GFP-tagged EFHC1 fusion protein by microinjection of the corresponding messager RNA. This EFHC1-GFP chimera includes the EFHC1 coding sequence from early embryonic RNA inserted into a plasmid to encode the full length EFHC1 in-frame through its C-terminal to GFP. As revealed in Figure4-1, bulk EFHC1 RNA was found in the ciliated ectoderm tissue. Therefore I examined the cellular localization of EFHC1-GFP in the ectodermal explants dissected from blastula stage embryos. Upon dissection, explants developed into atypical epidermis spattered with multiciliated cells at a similar rate as observed in the intact embryo. Compared with whole embryo, explants have an advantage in that they have a simpler, albeit abnormal developmental fate, since they lack mesodermally and endodermally derived inductive signaling systems (Ariizumi et al. 2009). Explants expressing EFHC1-GFP were fixed and analyzed by confocal microscopy. Images collected revealed that the GFP signal was found in a ciliary like structure with punctate foci similar to basal bodies. This data indicated, as in the other organisms, EFHC1 is a ciliary component in *X. laevis*. Cytoplasm and cell boundary were also labeled by EFHC1-GFP signal, although this localization might be non-specific due to overexpression of the chimera. The GFP-only control was also found in cytoplasm and cell boundary in explants. To confirm the association of EFHC1 with cilia and/or basal bodies, immuno-fluorescence was applied to the explants. Acetylated tubulin and centrin2 were stained as cilia and basal body markers, respectively. EFHC1-GFP co-localized well with acetylated tubulin. EFHC1-GFP was present in the full length of the cilia, proving it is a ciliary protein as other homologs. The basal body marker centrin 2 did not colocalize with EFHC1-GFP. However, because of the low quality of centrin2 antibody, we were not able to get images with high

resolution for a solid conclusion. To overcome the antibody issue, we turned to centrin2-RFP, which is reported to give basal body labeling (Brooks and Wallingford, 2015). Centrin2-RFP and EFHC1-GFP were co-injected in the embryos. Animal caps expressing both fusions were fixed and subjected to confocal microscopy (Fig4-2A). There is no colocalization of centrin2-RFP and EFHC1-GFP at the basal bodies.

To extend our understanding of EFHC1 ciliary localization, we turned to the other two types of cilia in *X.laevis*. One is the single motile cilia on the gastrocoel roof plate, playing a role in establishing the left-right asymmetry as the mouse embryonic nodal cilia. GRP tissues expressing EFHC1-GFP were dissected from stage 19 embryos and then fixed and stained with acetylated tubulin antibody. As figure 4-2B showed, the GRP cilia were visualized by artificial red color of acetylated tubulin staining and EFHC1-GFP was overlapped with the cilia marker. This data first established the presence of EFHC1 in nodal-like cilia, suggesting it may function in building embryonic left-right asymmetry. Current literature reported that EFHC1 is only associated with motile cilia and there are no reports of EFHC1 in primary cilia. I investigated whether this is the case in *Xenopus*. Primary cilia are present in various tissues in *Xenopus* embryos. One such tissue is the embryonic neural tube developing from stage 16, coordinating tissue homeostasis and signaling transduction. Embryos were injected with EFHC1-GFP RNA and harvested at stage 26. After fixation, these embryos were sectioned into 300um thick slides and immuno-stained with acetylated tubulin. I examined individual sections of neural tube of a single embryo by confocal microscopy. Surprisingly, this GFP chimera was found at the primary cilia based on colocalization with acetylated tubulin staining. Strong cytoplasm GFP signal was also present in cells at the neural tube (Fig4-2C). This is the first evidence of EFHC1 associated with the primary cilia, suggesting this protein may function in signaling transduction in addition to being a building block of ciliary axoneme. Taken together, these data demonstrated EFHC1 is a protein associated with both motile cilia and non-motile primary cilia, and it may play broader physiological roles than we expected.

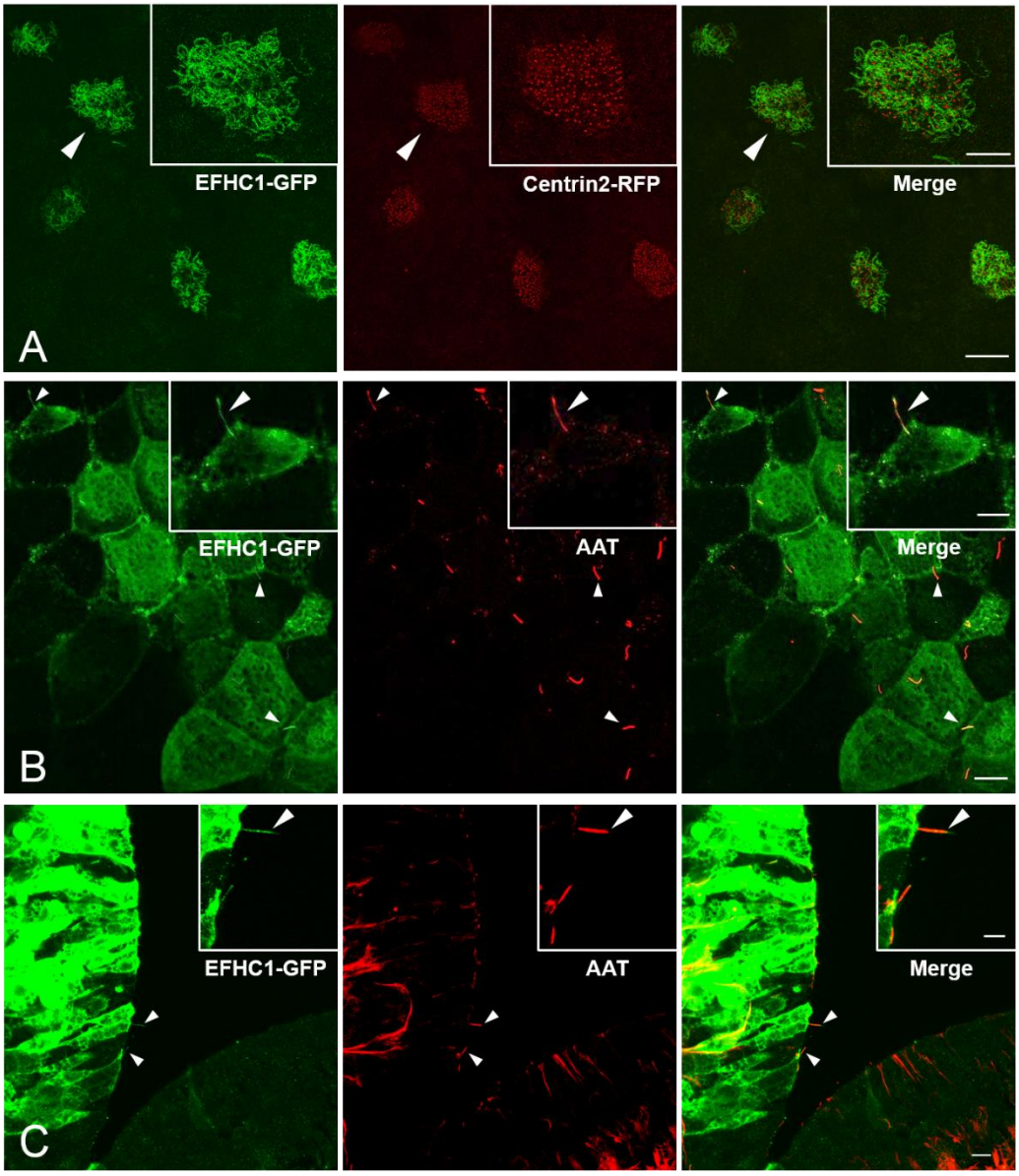

Figure4-2. Localization of EFHC1 in various cilia. (A) EFHC1-GFP localizes to the motile cilia. Fertilized eggs were injected with RNAs encoding EFHC1-GFP and centrin2-RFP; ectodermal explants were dissected at ~stage 9 and fixed at stage22 for fluorescence microscopy analysis. EFHC1-GFP is localized to the cilia of multiciliated cells in ectodermal explants. Scale bar: 20µm (main) and 10µm (insert). (B) EFHC1-GFP localizes to the single cilia in the gastrocoele roof plate regions. Embryos injected with EFHC1-GFP RNA were dissected at stage 19 and fixed and probed with antibodies against GFP (green) and acetylated tubulin (AAT, red). Arrows indicate the GRP cilia with EFHC1-GFP signal. Scale bar: 15µm (main) and 8µm (insert). (C) EFHC1-GFP localizes to the primary cilia at the ventral surface of the neural tube. The neural tube region of stage 26 embryos were sectioned and stained for injected EFHC1-GFP (green) and acetylated tubulin (grey). Arrow indicates the primary cilium with EFHC1-GFP signal. Scale bar: 10µm (main) and 5µm (insert).

The N-terminal domain is required for EFHC1 ciliary localization

EFHC1 is a conserved protein with three DM10 domain of unknown function and a putative EF hand calcium binding motif at its C terminus. The *Xenopus* EFHC1 lacks the EF hand motif, suggesting this region is less evolutional conserved and not necessary for its ciliary association. To determine which domain is involved in EFHC1 ciliary localization, we made several GFP tagged truncation mutants; each of them lacks an individual DM10 domain or only contains the very N-terminal region (Fig4-3A). Again, the ectoderm explants and the confocal microscopy were applied to study the localization of these mutants in multiciliated cells. The results showed that both EFHC1-Δ2 and EFHC1-Δ3 still localized to the cilia on the explants. In contrast, GFP signal of EFHC1-Δ1 was no longer observed in the cilia. It suggested the N-terminus and the first DM10 domain are critical for EFHC1 ciliary association. The last mutant we tested is GFP fused with N-terminal 92 amino acids. Surprisingly, this truncation was able to localize to the cilia region in multiciliated cells. For each mutant, a cytoplasmic pool of GFP was observed as seen with full length protein (Fig4-3B). Together, this mutation analysis indicates the N-terminus itself is required and sufficient for the localization of EFHC1 at the motile cilia, while deletion of each individual DM10 domain does not influence its localization.

EFHC1b morpholino specificly reduces EFHC1b protein expression

To define the function of EFHC1 in the early embryo we designed and synthesized a translation blocking morpholino (EFHC1 MO) from GeneTools, LLC. The morpholino sequence was used in a blast search against the latest (7.1) version of the *X. laevis* genome. The only two hits are EFHC1a and EFHC1b. It is not known whether EFHC1a is expressed in *X.laevis* and the start site remains to be annotated. Two rescue plasmids were built respectively. The pCS2-EFHC1-match plasmid encodes an RNA that contains an exact match to the EFHC1 MO sequence, while the pCS2-EFHC1-GFP-rescue plasmid encodes an RNA in which the region targeted by the EFHC1 MO was altered to reduce

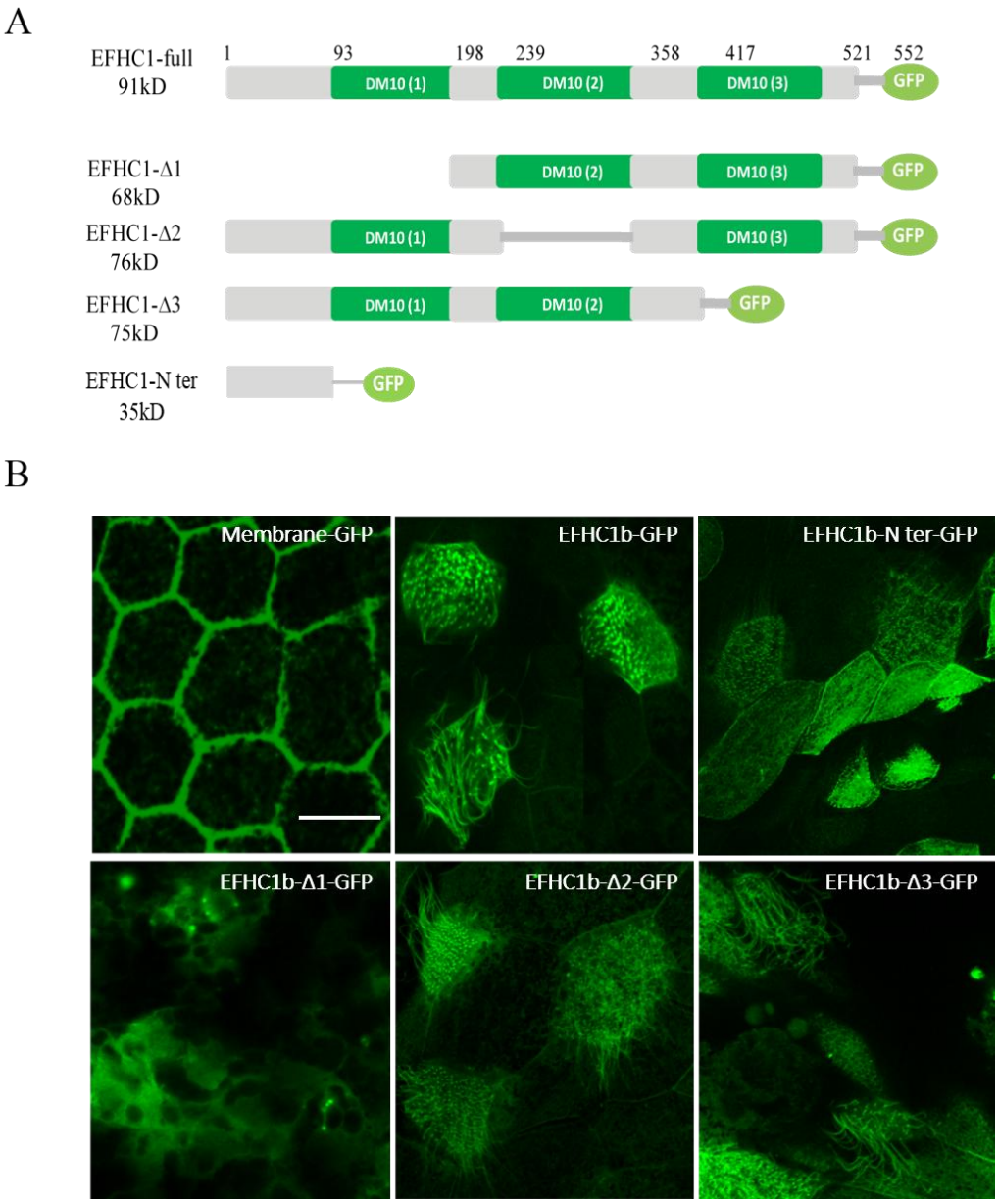

Figure4-3. The N-terminus of EFHC1 is required for its ciliary localization. (A) Schematic of truncation EFHC1 mutant alleles designed for the localization analysis of structural domains. (B) Subcellular localization of EFHC1 mutants. Ectoderm transplant from embryos injected with RNAs of membrane-GFP, EFHC1-GFP, EFHC1-N ter-GFP, EFHC1-Δ1-GFP, EFHC1-Δ2-GFP, and EFHC1-Δ3-GFP. The fusion proteins were visualized by GFP fluorescence. Scale bar: 10μm.

complementarity to the morpholino but without changing the final polypeptide sequence (Fig4-4A). Both plasmids were sequenced to confirm the absence of mutations introduced in the process of construction. We first confirmed the effectiveness of the EFHC1 MO by injecting fertilized eggs with RNAs encoding GFP or EFHC1-GFP-match together with either a control or EFHC1 MO. The level of EFHC1-GFP protein that accumulated was dramatically reduced by the EFHC1 MO but unaffected by the control MO (Fig4-4B).

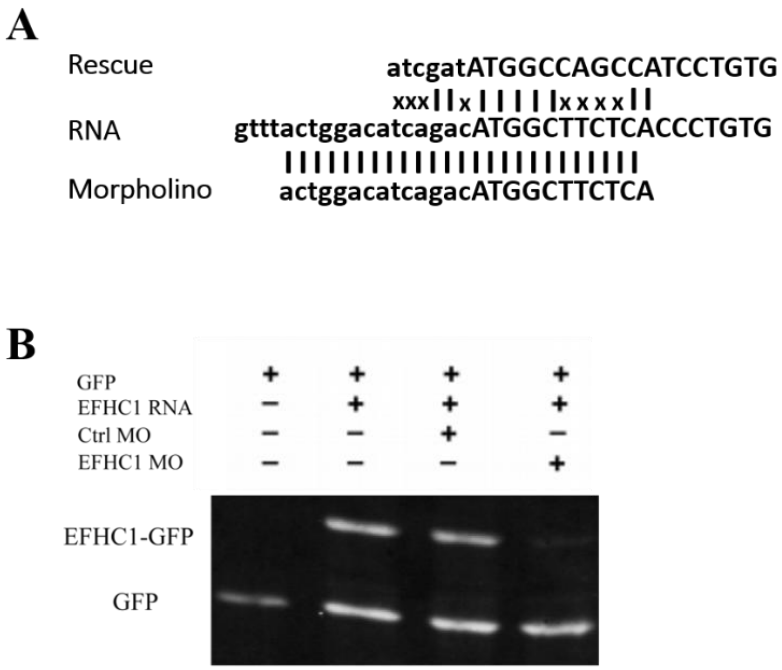

Figure4-4. Specificy of EFHC1 morpholino. (A) The EFHC1b MO aligns with the translation start region of the *EFHC1* RNA; this same sequence is present in the EFHC1-GFP-match RNA. EFHC1-GFP-rescue has a number of mismatches in the morpholino-binding region. (B) Immunoblot analysis was carried out using an anti-GFP antibody. Embryos were injected with RNAs encoding GFP and EFHC1-GFP match and either control or EFHC1 MO and analyzed at stage 11. EFHC1 MO reduced EFHC1-GFP protein levels.

Loss of EFHC1 affects ciliated cell and cilia formation

Given the association of EFHC1 with ciliary axonemes (Fig4-2), we characterized the effect of reducing EFHC1 protein levels on the formation of multiciliated cells in ectodermal explants as well as the number of cilia per ciliated cell. Typically, control or EFHC1 morpholino was co-injected with RNA encoding a membrane-bound form of GFP that marks cell outlines. Explants were generated from embryos at stage 9 and examined when control embryos reached stage 18. Using confocal microscopy and a semi-automated quantitation system (described in Shi et al., 2014), we found that both the number of ciliated cells per unit area (ciliated cell density) and the number of cilia per ciliated cell were reduced in EFHC1 morphants (Fig4-5). Both EFHC1 morphant phenotypes were rescued by the injection of RNA encoding the EFHC1-GFP-rescue construct. None of the EFHC1 deletion mutants can rescue this ciliary phenotype (Fig4-6).Additionally, we have found fewer and shorter gastrocoele roof plate cilia in EFHC1 morphant embryos (data not shown). Effects of the EFHC1 MO on primary cilia were more difficult to discern, since neural tube morphology was disrupted in morphant embryos (see below).

EFHC1 functions in embryonic patterning

Two types of whole embryo morpholino studies were carried out for the purpose of determining whether EFHC1 has a role in embryonic patterning. “Two of two” experiments can be used to check the general growth of embryos (Shi et al., 2014). Both cells of two-cell embryos were injected with MO. Two of two EFHC1 MO injections produced embryos that were visibly abnormal, smaller, with a number of defects including a delayed development. Since EFHC1 RNA was found in neural crest and central nervous system, I decided to specifically study these two tissues in EFHC1 morpholino knockdown embryos. For this study, I used “one of two” experiments, in which one blastomere of a two cell stage embryo was injected equatorially with morpholino together with RNA encoding β-galactosidase as a lineage tracer. In situ hybridization-based analyses of early neurula stage embryos revealed defects in the expression of the neural crest markers of Twist1 and Sox9. The signal of these two markers

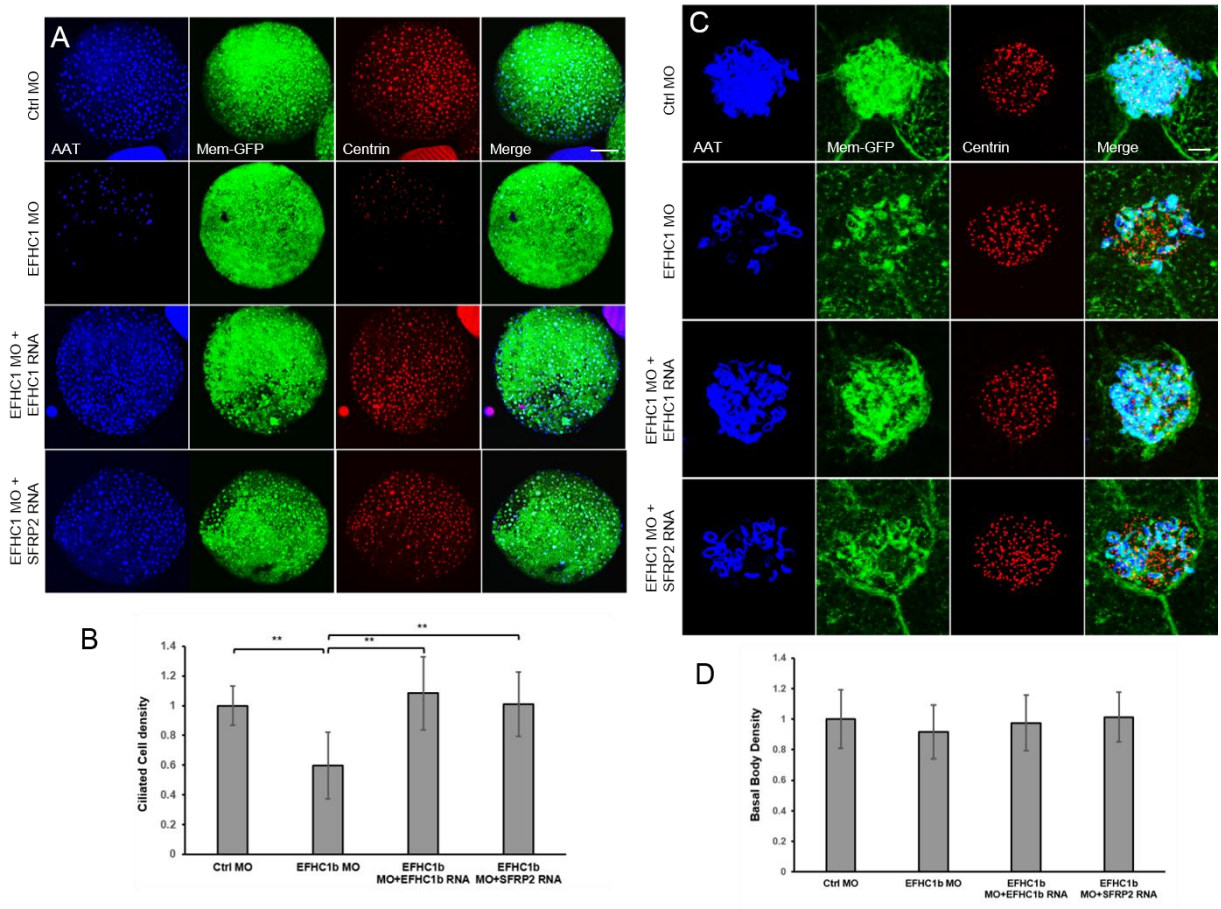

Figure4-5. Loss of EFHC1 leads to motile cilia defects on ectoderm explants. (A) Ciliated cell density is decreased in explants from EFHC1 morphants. Explants were stained with GFP, Cen2 and acetylated tubulin (AAT) antibodies. Scale bar: 100µm. (B) Quantification of of ciliated cell density shown in A. (C) The number of cilia per cell is affected in EFHC1 morphants while basal body density remains the same. Scale bar: 5µm. (D) Quantitation of the EFHC1 morpholino's effect on basal body density. Explants were dissected from embryos injected with either control MO, EFHC1 MO as well as the indicated RNAs. Membrane GFP is used as a tracer for injection. Membrane-GFP was visualized using an anti-GFP antibody, while anti-acetylated tubulin and anti-centrin antibodies were used to visualized cilia and basal bodies, respectively. (Comparisons between conditions are marked by horizontal bars (** for p<0.01).

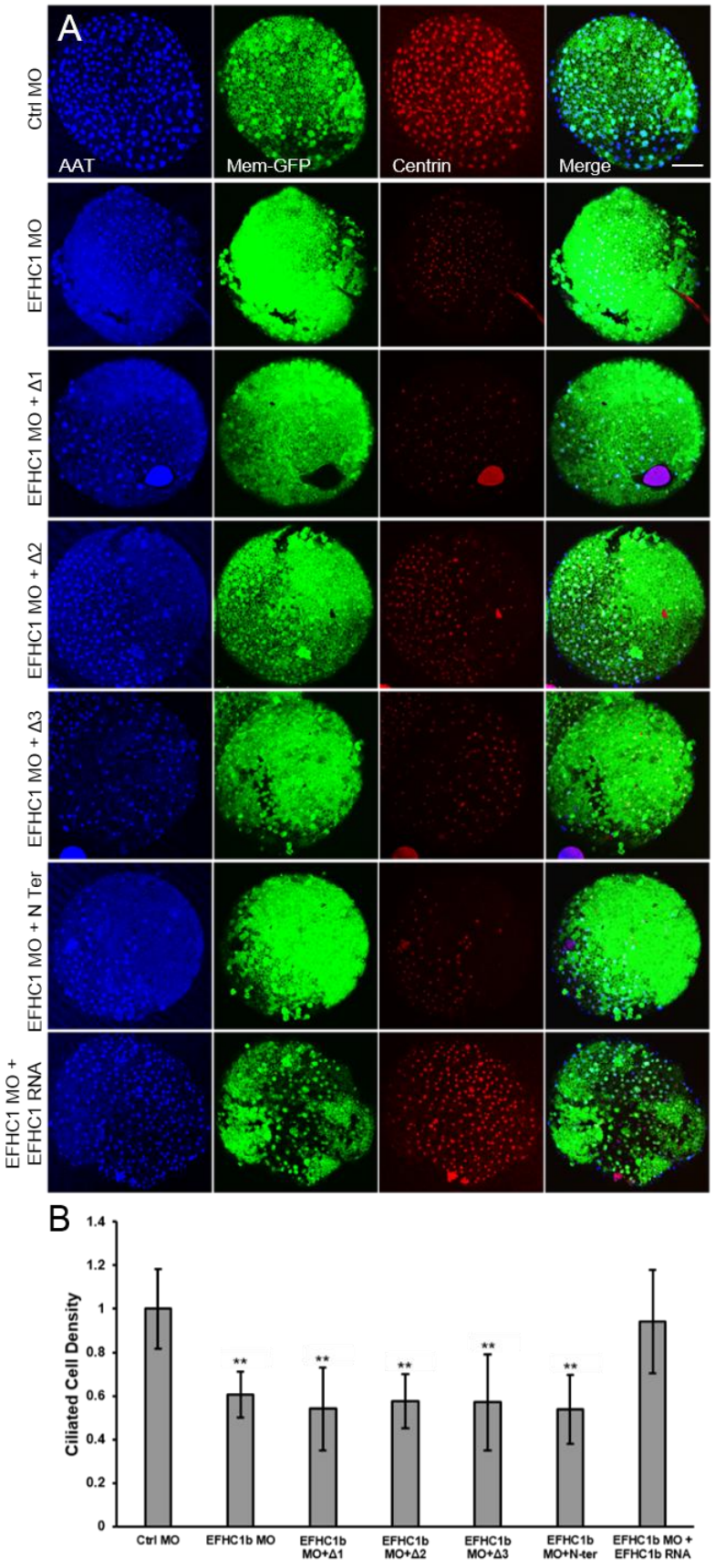
A
Ctrl MO
EFHC1 MO
EFHC1 MO + Δ1
EFHC1 MO + Δ2
EFHC1 MO + Δ3
EFHC1 MO + N Ter
EFHC1 MO + EFHC1 RNA
AAT
Mem-GFP
Centrin
Merge
B
Ciliated Cell Density
1.4
1.2
1
0.8
0.6
0.4
0.2
0
**
Ctrl MO
EFHC1b MO
EFHC1b MO+Δ1
EFHC1b MO+Δ2
EFHC1b MO+Δ3
EFHC1b MO+N-ter
EFHC1b MO + EFHC1b RNA

Figure4-6. EFHC1 truncation mutants cannot rescue the ciliary defects in EFHC1b morphants. (A) Immuno-fluorescence images of explants from embryos injected with EFHC1 MO, as well as the indicated RNAs of EFHC1 mutant alleles shown in Fig4-3.Membrane-GFP was visualized using an anti-GFP antibody, while anti-acetylated tubulin and anti-centrin antibodies were used to visualized cilia and basal bodies, respectively. Scale bar: 100µm. (B) Quantification of ciliated cell density is shown. (** for $p<0.01$).

was reduced in the morpholino injected side (Fig4-7A). When EFHC1-R-GFP was co-injected with EFHC1-morpholino, the reduced signal of Sox9 and twist was restored.

Once induced, neural crest cells undergo migration to their destination. Since defects in neural crest induction at stage18 embryos was observed, I followed migration behavior of neural crest in EFHC1 morphants. For this experiment, less EFHC1 morpholino was injected, so that neural crest was formed at neurula stage. Then the embryos were allowed to grow to stage25 when neural crest migration is well underway. Embryos injected with control morpholino had the neural crest markers forms the expected three striped pattern, which is totally absent in the EFHC1 morphants (Fig4-7B). The loss of Twist1 and Sox9 expression in morphants was rescued by injection of EFHC1-R-GFP and by the EFHC1-DM10-Δ3-GFP mutant RNA. Quantitation of these rescue studies is shown in Fig4-7C. Approximately 75% of the embryos showed this defect when EFHC1 MO was injected. When rescued with full length EFHC1 protein and mutant missing the last DM10 domain, only 30% embryos had the abnormal expression of neural crest. Taken together, morpholino mediated EFHC1 knockdown causes defects in both neural crest induction and neural crest migration.

Neural crest migration is a complex developmental process, involving significant changes of cytoskeleton reorganization, cell adhesion, matrix adhesion and cross talk between these components. To distinguish which component is responsible for the inhibition of neural crest migration in EFHC1 morphants, the neural crest cells or the surrounding environment, a transplant assay was performed. Premigratory neural crest tissue was dissected from neurula donor embryos injected with EFHC1 or control morpholino and GFP RNA as a tracer. Then the premigratory neural crest from host wild type embryos was removed and replaced with the donor tissue. The migration of the neural crest cells in the chimera was visualized by GFP signal and monitored until stage 24. Both of the tissue grafts were successful as shown by constant fluorescence signal. The donor neural crest cells from control embryos migrated normally, producing three seperate GFP streams. In contrast, transplanted neural crest from

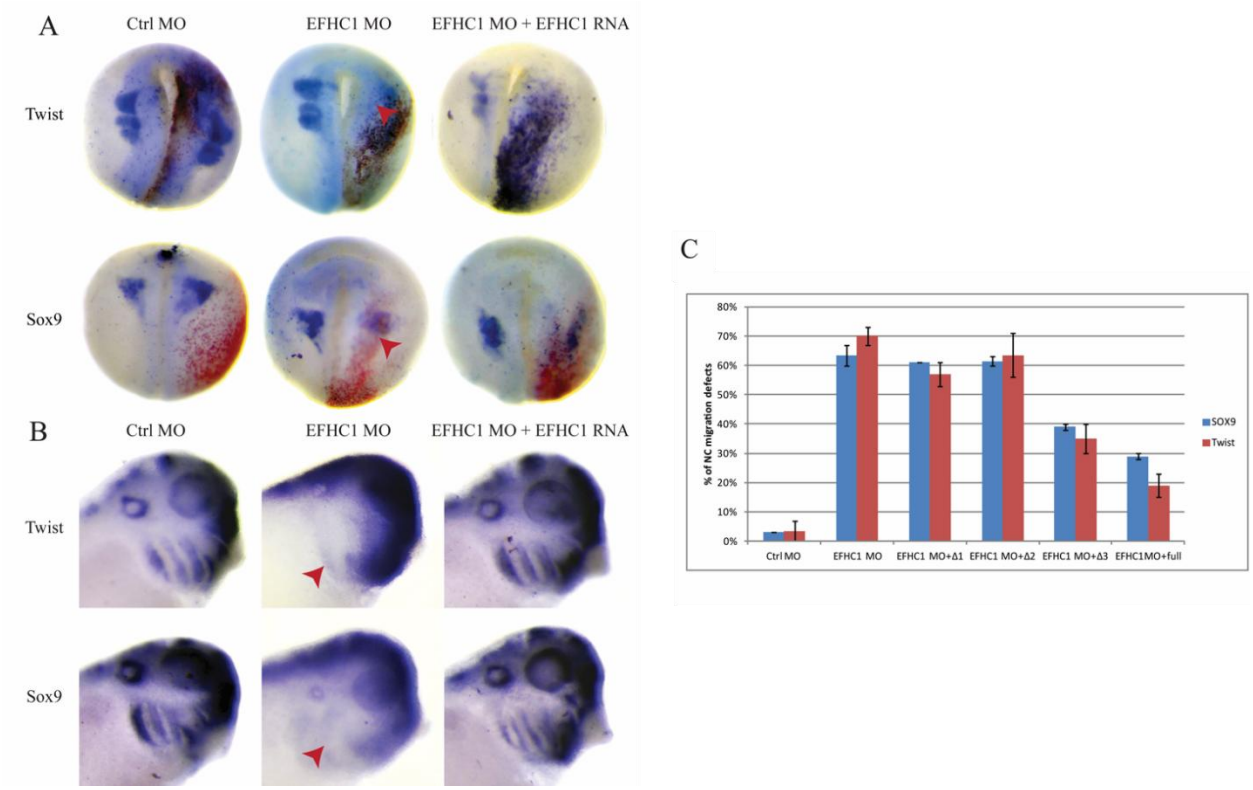

Figure4-7. Depletion of EFHC1 affects neural crest induction and migration. (A) *In situ* hybridization studies showed knockdown of EFHC1 produced a dramatic reduction in both *Sox9* and *Twist1* in stage 18 (A) and stage 25(B) embryos. These effects were rescued by the co-injection of EFHC1-GFP-rescue RNA with EFHC1 MO. Loss of neural crest markers was rescued by EFHC1-Δ3 mutant**.** All embryos tested in (A) were coinjected with RNA encoding β -galactosidase (red) as a lineage. Twist and Sox9 are visualized by the blue staining. Red arrows indicate the regions where the level of neural crest markers are reduced. (C) Quantification of (B) and the embryos co injected of EFHC1 MO with the EFHC1 mutants. Blue refers to Sox9 and red refers to twist.

EFHC1 morphants remained in the grafted region and failed to migrate to the peripheral destination (Fig4-8B). In addition, an in vitro assay of neural crest migration was performed as described previously (Alfandari et al., 2003). Neural crest tissues were dissected from EFHC1 or control morpholino injected neurula stage embryos. Then the explants were seeded into fibronectin treated 24-well plates and monitored by live cell images for 24hrs. For control tissues, migration of neural crest cells started 1hr after seeding and a single layer of cells were seen after 8hrs at the migratory leading range. In contrast, neural crest from EFHC1 morphants remained in the original seeding place and there was no obvious migratory behavior during the entire 24hr time window. Occasionally, single cells were seen at the peripheral of the explants (Fig4-8C).

An observation in the stage18 embryo experiment when EFHC1-GFP RNA was coinjected to rescue the neural crest defect. There was ectopic expression of Twist in the injection side. In contrast, the Sox9 expression with EFHC1-R-GFP rescue was quite normal. This twist specific ectopic expression may be caused by over expression of EFHC1. To test this idea, we repeated this "one of two" experiment by injecting EFHC1-GFP alone without EFHC1 morpholino. First, overexpression of EFHC1 produced embryos of morphologically normal appearance at stage 22 compared to control embryos (Fig4-9A). Then we analyzed the twist expression by in situ hybridization on stage18 embryos as before. The whole injected blastomere was covered by the ectopic twist signal. Two more neural crest markers snail and slug were tested and both of their expression pattern stayed normal, similar to Sox9 (Fig4-9B, C). Thus, this data confirmed that overexpression of EFHC1 expanded twist expression domain in neurula stage embryos. I investigated which domain of EFHC1 is responsible for the altered twist expression. Besides the EFHC1 mutants that were studies previously for ciliary localization, additional mutants containing individual DM10 domains and the missing N-terminus with GFP tag were generated accordingly. Surprisingly, over expression of each mutant could trigger this irregular twist expression. Almost all of the injected

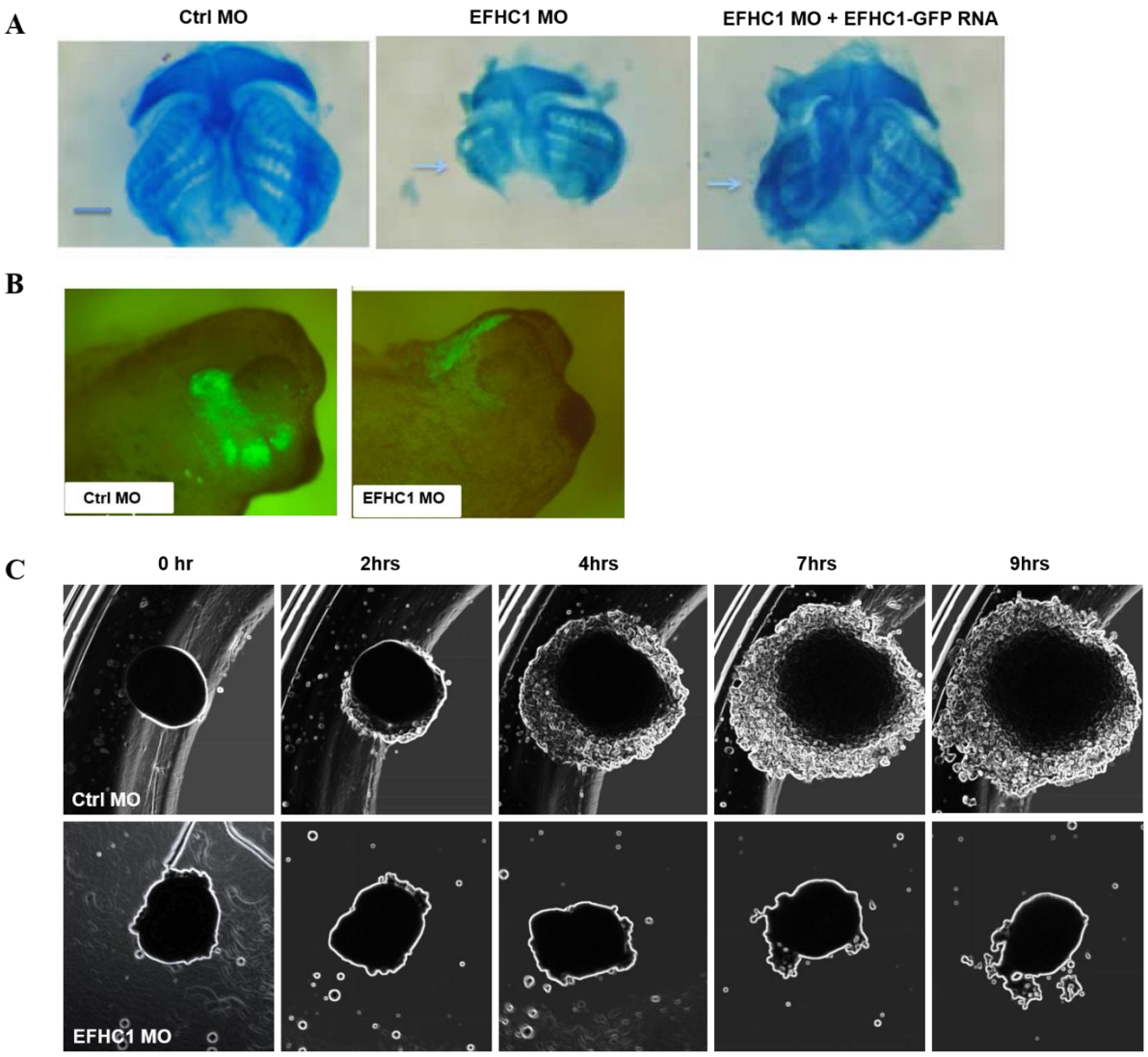

Figure4-8. Knocked down of EFHC1 results in Neural crest migration both in vivo and in vitro. (A) Alcian Blue staining revealed defects in EFHC1 MO injected embryos at later stage, compared to control embryos; these defects were rescued by co-injection of EFHC1-GFP-rescue RNA. (B) Neural crest transplants from GFP injected embryos migrate normally, while the analogous region from EFHC1 morphant embryos failed to migrate. (C) Neural crest explants from EFHC1 morphants fail to migrate in vitro. Live cell images of the neural crest explants from embryos injected either control MO or EFHC1 MO. Migration events were monitored for entire 24hrs and the first 9hr period is shown here. The explant from control morphant migrates to peripheral environment. In contrast, the explant from EFHC1 morphant remains the same shape without cell migration. The experiments in (A) and (B) were done by Dr. Jianli Shi.

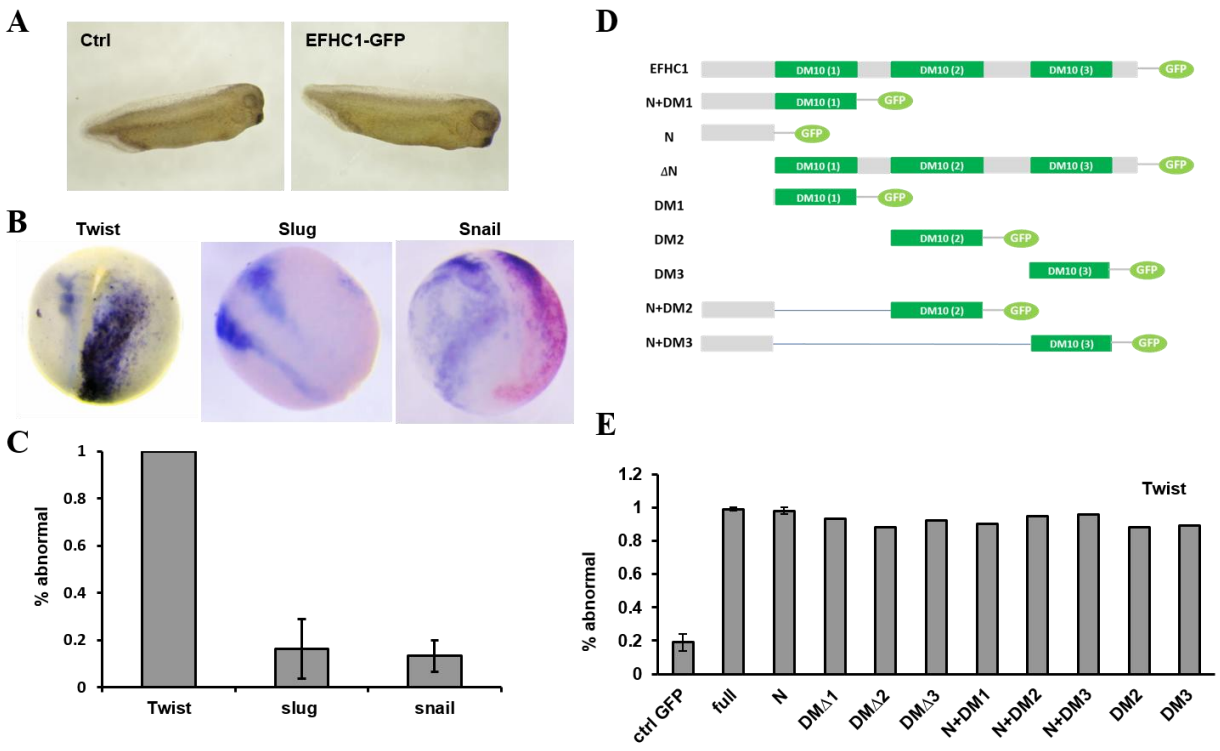

Figure4-9. Effects of EFHC1 overexpression on neural crest markers. (A) Morphology of whole embryos is normal when EFHC1 is overexpressed. (B) No defects are seen in Slug and Snail expression when EFHC1 is overexpressed. In situ hybridization of neural crest markers, Twist, Slug and Snail. (C) Quantification of the in situ experiment in B. (D) Schematic of EFHC1 mutants. (E) All of the EFHC1 mutants lead to the ectopic Twist expression.

embryos showed this phenotype (Fig4-9D, E). With the presence of the endogenous full length EFHC1 and limited knowledge of interacting proteins, we cannot draw a clear conclusion about this experiment. Further study is required to better understand how EFHC1 influences Twist expression.

In early neurula stage embryos, the central nervous system develops specific spatial pattern of various markers. To define the function of EFHC1 in this tissue, three common markers were used for in situ hybridization-based analyses. EFHC1 knockdown produced disrupted central nervous system patterning of neural-β-tubulin (Tubb2b), Engrailed, and Krox20. Both the uninjected blastomere and the embryos injected with control morpholino exhibited ordered expression patterns. Again, these defects were reversed by the co-injection of EFHC1-R- GFP and the EFHC1-DM10-Δ3-GFP mutant RNA (Fig4-10A). More than 70% of EFHC1 morphants harbored this phenotype and EFHC1-R-GFP and EFHC1-DM10-Δ1-GFP suppressed the abnormal rate to 30% (Fig4-10B). In contrast, there was no difference observed when EFHC1-DM10-Δ1-GFP and EFHC1-DM10-Δ2-GFP were co-injected. Together, the data above indicates EFHC1 plays a role in embryonic patterning and neural crest migration. The first two DM10 domains are critical for this function, which further suggests that the last DM10 domain along with the C terminus (including the EF hand calcium binding motif in orthologs) may be less conserved for the proteins's functions.

Our previous study on Chibby showed that depletion of Chibby caused similar embryonic patterning defects in both neurula and later stage embryos. It is possible that the two proteins function together in the same pathway. To define the relation of the two proteins, I investigated whether Chibby-R-GFP can rescue the EFHC1 depletion defects observed in the neural crest and in the central nervous system. Embryos were co-injected with EFHC1 morphlino and Chibby-R-GFP RNA. Unlike EFHC1-R-GFP, there were still approximately 70% of the embryos exhibiting deficient neural crest migration despite Chibby-R-GFP expression (Fig4-11). This suggested that EFHC1 is not functioning through Chibby in neural crest migration.

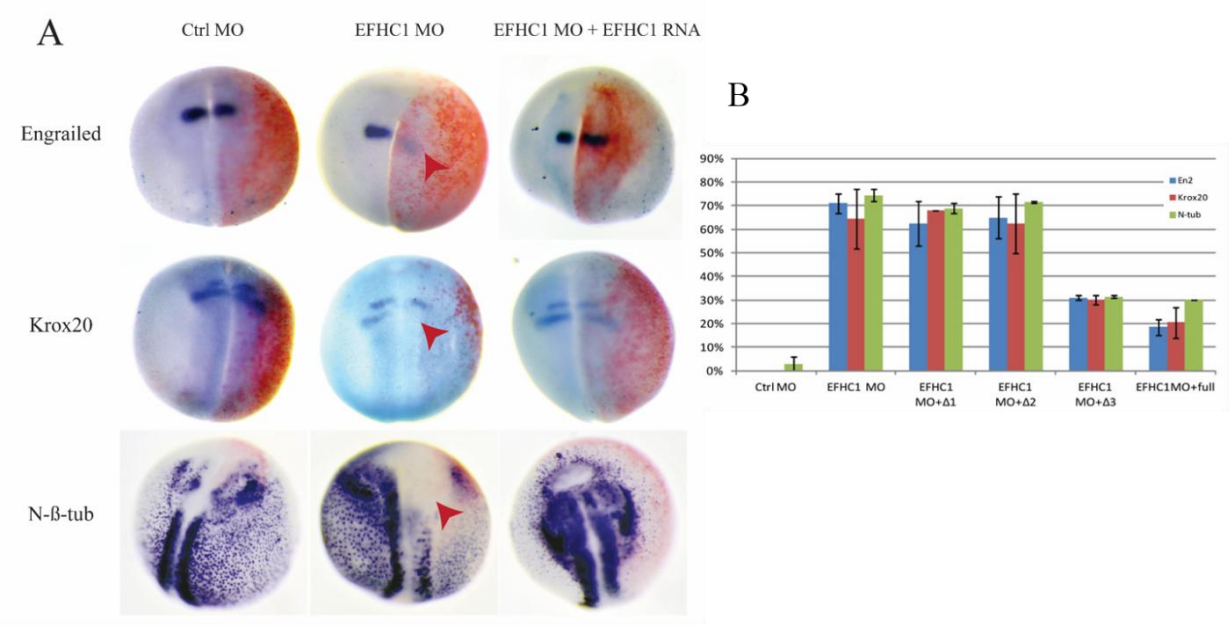

Figure4-10. Depletion of EFHC1 disrupts central nervous system patterning. (A) *In situ* hybridization studies revealed the loss of the neural patterning markers *Engrailed*, *Krox20* and *N-b-tub* (in blue). These phenotypes were rescued by injection of EFHC1-GFP-rescue RNA. Embryos were injected with either control MO, EFHC1 MO, or EFHC1 MO together with EFHC1-GFP RNA. All embryos were injected with RNA encoding β -galactosidase (red) as a lineage tracer. (B) Loss of neural patterning marker was rescued by EFHC1-Δ3 mutant. Quantitation of (A) and the embryos co-injected of EFHC1 MO and the truncation mutants.

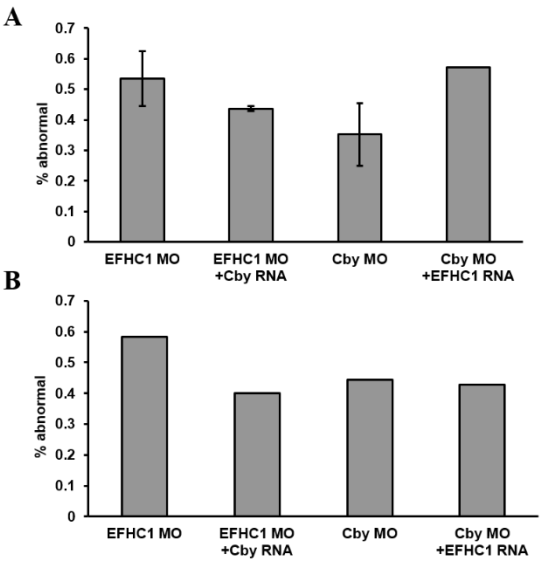

Figure4-11. The CNS and NC defects in EFHC1 morphants cannot be rescued by Cby RNA, and vice versa. (A) Quantification of embryos showing disrupted central nervous system marker En2. (B) Quantification of embryos showing disrupted neural crest marker Twist.

EFHC1 regulates gene expression and Wnt8 signaling.

In the course of analyzing EFHC1 morphant embryos, we noted the loss of Tubb2b expression (as monitored by in situ hybridization) in neural ectoderm (see above) and in ectodermal explants. This change in Tubb2b RNA levels in explants and the changes in the expression of CNS and neural crest markers seen in EFHC1 morphants are similar to those described previously in Cby morphants (Shi et al., 2014). Cby is a basal body associated protein that is known to act as intracellular antagonist of β-catenin mediated Wnt signaling (Shi et al., 2014). This led us to examine the levels of Wnt8, Tubb2b, BMP4, Noggin, and FGF8 RNAs in EFHC1 morphant ectodermal explants at stage 18. As in the case of Cby, EFHC1 morphant explants displayed a dramatic increase in the level of Wnt8A and a decrease in Tubb2b levels – the change in Wnt8A RNA level was greater in explants (at stage 18) than in whole embryos (at stage 11). Unlike Cby morphant explants, there was no apparent change in the levels of BMP4 or Noggin RNA levels (Fig4-12B). Among the truncation mutants, only EFHC1-DMΔ3 rescued the level of Wnt8 RNA. This conclusion is supported by studies using the TOPFLASH reporter, which responds to increased levels of β-catenin. While reduction of EFHC1 levels increases TOPFLASH activity, EFHC1-GFP does not directly inhibit the activation of the TOPFLASH reporter by G-β-catenin (a stabilized form of β-catenin) (Fig4-12D). Together, the rescue data suggested the changes in RNA level were secondary "feedback" effects associated with increased canonical Wnt signaling.

It is known that many transcriptional factors play roles in ciliogenesis and various signaling pathways are reportedly influenced by depletion of ciliary protein (Chung et al., 2012). I used qPCR experiments on several genes involved in regulating cilia formation and ciliated cell differentiation to determine whether the RNA level of them are affect in EFHC1 morphants . Preliminary data showed that the mRNA level of Notch1 is slightly upregulated in the explants of EFHC1 morphants. The change of Notch1 RNA level may be related to the defect in ciliated cell formation (Fig4-13).

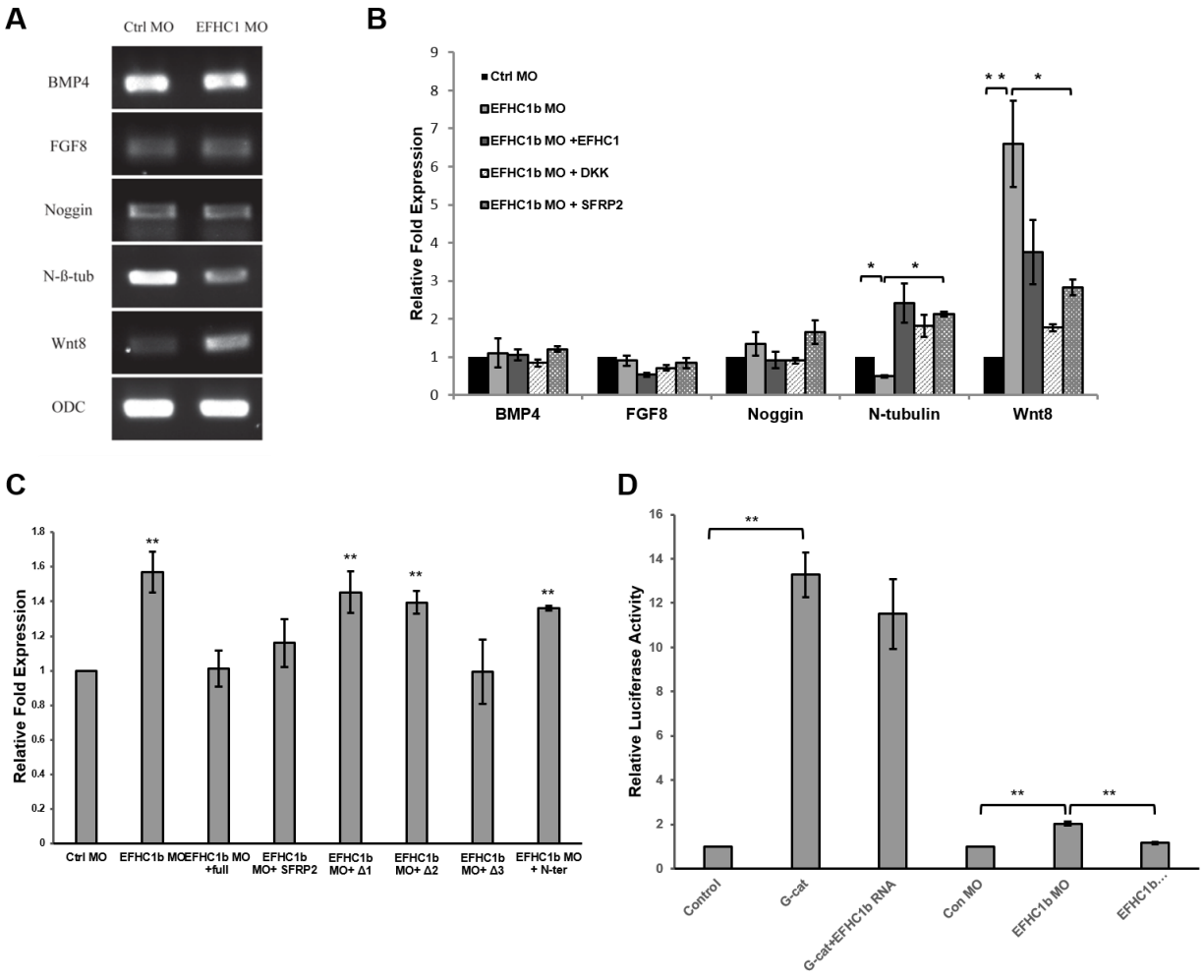

Figure4-12. Gene expression and Wnt signaling are altered in EFHC1b morphants. (A) Control and EFHC1 morpholino explants were analyzed at stage 18 using RT-PCR; EFHC1 morphant explants displayed decreased levels of *Neural tubulin* RNAs, and increased levels of *Wnt8* RNA. Levels of BMP4, Noggin and *FGF8* RNA were unchanged. (B) qPCR analyses of control and EFHC1 morphant explants co-injected with EFHC1-GFP-rescue, Dkk1, or *SRFP2* RNAs. Both EFHC1-GFP and the two Wnt signaling inhibitors returned all RNAs to control levels. (C) qPCR analyses of control and EFHC1 morphant explants co-injected with EFHC1-GFP-rescue, *SRFP2 or EFHC1 mutant* RNAs on *Wnt8* RNA. Besides the EFHC1-GFP and the Wnt inhibitor SFRP2, EFHC1-Δ3-GFP also brought the Wnt8 RNA to control level. (D**)** Embryos were injected with TOPFLASH and FOPFLASH (control) plasmid DNAs together with Δ G-β -catenin RNA either alone or together with GFP or EFHC1-GFP RNAs or control, EFHC1 MO and EFHC1 MO with SFRP2. The Y-axis indicates fold increase relative to the control TOPFLASH/FOPFLASH value (set equal to 1). Comparisons between conditions are marked by horizontal bars; in each case, *p*-values were<0.05. The experiments in D was done by Dr. Jianli Shi.

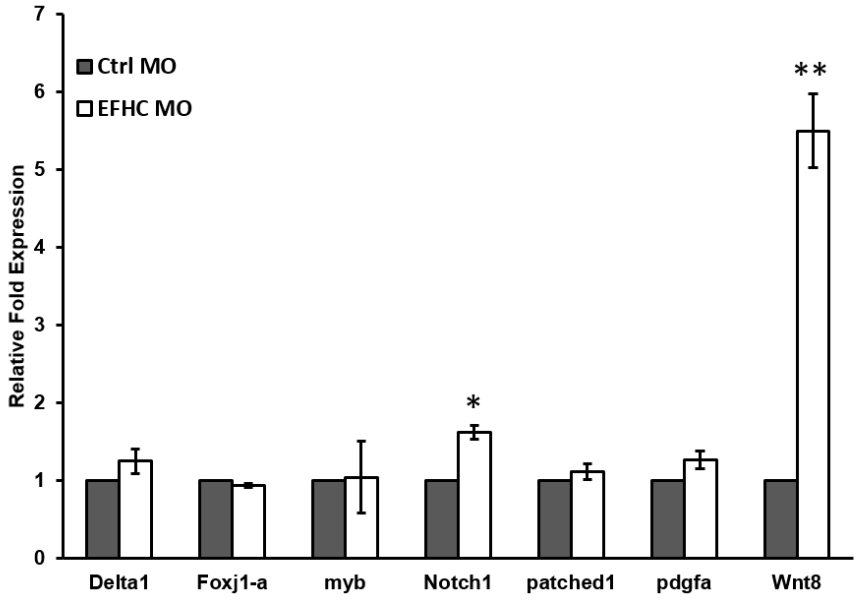

Figure4-13. Notch1 RNA level is changed in EFHC1 morphant explants. Control and EFHC1 morpholino explants were analyzed at stage 18 using qPCR; EFHC1 morphant explants displayed increased levels of *Notch1* RNAs and *Wnt8* RNA as positive control. Levels of Delta1, Foxj1-a and *myb,* patched1 and pdgfa RNA were unchanged.

IV. Discussion

The EFHC proteins, EFHC1 and EFHC2, are a highly conserved but poorly understood eukaryotic protein family. While mutations in hEFHC1 have been reported to account for between 3 to 9% of all cases of JME around the world(de Nijs et al., 2012), how changes in EFHC1 lead to disease effects remain obscure. The situation is further complicated by the observation that JME-associated mutations are also found in apparently normal individual(Bai et al., 2009; Pal and Helbig, 2015; Subaran et al., 2015) and different EFHC1 alleles may act in distinctly different mechanisms(Stogmann et al., 2006).

Previous studies have found that EFHC1 to be a component of the motile ciliary axonemal component. In *Chlamydomonas* Rib72 was identified as a component of the protofilament ribbon in

axonemal doublet microtubule(Ikeda et al., 2003). My own studies in *Tetrahymena* indicate that EFHC1 and EFHC2 are associated with both the basal body and the cilia (Chapter2 and3). Both of them are required for MIP structure inside the doublet microtubule. In the mouse, EFHC1 has been found associated with motile cilia and the sperm flagella. Earlier reports that EFHC1 was associated with cytoplasmic microtubule and spindle systems appear to have been due to antibody cross-reactivity(Yamakawa and Suzuki, 2013). In *Xenopus* explants and embryos, I found that EFHC1-GFP was localized to both motile cilia on the multiciliated cells on the ectodermal explants and the cells on gastrocoele roof plate. In contrast to a report in the mouse(Ikeda et al., 2005), I do find EFHC1-GFP to be associated with primary cilia in the developing neural tube. Originally no EFHC2 gene had been identified in X. laevis, but a BLAST search of the 7.1 genome assembly using the X. tropicalis EFHC2 coding region sequence reveals two likely EFHC2 genes. However, it is not known whether the two genes are expressed.

Although cilia are still present in EFHC1 null mice (Narita et al. 2012), we observed a decrease of ciliated cells and the number of cilia per cell in EFHC1b morphant ectodermal explants, as well as effects on gastrocoel cilia, and severe defects in the CNS and in neural crest development. The differences between the *X. laevi*s EFHC1b morphant and the mouse EFHC1 null phenotypes presumably arises from the dramatically different modes of development between the two organisms. It is also possible that in the mouse the presence of EFHC2 partially suppresses the EFHC1 null phenotype.

The mechanism by which mutations in EFHC1 lead to JME remains unclear. EFHC1 has been reported to interact with redox-sensitive TRPM2 channel protein and mutations in EFHC1 have been proposed to lead to increased cell death (Katano et al., 2012). It has also been reported that mutations in EFHC1 act in a dominant-negative mechanism disrupting brain development to various extents(de Nijs et al., 2009). What is clear from my studies is that down-regulating EFHC1 expression in *Xenopus*, even at time when there are no cilia present, leads to effects on gene expression, specifically changes in

Wnt8a RNA levels. The mechanism of these EFHC1 morpholino effects is not clear, but it is clearly distinct from the mechanism by which Chibby acts, that is directly through effects on β-catenin. One possibility is that the mechanism is related to that described for the loss of the ciliopathy-associated proteins BBS4 and OFD1, which lead to defects in the centrosomal proteosome and the stabilization of a number of target involved in signaling(Liu et al., 2014). Recently, two transcription factors, the β-catenin-binding HMG box protein TCF4 and the Zinc finger transcription factor ZBED1 is indicated to interact with EFHC1(Sahni et al., 2015), which may explain why down-regulation of EFHC1 influence the gene expression. The ability of the secreted Wnt inhibitor SFRP2 to return the density of multiciliated cells and the levels of *Wnt8a* and *Tubb2b* RNAs to near control levels suggests that an autocrine (and perhaps paracrine) Wnt signaling feedback loop, blocked by SFRP2, is involved in these effects.

Chapter 5. Conclusion

Basal bodies and cilia are conserved organelles composed of hundreds of polypeptide components. Basal bodies are closely related to the centrioles within the centrosomes, which are critical for cellular division and cellular organization. Centrosome and centriole abnormalities are reported to be the markers for malignant tumors(Schatten et al., 2000). Basal bodies and centrioles are interconverted in many cell types in the context of ciliogenesis, where basal bodies are the platforms to nucleate the axonemes of cilia. Different types of cilia have various and often over-lapping functions, from driving fluid flow and cellular motility, to the establishment of distinct cellular domains and morphologies, to modulating intracellular signaling involved in tissue patterning. Defects in cilia formation and function have been implicated in a wide range of human pathologies, including brain malformations and malfunctions, retinal dystrophies, cystic kidney disease, liver fibrosis, and skeletal abnormalities. Developing a molecular level understanding of the structural and functional aspects of cilia and cilia-associated proteins is therefore critical to understanding basic biological processes involved in cilia-related human pathologies. With the application of genomic and proteomic tools in recent years, more and more novel components have been identified within these organelles. However, we are not yet at the destination because these new techniques have provided us a long list of basal body and ciliary components to determine how they cooperate to keep cilia and basal bodies functional.

My work here investigates the localization of four basal body candidate components identified from a basal body proteome in *Tetrahymena*(Kilburn et al., 2007). All of the candidates, BBC31, BBC52, BBC57 and BBC73, are conserved through eukaryotes and human orthologues have been identified by sequencing analysis. Structural domains known to be involved in ciliary functions are found in each of the four candidates, such as the EF-hand motif in Bbc52, Bbc57, and Bbc73 and CH domain in Bbc31. By endogenous tagging of the BBC proteins with mCherry, I found Bbc31 is not associated with the core

structures of either the basal body or the cilium. Bbc31-mCherry is predominantly present at the microtubule based accessory structures of basal body in *Tetrahymena*. Basal body accessory structures, such as the striated rootlet in vertebrates and its analog kinetodesmal fibers in *Tetrahymena*, play important roles in stabilizing basal body orientation and ensuring ciliary alignment coupled to increasing mechanical cilia force(Chien et al., 2013; Galati et al., 2014). My preliminary analysis on somatic *bbc31Δ* cells showed disrupted basal body cortical row organization. Bbc31 is accumulated within the postciliary and transverse microtubule bundles, which are highly stable and not easily disaggregated by regular treatments that disrupt microtubules (Wloga and Frankel, 2012). This suggests Bbc31 may also function in stabilizing microtubules more generally. Studies of Bbc31 homolog CLAMP in mouse and *Xenopus* reveal that these proteins are associated with well-organized microtubule bundles and dynamically interact with and stabilize microtubules(Dougherty et al., 2005; Werner et al., 2014).

Bbc52 and BBC57 are paralogs in *Tetrahymena*, and their human orthologues, C15orf26 and CAPSL, have been linked to primary ciliary dyskinesia and type I diabetes diseases (Austin-Tse et al., 2013; Santiago et al., 2008). However, there is very little information about the cellular localization and functions of C15orf26 and Capsl, as well as the pathological cause for the human diseases. My data shows that both protein are associated with basal bodies and cilia in *Tetrahymena*. In contrast, the human protein Capsl does not localize to the centrosome in U2OS cells. It would be worthwhile to determine whether C15orf26 is ciliary component in human cells, as the reduction of C15orf26 protein level leads to abnormal cilia structure and impaired cilia motility in Zebrafish (Austin-Tse et al., 2013).There is no doubt that future work on Bbc52 and Bbc57, as well as their human orthologues will shed light on the foundation of the related human diseases.

The main body of my thesis is focused on the functional analysis of Bbc73/EFHC1 in *Tetrahymena* and *Xenopus*. The EFHC family, including EFHC1 and EFHC2, consists of conserved but poorly understood proteins associated with microtubule-based structures, membrane-bound ion

channels, and human diseases. EFHC1 is conserved throughout eukaryotes possessing the centriole/basal body and cilia structures. Notably, neither *C. elegans* nor *S. cerevisiae* has an apparent homolog of EFHC1. *C.elegans* does not have any motile cilia and the centrioles are composed of singlet microtubules. Budding yeast use the spindle pole body as its microtubule organization center, which is quite structurally divergent despite many conserved components and regulators. Furthermore, no cilia or flagella are present in yeast cells. EFHC proteins contain three conserved DM10 (domains of unknown function). In EFHC1 there is a putative Ca^{2+} binding EF-hand domain in the C-terminal region (FIG. 1). This C-terminal EF-hand domain is absent in EFHC2 proteins. Mutations of EFHC1 are linked to juvenile myoclonic epilepsy and dysfunction of EFHC2 is thought to be involved in Turner syndrome(Blaya et al., 2009; Suzuki et al., 2004; Weiss et al., 2007).

I have described the identification of EFHC genes in both *Tetrahymena thermophila* and *Xenopus laveis*. Similar to human, a single EFHC1-like gene, *BBC73*, as well as a single EFHC2-like gene, *BBC60* were identified in *Tetrahymena* genome. In contrast, *X. laevis* is allotetraploid and often contains –a and –b alloalleles of genes present in single copies in the diploid species *X. tropicalis* (Hellsten et al., 2007). A BLAST search of the latest (7.1) version of the *X. laevis* genome using the previously identified EFHC1 coding region reveals two EFHC1-related chromosomal scaffolds. One scaffold contains the originally annotated EFHC1-like gene, termed EFHC1b. The second EFHC1 scaffold identified has yet to be annotated and its putative start site remains to be identified. We tentatively identify this gene as EFHC1a. Using the same method, two EFHC2 scaffolds were identified and neither of their expression have been confirmed. Sequence alignment clearly shows that the DM10 domains are much more conserved than the N- and C-termini across these species.

EFHC1 is reported to be a cilia and flagellar component in mouse, *Chlamydomonas*, as well as a microtubule associated protein in fly and human cells (Ikeda et al., 2003, 2005; de Nijs et al., 2009; Rossetto et al., 2011). The association of EFHC1 within the cilia from the above studies is restricted the

motile cilia and there is no evidence of EFHC1 localizing to primary cilia. Kilburn et al confirmed the association of overexpressed EFHC1 homolog with basal bodies in *Tetrahymena* upon the identification of the protein in the basal body proteome (Kilburn et al., 2007). No localization data was previously available for EFHC2. My results are consistent with the current knowledge on EFHC1 cellular localization and I made new discoveries about the localization of protein. In *Tetrahymena*, endogenous Bbc73-mCherry is found at both the basal bodies and the cilia. The fusion protein is also observed at the contractile vacuolar pores, a different microtubule-based structure in ciliates. Immuno-electron microscopy reveals that Bbc73 is mainly associated with the microtubule walls of basal bodies and the axonemes of cilia. Bbc60, the homology of human EFHC2, although missing from the basal body proteome, has a similar localization pattern to Bbc73. In *Xenopus*, EFHC1b-GFP is found at the motile cilia on multiciliated cells in ectoderm explants. Surprisingly, the protein is also detected at the gastrocoel roof plate cilia and at the primary cilia in the ventral surface of neural tube. Gastrocoel roof plate cilia are analogous to the nodal cilia in mouse embryos, which are critical for establishing the left-right asymmetry. Primary cilia are required for multiple signaling transduction events during vertebrate development (Eggenschwiler and Anderson, 2007). The accumulation of EFHC1b polypeptides at these two organelles suggests EFHC1b may play a role in regulating signaling.

The N-terminus of EFHC1 is required and sufficient for its association with microtubules in human cells (de Nijs et al., 2006). It is remarkable that determinants of EFHC1 localization in *Tetrahymena* and *Xenopus* are different. Analysis on Bbc73 truncation mutations showed that as the case of human EFHC1, the N-terminus itself is able to localize to the basal body and the cilium, although the signal is much weak than the wild type protein. Unexpectedly, without the N-terminus, the protein can still maintain its association with the basal body and the cilium, which suggests that a second localization determinant exists outside the N-terminal motif of Bbc73. In contrast to *Tetrahymena*, but similar to human EFHC1, EFHC1b requires its N-terminus for its ciliary association in *Xenopus*. This could

be explained by the divergence of the N-terminal sequences between the human, *Tetrahymena* and *Xenopus* EFHC1 genes. It would be interesting to determine which domain within Bbc60 ensures its localization.

Efhc1$^{-/-}$ mice are viable with a subtle ciliary defect (Suzuki et al., 2009). I have generated the *Tetrahymena BBC73* null strains, which display normal growth rate. The viability of *bbc73Δ* cells, as well as *bbc60Δ* cells from the Gaertig lab proves that neither of these genes are essential, similar to the mouse homolog. Loss of EFHC1 in mice leads to spontaneous myoclonus and increased seizure susceptibility (Suzuki et al., 2009). Similarly, *bbc73Δ* cells are hyperreactive to the food stimuli. It is reported that the cilia structure remains intact in Efhc1$^{-/-}$ mice. Depletion of *BBC73* in *Tetrahymena* results in the lack of MIP complexes in the doublet microtubule lumen while the overall 9+2 axoneme structure is not affected. A similar defect is found in the axonemes of *bbc60Δ* cells. MIPs are complexes identified inside the microtubule by cryo-EM recently. Despite the morphological description of these structures, there is no published data on the composition and function of MIPs. This new discovery will surely shed light on our understanding on the molecular assembly and biological roles of MIPs. My hypothesis on the relationship between MIPs and Bbc73/ Bbc60 is that the two proteins may be the molecular components or the regulator of MIPs. To address this question, constructs encoding chimeras of large tags with Bbc73 or Bbc60 were introduced into the appropriate null mutant strains that were used for cryo-EM analysis. If the proteins are the components of MIPs, the additional mass from the tag would be resolved. This work is currently underway. Besides the structural defect, no other ciliary phenotypes are observed in *bbc73Δ* cells. One explanation is that Bbc73 and Bbc60 are functionally redundant. I have attempted to knockout both genes in *Tetrahymena* simultaneously. Although the individual null mutant strains shows the same structural defect, I would predict that the double knockout would result in a more severe ciliary phenotype. The structural findings described here provides a useful foundation for future work on understanding the functions of MIPs.

Because we have little knowledge about the dependencies between EFHC1 and EFHC2, I conducted the first localization analysis of the individual protein without its paralog in *Tetrahymena*. It appears that the localization of Bbc73 and of Bbc60 are independent on each other. However, this cannot rule out the possibility that they are present in the same complex, such as MIP1. There is no published data on whether Bbc73 and Bbc60 physically interact with each other, but it is feasible. The axoneme of cilia is composed of well-arranged doublet microtubules with multiple complexes attached to the microtubule wall. Identifying EFHC1 interactors would assist to understand how it functions in this complex structure. However, little is known of EFHC1 interacting proteins. EFHC1 has been described to interact with the redox-sensitive TRPM2 plasma membrane protein (Katano et al. 2012). EFHC1 is also reported to be associated with tektin filaments in Sea urchin flagella (Setter et al. 2006). This direction is worthwhile to pursue for building a Bbc73 interactome network and expanding our knowledge on the mechanisms of Bbc73 cellular functions.

Although cilia are still present in Efhc1$^{-/-}$ mice (Suzuki et al., 2009), my work in *Xenopus* shows that loss of EFHC1b leads to reduced multiciliated cell density and a decreased number of cilia per multiciliated cell. Basal body density is not affected. This difference between mice and *Xenopus* may be due to the fact that EFHC2 present in the mutant mice could cover the potential phenotype, while EFHC2 in *X. laveis* may not be expressed or redundant with EFHC1. It would be interesting to determine whether the *Xenopus* ciliary defects can be rescued by co-injection of the full length EFHC2 RNA.

Besides the ciliary defects, I found many additional phenotypes caused by reducing EFHC1b protein level during embryonic development in *Xenopus*, including the disrupted central nervous system patterning and impaired neural crest migration. The same defects were described previously for the basal body associated protein Cby (Shi et al., 2014). However, the EFHC1b defects appear to be distinct from Cby, as I note that injection of Cby-GFP (which rescues the Cby morphant phenotype), does not rescue EFHC1 morphant phenotypes. What is novel in my findings of EFHC1b functions is the effect of

reducing EFHC1b levels on β-catenin-mediated Wnt signaling, as monitored by qPCR on RNA level of Wnt8 and the activation of the TOPFLASH reporter in early gastrula stage embryos. In this experiment Wnt8 levels are increased before the on-set of ciliogenesis. The mechanistic details of EFHC1-mediated regulation remain to be identified, but it is worth noting the Kif3a protein has been found to have non-ciliogenesis associated effects on β-catenin-mediated Wnt signaling (Corbit et al., 2008).

An important aspect of the observations in *Xenopus* is that many of the effects associated with the down regulation of EFHC1 appear to be indirect, the result of autocrine and/or paracrine effects of increased Wnt8a signaling; these effects are inhibited by the expression of secreted Wnt antagonists. In fact, the only EFHC1 morphant phenotype not inhibited by the secreted Wnt inhibitor SFRP2 was the effect on axoneme formation. This appears to reflect a structural role for the EFHC1 protein that only the full-length protein can rescue in EFHC1 morphant explants. On the other hand, reduction in multiciliated cells in ectodermal explants was rescued by the expression of SFRP2. This is similar to our observations in Cby morphant explants (Shi et al., 2014), and supports the conclusion the formation of multiciliated cells is inhibited by high levels of Wnt signaling.

From the perspective of the etiology of JME and Wnt signaling is the reduction of EFHC1 that leads to an increased in β-catenin-dependent Wnt signaling activity, and initiates a Wnt mediated autocrine/paracrine feedback loop that can have dramatic effects on CNS and neural crest patterning. Presumably analogous, but less severe effects associated with EFHC1 mutations could influence the development of the human CNS leading to the onset of JME in some individuals.

References:

Alfandari, D., Cousin, H., Gaultier, A., Hoffstrom, B.G., and DeSimone, D.W. (2003). Integrin alpha5beta1 supports the migration of Xenopus cranial neural crest on fibronectin. Dev. Biol. *260*, 449–464.

Allen, R.D. (1967). Fine Structure, Reconstruction and Possible Functions of Components of the Cortex of Tetrahymena pyriformis. J. Protozool. *14*, 553–565.

Van Amerongen, R., and Nusse, R. (2009). Towards an integrated view of Wnt signaling in development. Dev. Camb. Engl. *136*, 3205–3214.

Andersen, J.S., Wilkinson, C.J., Mayor, T., Mortensen, P., Nigg, E.A., and Mann, M. (2003). Proteomic characterization of the human centrosome by protein correlation profiling. Nature *426*, 570–574.

Armijo, J.A., Shushtarian, M., Valdizan, E.M., Cuadrado, A., de las Cuevas, I., and Adín, J. (2005). Ion channels and epilepsy. Curr. Pharm. Des. *11*, 1975–2003.

Austin-Tse, C., Halbritter, J., Zariwala, M.A., Gilberti, R.M., Gee, H.Y., Hellman, N., Pathak, N., Liu, Y., Panizzi, J.R., Patel-King, R.S., et al. (2013). Zebrafish Ciliopathy Screen Plus Human Mutational Analysis Identifies C21orf59 and CCDC65 Defects as Causing Primary Ciliary Dyskinesia. Am. J. Hum. Genet. *93*, 672–686.

Avidor-Reiss, T., Maer, A.M., Koundakjian, E., Polyanovsky, A., Keil, T., Subramaniam, S., and Zuker, C.S. (2004). Decoding cilia function: defining specialized genes required for compartmentalized cilia biogenesis. Cell *117*, 527–539.

Bachmann-Gagescu, R. (2014). [Genetic complexity of ciliopathies and novel genes identification]. Médecine Sci. MS *30*, 1011–1023.

Bai, D., Bailey, J.N., Durón, R.M., Alonso, M.E., Medina, M.T., Martínez-Juárez, I.E., Suzuki, T., Machado-Salas, J., Ramos-Ramírez, R., Tanaka, M., et al. (2009). DNA variants in coding region of EFHC1: SNPs do not associate with juvenile myoclonic epilepsy. Epilepsia *50*, 1184–1190.

Basten, S.G., and Giles, R.H. (2013). Functional aspects of primary cilia in signaling, cell cycle and tumorigenesis. Cilia *2*, 6.

Bergmann, C., Fliegauf, M., Brüchle, N.O., Frank, V., Olbrich, H., Kirschner, J., Schermer, B., Schmedding, I., Kispert, A., Kränzlin, B., et al. (2008). Loss of nephrocystin-3 function can cause embryonic lethality, Meckel-Gruber-like syndrome, situs inversus, and renal-hepatic-pancreatic dysplasia. Am. J. Hum. Genet. *82*, 959–970.

Blaya, C., Moorjani, P., Salum, G.A., Gonçalves, L., Weiss, L.A., Leistner-Segal, S., Manfro, G.G., and Smoller, J.W. (2009). Preliminary evidence of association between EFHC2, a gene implicated in fear recognition, and harm avoidance. Neurosci. Lett. *452*, 84–86.

Broadhead, R., Dawe, H.R., Farr, H., Griffiths, S., Hart, S.R., Portman, N., Shaw, M.K., Ginger, M.L., Gaskell, S.J., McKean, P.G., et al. (2006). Flagellar motility is required for the viability of the bloodstream trypanosome. Nature *440*, 224–227.

Brooks, E.R., and Wallingford, J.B. (2015). In vivo investigation of cilia structure and function using Xenopus. Methods Cell Biol. *127*, 131–159.

Carvalho-Santos, Z., Azimzadeh, J., Pereira-Leal, J.B., and Bettencourt-Dias, M. (2011). Tracing the origins of centrioles, cilia, and flagella. J. Cell Biol. *194*, 165–175.

Cassidy-Hanley, D.M. (2012). Tetrahymena in the Laboratory: Strain Resources, Methods for Culture, Maintenance, and Storage. Methods Cell Biol. *109*, 237–276.

Chan, S.W., Fowler, K.J., Choo, K.H.A., and Kalitsis, P. (2005). Spef1, a conserved novel testis protein found in mouse sperm flagella. Gene *353*, 189–199.

Chien, Y.-H., Werner, M.E., Stubbs, J., Joens, M.S., Li, J., Chien, S., Fitzpatrick, J.A.J., Mitchell, B.J., and Kintner, C. (2013). Bbof1 is required to maintain cilia orientation. Development *140*, 3468–3477.

Chung, M.-I., Peyrot, S.M., LeBoeuf, S., Park, T.J., McGary, K.L., Marcotte, E.M., and Wallingford, J.B. (2012). RFX2 is broadly required for ciliogenesis during vertebrate development. Dev. Biol. *363*, 155–165.

Conte, F.F., Ribeiro, P.A.O., Marchesini, R.B., Pascoal, V.D.B., Silva, J.M., Oliveira, A.R., Gilioli, R., Sbragia, L., Bittencourt, J.C., and Lopes-Cendes, I. (2009). Expression profile and distribution of Efhc1 gene transcript during rodent brain development. J. Mol. Neurosci. MN *39*, 69–77.

Corbit, K.C., Aanstad, P., Singla, V., Norman, A.R., Stainier, D.Y.R., and Reiter, J.F. (2005). Vertebrate Smoothened functions at the primary cilium. Nature *437*, 1018–1021.

Corbit, K.C., Shyer, A.E., Dowdle, W.E., Gaulden, J., Singla, V., Chen, M.-H., Chuang, P.-T., and Reiter, J.F. (2008). Kif3a constrains beta-catenin-dependent Wnt signalling through dual ciliary and non-ciliary mechanisms. Nat. Cell Biol. *10*, 70–76.

Cossette, P., Liu, L., Brisebois, K., Dong, H., Lortie, A., Vanasse, M., Saint-Hilaire, J.-M., Carmant, L., Verner, A., Lu, W.-Y., et al. (2002). Mutation of GABRA1 in an autosomal dominant form of juvenile myoclonic epilepsy. Nat. Genet. *31*, 184–189.

Culver, B.P., Meehl, J.B., Giddings, T.H., and Winey, M. (2009). The Two SAS-6 Homologs in Tetrahymena thermophila Have Distinct Functions in Basal Body Assembly. Mol. Biol. Cell *20*, 1865–1877.

Cyrklaff, M., Kudryashev, M., Leis, A., Leonard, K., Baumeister, W., Menard, R., Meissner, M., and Frischknecht, F. (2007). Cryoelectron tomography reveals periodic material at the inner side of subpellicular microtubules in apicomplexan parasites. J. Exp. Med. *204*, 1281–1287.

Delgado-Escueta, A.V., Koeleman, B.P.C., Bailey, J.N., Medina, M.T., and Durón, R.M. (2013). The quest for Juvenile Myoclonic Epilepsy genes. Epilepsy Behav. *28, Supplement 1*, S52–S57.

Dougherty, G.W., Adler, H.J., Rzadzinska, A., Gimona, M., Tomita, Y., Lattig, M.C., Merritt, R.C., and Kachar, B. (2005). CLAMP, a novel microtubule-associated protein with EB-type calponin homology. Cell Motil. Cytoskeleton *62*, 141–156.

Dutcher, S.K. (1995). Purification of basal bodies and basal body complexes from Chlamydomonas reinhardtii. Methods Cell Biol. *47*, 323–334.

Eggenschwiler, J.T., and Anderson, K.V. (2007). Cilia and Developmental Signaling. Annu. Rev. Cell Dev. Biol. *23*, 345–373.

Escayg, A., De Waard, M., Lee, D.D., Bichet, D., Wolf, P., Mayer, T., Johnston, J., Baloh, R., Sander, T., and Meisler, M.H. (2000). Coding and noncoding variation of the human calcium-channel beta4-subunit gene CACNB4 in patients with idiopathic generalized epilepsy and episodic ataxia. Am. J. Hum. Genet. *66*, 1531–1539.

Ferkol, T.W., and Leigh, M.W. (2012). Ciliopathies: the central role of cilia in a spectrum of pediatric disorders. J. Pediatr. *160*, 366–371.

Frankel, J. (2000). Cell biology of Tetrahymena thermophila. Methods Cell Biol. *62*, 27–125.

Gaertig, J., Cruz, M.A., Bowen, J., Gu, L., Pennock, D.G., and Gorovsky, M.A. (1995). Acetylation of lysine 40 in alpha-tubulin is not essential in Tetrahymena thermophila. J. Cell Biol. *129*, 1301–1310.

Galati, D.F., Bonney, S., Kronenberg, Z., Clarissa, C., Yandell, M., Elde, N.C., Jerka-Dziadosz, M., Giddings, T.H., Frankel, J., and Pearson, C.G. (2014). DisAp-dependent striated fiber elongation is required to organize ciliary arrays. J. Cell Biol. *207*, 705–715.

Ganesh, S. (2010). Juvenile myoclonic epilepsy: EFHC1 at the cross–roads? Ann. Neurosci. *17*, 57–59.

Gao, C., and Chen, Y.-G. (2010). Dishevelled: The hub of Wnt signaling. Cell. Signal. *22*, 717–727.

Garvalov, B.K., Zuber, B., Bouchet-Marquis, C., Kudryashev, M., Gruska, M., Beck, M., Leis, A., Frischknecht, F., Bradke, F., Baumeister, W., et al. (2006a). Luminal particles within cellular microtubules. J. Cell Biol. *174*, 759–765.

Garvalov, B.K., Zuber, B., Bouchet-Marquis, C., Kudryashev, M., Gruska, M., Beck, M., Leis, A., Frischknecht, F., Bradke, F., Baumeister, W., et al. (2006b). Luminal particles within cellular microtubules. J. Cell Biol. *174*, 759–765.

Gerdes, J.M., Liu, Y., Zaghloul, N.A., Leitch, C.C., Lawson, S.S., Kato, M., Beachy, P.A., Beales, P.L., DeMartino, G.N., Fisher, S., et al. (2007). Disruption of the basal body compromises proteasomal function and perturbs intracellular Wnt response. Nat. Genet. *39*, 1350–1360.

Geremek, M., Schoenmaker, F., Zietkiewicz, E., Pogorzelski, A., Diehl, S., Wijmenga, C., and Witt, M. (2008). Sequence analysis of 21 genes located in the Kartagener syndrome linkage region on chromosome 15q. Eur. J. Hum. Genet. *16*, 688–695.

Gibbons, I.R. (1981). Cilia and flagella of eukaryotes. J. Cell Biol. *91*, 107s – 124s.

Giddings, T.H., Meehl, J.B., Pearson, C.G., and Winey, M. (2010). Electron tomography and immuno-labeling of Tetrahymena thermophila basal bodies. Methods Cell Biol. *96*, 117–141.

Goetz, S.C., and Anderson, K.V. (2010). The primary cilium: a signalling centre during vertebrate development. Nat. Rev. Genet. *11*, 331–344.

Grünewald, R.A., and Panayiotopoulos, C.P. (1993). Juvenile myoclonic epilepsy. A review. Arch. Neurol. *50*, 594–598.

Gu, W., Sander, T., Heils, A., Lenzen, K.P., and Steinlein, O.K. (2005). A new EF-hand containing gene EFHC2 on Xp11.4: tentative evidence for association with juvenile myoclonic epilepsy. Epilepsy Res. *66*, 91–98.

Habas, R., and Dawid, I.B. (2005). Dishevelled and Wnt signaling: is the nucleus the final frontier? J. Biol. *4*, 2.

Haug, K., Warnstedt, M., Alekov, A.K., Sander, T., Ramírez, A., Poser, B., Maljevic, S., Hebeisen, S., Kubisch, C., Rebstock, J., et al. (2003). Mutations in CLCN2 encoding a voltage-gated chloride channel are associated with idiopathic generalized epilepsies. Nat. Genet. *33*, 527–532.

Haycraft, C.J., Banizs, B., Aydin-Son, Y., Zhang, Q., Michaud, E.J., and Yoder, B.K. (2005). Gli2 and Gli3 Localize to Cilia and Require the Intraflagellar Transport Protein Polaris for Processing and Function. PLoS Genet. *1*.

Hellsten, U., Khokha, M.K., Grammer, T.C., Harland, R.M., Richardson, P., and Rokhsar, D.S. (2007). Accelerated gene evolution and subfunctionalization in the pseudotetraploid frog Xenopus laevis. BMC Biol. *5*, 31.

Hennessey, T.M., and Lampert, T.J. (2012). Behavioral bioassays and their uses in Tetrahymena. Methods Cell Biol. *109*, 393–410.

Hildebrandt, F., Benzing, T., and Katsanis, N. (2011). Ciliopathies. N. Engl. J. Med. *364*, 1533–1543.

Huang, P., and Schier, A.F. (2009). Dampened Hedgehog signaling but normal Wnt signaling in zebrafish without cilia. Dev. Camb. Engl. *136*, 3089–3098.

Huangfu, D., and Anderson, K.V. (2005). Cilia and Hedgehog responsiveness in the mouse. Proc. Natl. Acad. Sci. U. S. A. *102*, 11325–11330.

Huangfu, D., Liu, A., Rakeman, A.S., Murcia, N.S., Niswander, L., and Anderson, K.V. (2003). Hedgehog signalling in the mouse requires intraflagellar transport proteins. Nature *426*, 83–87.

Ibañez-Tallon, I., Heintz, N., and Omran, H. (2003). To beat or not to beat: roles of cilia in development and disease. Hum. Mol. Genet. *12 Spec No 1*, R27–R35.

Ikeda, T. (2010). NDP kinase 7 is a conserved microtubule-binding protein preferentially expressed in ciliated cells. Cell Struct. Funct. *35*, 23–30.

Ikeda, K., Brown, J.A., Yagi, T., Norrander, J.M., Hirono, M., Eccleston, E., Kamiya, R., and Linck, R.W. (2003). Rib72, a conserved protein associated with the ribbon compartment of flagellar A-microtubules and potentially involved in the linkage between outer doublet microtubules. J. Biol. Chem. *278*, 7725–7734.

Ikeda, T., Ikeda, K., Enomoto, M., Park, M.K., Hirono, M., and Kamiya, R. (2005). The mouse ortholog of EFHC1 implicated in juvenile myoclonic epilepsy is an axonemal protein widely conserved among organisms with motile cilia and flagella. FEBS Lett. *579*, 819–822.

Ishikawa, T. (2015). Cryo-electron tomography of motile cilia and flagella. Cilia *4*, 3.

Kapoor, A., Vijai, J., Ravishankar, H.M., Satishchandra, P., Radhakrishnan, K., and Anand, A. (2003). Absence of GABRA1 Ala322Asp mutation in juvenile myoclonic epilepsy families from India. J. Genet. *82*, 17–21.

Katano, M., Numata, T., Aguan, K., Hara, Y., Kiyonaka, S., Yamamoto, S., Miki, T., Sawamura, S., Suzuki, T., Yamakawa, K., et al. (2012). The juvenile myoclonic epilepsy-related protein EFHC1 interacts with the redox-sensitive TRPM2 channel linked to cell death. Cell Calcium *51*, 179–185.

Keller, L.C., Romijn, E.P., Zamora, I., Yates III, J.R., and Marshall, W.F. (2005). Proteomic Analysis of Isolated Chlamydomonas Centrioles Reveals Orthologs of Ciliary-Disease Genes. Curr. Biol. *15*, 1090–1098.

Kilburn, C.L., Pearson, C.G., Romijn, E.P., Meehl, J.B., Giddings, T.H., Culver, B.P., Yates, J.R., and Winey, M. (2007a). New Tetrahymena basal body protein components identify basal body domain structure. J. Cell Biol. *178*, 905–912.

Kilburn, C.L., Pearson, C.G., Romijn, E.P., Meehl, J.B., Giddings, T.H., Culver, B.P., Yates, J.R., and Winey, M. (2007b). New Tetrahymena basal body protein components identify basal body domain structure. J. Cell Biol. *178*, 905–912.

King, S.M. (2006). Axonemal protofilament ribbons, DM10 domains, and the link to juvenile myoclonic epilepsy. Cell Motil. Cytoskeleton *63*, 245–253.

Kobayashi, T., and Dynlacht, B.D. (2011). Regulating the transition from centriole to basal body. J. Cell Biol. *193*, 435–444.

Koppelhus, U., Hellung-Larsen, P., and Leick, V. (1994). An improved quantitative assay for chemokinesis in Tetrahymena. Biol. Bull. *187*, 8–15.

Korenbaum, E., and Rivero, F. (2002). Calponin homology domains at a glance. J. Cell Sci. *115*, 3543–3545.

Lee, J.E., and Gleeson, J.G. (2011). A systems-biology approach to understanding the ciliopathy disorders. Genome Med. *3*, 59.

Li, J.B., Gerdes, J.M., Haycraft, C.J., Fan, Y., Teslovich, T.M., May-Simera, H., Li, H., Blacque, O.E., Li, L., Leitch, C.C., et al. (2004). Comparative Genomics Identifies a Flagellar and Basal Body Proteome that Includes the BBS5 Human Disease Gene. Cell *117*, 541–552.

Linck, R., Fu, X., Lin, J., Ouch, C., Schefter, A., Steffen, W., Warren, P., and Nicastro, D. (2014). Insights into the Structure and Function of Ciliary and Flagellar Doublet Microtubules TEKTINS, Ca2+-BINDING PROTEINS, AND STABLE PROTOFILAMENTS. J. Biol. Chem. *289*, 17427–17444.

Liu, Y.P., Tsai, I.-C., Morleo, M., Oh, E.C., Leitch, C.C., Massa, F., Lee, B.-H., Parker, D.S., Finley, D., Zaghloul, N.A., et al. (2014). Ciliopathy proteins regulate paracrine signaling by modulating proteasomal degradation of mediators. J. Clin. Invest. *124*, 2059–2070.

MacDonald, B.T., Tamai, K., and He, X. (2009). Wnt/β-catenin signaling: components, mechanisms, and diseases. Dev. Cell *17*, 9–26.

Marshall, W.F. (2008). Basal bodies platforms for building cilia. Curr. Top. Dev. Biol. *85*, 1–22.

Marshall, W.F., and Nonaka, S. (2006). Cilia: tuning in to the cell's antenna. Curr. Biol. CB *16*, R604–R614.

Marshall, W.F., and Rosenbaum, J.L. (2001). Intraflagellar transport balances continuous turnover of outer doublet microtubules. J. Cell Biol. *155*, 405–414.

May, S.R., Ashique, A.M., Karlen, M., Wang, B., Shen, Y., Zarbalis, K., Reiter, J., Ericson, J., and Peterson, A.S. (2005). Loss of the retrograde motor for IFT disrupts localization of Smo to cilia and prevents the expression of both activator and repressor functions of Gli. Dev. Biol. *287*, 378–389.

Meador, K.J. (2010). Brain Function and Anatomy in Juvenile Myoclonic Epilepsy. Epilepsy Curr. *10*, 13–14.

Meehl, J.B., Giddings, T.H., and Winey, M. (2009). High pressure freezing, electron microscopy, and immuno-electron microscopy of Tetrahymena thermophila basal bodies. Methods Mol. Biol. Clifton NJ *586*, 227–241.

Murai, M.J., Sassonia, R.C., Zamboni, A.H., Conte, F.F., Martins-de-Souza, D., Aparicio, R., de Oliveira, M.G., and Lopes-Cendes, I. (2008). Characterization of the C-terminal half of human juvenile myoclonic epilepsy protein EFHC1: dimer formation blocks Ca2+ and Mg2+ binding to its functional EF-hand. Arch. Biochem. Biophys. *477*, 131–138.

Nauli, S.M., Alenghat, F.J., Luo, Y., Williams, E., Vassilev, P., Li, X., Elia, A.E.H., Lu, W., Brown, E.M., Quinn, S.J., et al. (2003). Polycystins 1 and 2 mediate mechanosensation in the primary cilium of kidney cells. Nat. Genet. *33*, 129–137.

Nicastro, D., Schwartz, C., Pierson, J., Gaudette, R., Porter, M.E., and McIntosh, J.R. (2006). The molecular architecture of axonemes revealed by cryoelectron tomography. Science *313*, 944–948.

Nicastro, D., Fu, X., Heuser, T., Tso, A., Porter, M.E., and Linck, R.W. (2011). Cryo-electron tomography reveals conserved features of doublet microtubules in flagella. Proc. Natl. Acad. Sci. U. S. A. *108*, E845–E853.

De Nijs, L., Lakaye, B., Coumans, B., Léon, C., Ikeda, T., Delgado-Escueta, A.V., Grisar, T., and Chanas, G. (2006). EFHC1, a protein mutated in juvenile myoclonic epilepsy, associates with the mitotic spindle through its N-terminus. Exp. Cell Res. *312*, 2872–2879.

De Nijs, L., Léon, C., Nguyen, L., Loturco, J.J., Delgado-Escueta, A.V., Grisar, T., and Lakaye, B. (2009). EFHC1 interacts with microtubules to regulate cell division and cortical development. Nat. Neurosci. *12*, 1266–1274.

De Nijs, L., Wolkoff, N., Coumans, B., Delgado-Escueta, A.V., Grisar, T., and Lakaye, B. (2012). Mutations of EFHC1, linked to juvenile myoclonic epilepsy, disrupt radial and tangential migrations during brain development. Hum. Mol. Genet. *21*, 5106–5117.

Ocbina, P.J.R., Tuson, M., and Anderson, K.V. (2009). Primary cilia are not required for normal canonical Wnt signaling in the mouse embryo. PloS One *4*, e6839.

Oda, T., and Kikkawa, M. (2013). Novel structural labeling method using cryo-electron tomography and biotin-streptavidin system. J. Struct. Biol. *183*, 305–311.

Pal, D., and Helbig, I. (2015). Commentary: Pathogenic EFHC1 mutations are tolerated in healthy individuals dependent on reported ancestry. Epilepsia *56*, 195–196.

Park, T.J., Mitchell, B.J., Abitua, P.B., Kintner, C., and Wallingford, J.B. (2008). Dishevelled controls apical docking and planar polarization of basal bodies in ciliated epithelial cells. Nat. Genet. *40*, 871–879.

Pazour, G.J., Agrin, N., Leszyk, J., and Witman, G.B. (2005). Proteomic analysis of a eukaryotic cilium. J. Cell Biol. *170*, 103–113.

Pearson, C.G., and Winey, M. (2009). Basal body assembly in ciliates: the power of numbers. Traffic Cph. Den. *10*, 461–471.

Pearson, C.G., Osborn, D.P.S., Giddings, T.H., Beales, P.L., and Winey, M. (2009). Basal body stability and ciliogenesis requires the conserved component Poc1. J. Cell Biol. *187*, 905–920.

Popodi, E.M., Hoyle, H.D., Turner, F.R., and Raff, E.C. (2008). Cooperativity beween the β-tubulin carboxy tail and the body of the molecule is required for microtubule function. Cell Motil. Cytoskeleton *65*, 955–963.

Rohatgi, R., Milenkovic, L., and Scott, M.P. (2007). Patched1 regulates hedgehog signaling at the primary cilium. Science *317*, 372–376.

Romano Dallai, R.M. (2005). The sperm structure of Galloisiana yuasai (Insecta, Grylloblattodea) and implications for the phylogenetic position of Grylloblattodea. *124*, 205–212.

Ross, A.J., May-Simera, H., Eichers, E.R., Kai, M., Hill, J., Jagger, D.J., Leitch, C.C., Chapple, J.P., Munro, P.M., Fisher, S., et al. (2005). Disruption of Bardet-Biedl syndrome ciliary proteins perturbs planar cell polarity in vertebrates. Nat. Genet. *37*, 1135–1140.

Rossetto, M.G., Zanarella, E., Orso, G., Scorzeto, M., Megighian, A., Kumar, V., Delgado-Escueta, A.V., and Daga, A. (2011). Defhc1.1, a homologue of the juvenile myoclonic gene EFHC1, modulates architecture and basal activity of the neuromuscular junction in Drosophila. Hum. Mol. Genet. *20*, 4248–4257.

Sahni, N., Yi, S., Taipale, M., Fuxman Bass, J.I., Coulombe-Huntington, J., Yang, F., Peng, J., Weile, J., Karras, G.I., Wang, Y., et al. (2015). Widespread macromolecular interaction perturbations in human genetic disorders. Cell *161*, 647–660.

Santiago, J.L., Alizadeh, B.Z., Martínez, A., Espino, L., de la Calle, H., Fernández-Arquero, M., Figueredo, M.A., de la Concha, E.G., Roep, B.O., Koeleman, B.P.C., et al. (2008). Study of the association between the CAPSL-IL7R locus and type 1 diabetes. Diabetologia *51*, 1653–1658.

Satir, P., and Christensen, S.T. (2007). Overview of Structure and Function of Mammalian Cilia. Annu. Rev. Physiol. *69*, 377–400.

Schatten, H., Wiedemeier, A.M., Taylor, M., Lubahn, D.B., Greenberg, N.M., Besch-Williford, C., Rosenfeld, C.S., Day, J.K., and Ripple, M. (2000). Centrosome-centriole abnormalities are markers for abnormal cell divisions and cancer in the transgenic adenocarcinoma mouse prostate (TRAMP) model. Biol. Cell Auspices Eur. Cell Biol. Organ. *92*, 331–340.

Schmidt, K.N., Kuhns, S., Neuner, A., Hub, B., Zentgraf, H., and Pereira, G. (2012). Cep164 mediates vesicular docking to the mother centriole during early steps of ciliogenesis. J. Cell Biol. *199*, 1083–1101.

Seifert, J.R.K., and Mlodzik, M. (2007). Frizzled/PCP signalling: a conserved mechanism regulating cell polarity and directed motility. Nat. Rev. Genet. *8*, 126–138.

Setter, P.W., Malvey-Dorn, E., Steffen, W., Stephens, R.E., and Linck, R.W. (2006). Tektin interactions and a model for molecular functions. Exp. Cell Res. *312*, 2880–2896.

Shi, J., Zhao, Y., Galati, D., Winey, M., and Klymkowsky, M.W. (2014). Chibby functions in Xenopus ciliary assembly, embryonic development, and the regulation of gene expression. Dev. Biol. *395*, 287–298.

Simons, M., Gloy, J., Ganner, A., Bullerkotte, A., Bashkurov, M., Krönig, C., Schermer, B., Benzing, T., Cabello, O.A., Jenny, A., et al. (2005). Inversin, the gene product mutated in nephronophthisis type II, functions as a molecular switch between Wnt signaling pathways. Nat. Genet. *37*, 537–543.

Stemm-Wolf, A.J., Meehl, J.B., and Winey, M. (2013). Sfr13, a member of a large family of asymmetrically localized Sfi1-repeat proteins, is important for basal body separation and stability in Tetrahymena thermophila. J. Cell Sci. *126*, 1659–1671.

Stephens, R.E. (1997). Synthesis and Turnover of Embryonic Sea Urchin Ciliary Proteins during Selective Inhibition of Tubulin Synthesis and Assembly. Mol. Biol. Cell *8*, 2187–2198.

Stephens, R. e., and Lemieux, N. a. (1999). Molecular chaperones in cilia and flagella: Implications for protein turnover. Cell Motil. Cytoskeleton *44*, 274–283.

Stogmann, E., Lichtner, P., Baumgartner, C., Bonelli, S., Assem-Hilger, E., Leutmezer, F., Schmied, M., Hotzy, C., Strom, T.M., Meitinger, T., et al. (2006). Idiopathic generalized epilepsy phenotypes associated with different EFHC1 mutations. Neurology *67*, 2029–2031.

Subaran, R.L., Conte, J.M., Stewart, W.C.L., and Greenberg, D.A. (2015). Pathogenic EFHC1 mutations are tolerated in healthy individuals dependent on reported ancestry. Epilepsia *56*, 188–194.

Sui, H., and Downing, K.H. (2006). Molecular architecture of axonemal microtubule doublets revealed by cryo-electron tomography. Nature *442*, 475–478.

Suzuki, T., Delgado-Escueta, A.V., Aguan, K., Alonso, M.E., Shi, J., Hara, Y., Nishida, M., Numata, T., Medina, M.T., Takeuchi, T., et al. (2004). Mutations in EFHC1 cause juvenile myoclonic epilepsy. Nat. Genet. *36*, 842–849.

Suzuki, T., Delgado-Escueta, A.V., Alonso, M.E., Morita, R., Okamura, N., Sugimoto, Y., Bai, D., Medina, M.T., Bailey, J.N., Rasmussen, A., et al. (2006). Mutation analyses of genes on 6p12-p11 in patients with juvenile myoclonic epilepsy. Neurosci. Lett. *405*, 126–131.

Suzuki, T., Inoue, I., Yamagata, T., Morita, N., Furuichi, T., and Yamakawa, K. (2008). Sequential expression of Efhc1/myoclonin1 in choroid plexus and ependymal cell cilia. Biochem. Biophys. Res. Commun. *367*, 226–233.

Suzuki, T., Miyamoto, H., Nakahari, T., Inoue, I., Suemoto, T., Jiang, B., Hirota, Y., Itohara, S., Saido, T.C., Tsumoto, T., et al. (2009). Efhc1 deficiency causes spontaneous myoclonus and increased seizure susceptibility. Hum. Mol. Genet. *18*, 1099–1109.

Topalidou, I., Keller, C., Kalebic, N., Nguyen, K.C.Q., Somhegyi, H., Politi, K.A., Heppenstall, P., Hall, D.H., and Chalfie, M. (2012). Genetically separable functions of the MEC-17 tubulin acetyltransferase affect microtubule organization. Curr. Biol. CB *22*, 1057–1065.

Varjosalo, M., and Taipale, J. (2008). Hedgehog: functions and mechanisms. Genes Dev. *22*, 2454–2472.

Vonderfecht, T., Cookson, M.W., Giddings, T.H., Clarissa, C., and Winey, M. (2012). The two human centrin homologues have similar but distinct functions at Tetrahymena basal bodies. Mol. Biol. Cell *23*, 4766–4777.

Voronina, V.A., Takemaru, K.-I., Treuting, P., Love, D., Grubb, B.R., Hajjar, A.M., Adams, A., Li, F.-Q., and Moon, R.T. (2009). Inactivation of Chibby affects function of motile airway cilia. J. Cell Biol. *185*, 225–233.

Wallace, R. (2005). Identification of a New JME Gene Implicates Reduced Apoptotic Neuronal Death as a Mechanism of Epileptogenesis. Epilepsy Curr. *5*, 11–13.

Weiss, L.A., Purcell, S., Waggoner, S., Lawrence, K., Spektor, D., Daly, M.J., Sklar, P., and Skuse, D. (2007). Identification of EFHC2 as a quantitative trait locus for fear recognition in Turner syndrome. Hum. Mol. Genet. *16*, 107–113.

Werner, M.E., Mitchell, J.W., Putzbach, W., Bacon, E., Kim, S.K., and Mitchell, B.J. (2014). Radial intercalation is regulated by the Par complex and the microtubule-stabilizing protein CLAMP/Spef1. J. Cell Biol. *206*, 367–376.

Widelitz, R. (2005). Wnt signaling through canonical and non-canonical pathways: recent progress. Growth Factors Chur Switz. *23*, 111–116.

Wloga, D., and Frankel, J. (2012). From molecules to morphology: cellular organization of Tetrahymena thermophila. Methods Cell Biol. *109*, 83–140.

Wloga, D., and Gaertig, J. (2010). Post-translational modifications of microtubules. J. Cell Sci. *123*, 3447–3455.

Xia, L., Hai, B., Gao, Y., Burnette, D., Thazhath, R., Duan, J., Bré, M.-H., Levilliers, N., Gorovsky, M.A., and Gaertig, J. (2000). Polyglycylation of Tubulin Is Essential and Affects Cell Motility and Division in Tetrahymena thermophila. J. Cell Biol. *149*, 1097–1106.

Yamakawa, K., and Suzuki, T. (2013). Re-evaluation of myoclonin1 immunosignals in neuron, mitotic spindle, and midbody--nonspecific? Epilepsy Behav. EB *28 Suppl 1*, S61–S62.

Yamamoto, R., Song, K., Yanagisawa, H.-A., Fox, L., Yagi, T., Wirschell, M., Hirono, M., Kamiya, R., Nicastro, D., and Sale, W.S. (2013). The MIA complex is a conserved and novel dynein regulator essential for normal ciliary motility. J. Cell Biol. *201*, 263–278.

Yuan, S., and Sun, Z. (2013). Expanding horizons: ciliary proteins reach beyond cilia. Annu. Rev. Genet. *47*, 353–376.

Zhou, J. (2009). Polycystins and primary cilia: primers for cell cycle progression. Annu. Rev. Physiol. *71*, 83–113.

De Zio, D., Giunta, L., Corvaro, M., Ferraro, E., and Cecconi, F. (2005). Expanding roles of programmed cell death in mammalian neurodevelopment. Semin. Cell Dev. Biol. *16*, 281–294.